Elasticity of Entropy-Dominated Systems

Thesis submitted towards the degree of

Doctor of Philosophy

by

Oded Farago

Submitted to the Senate of Tel Aviv University

June 2001

This work was carried out under the supervision of

Professor Yacov Kantor

To Zahit and Yotam

Acknowledgments

Abstract

Methods which relate the elastic constants of thermodynamic systems to the fluctuations of the pressure or the volume are called "fluctuation" methods. In this thesis I derive expressions, within the fluctuation method, for determining the elastic constants in systems composed of hard spheres tethered by inextensible bonds. Such systems are frequently used as athermal models of real physical systems whose thermodynamic properties are primarily determined by entropy rather than energy. The new formalism relates the elastic constants to the probability densities of contacts between the spheres and the probability densities of having stretched bonds. In order to demonstrate the validity, efficiency and accuracy of the method, I present the results of Monte Carlo simulations which use the new formalism to determine the elastic properties of hard sphere systems. The numerical results agree well with analytical predictions.

The new method is also applied to compute the elastic constants of a two-dimensional net of fixed connectivity. The net (called, the "fisherman's net") is composed of point-like atoms each of which is tethered to six neighbors by a bond limiting the distance between them to a certain maximal separation, but having zero energy at all smaller lengths. I measure the elastic constants for many values of the ratio γ between the maximal and actual extensions of the net. When the net is very stretched ($\gamma \sim 1$), a simple transformation maps the system into a triangular hard disk solid, and it is shown that the elastic properties of both systems, coincide.

When the fisherman's net becomes looser ($\gamma \sim 3$) its elasticity approaches a behavior resembling that of a network consisting of springs whose energy is proportional to their squared end-to-end distance ($E = \frac{1}{2}Kr^2$). Such springs are called "Gaussian" because of the Gaussian form of their statistical weights. An exact analytical treatment of the elastic properties of Gaussian networks leads to two remarkable results: (1) The stress tensor of a Gaussian network coincides with the conductivity tensor of an equivalent resistor network. (2) The elastic constants of a single Gaussian net vanish. Perturbation theory is used to analyze the elastic behavior of networks of slightly non-Gaussian springs.

Special focus is given in the thesis to the problem of entropic elasticity of percolat-

ing systems, which are frequently used as models for gels. I consider both "phantom" (without excluded volume interactions) and "self-avoiding" (with excluded volume interactions) systems. In the phantom case, the results of the Gaussian model leads to the prediction that the shear modulus of the system has a power law dependence on the distance from the percolation threshold, $\mu \sim (p - p_c)^f$, where the rigidity exponent f is equal to t, the conductivity exponent in random resistor networks. The nearly Gaussian model leads to another conclusion that the elastic constants also have a power law dependence on $(p - p_c)$ with a critical exponent larger than the conductivity exponent. Numerical studies of the entropic elasticity of tethered percolating networks confirm the the validity of these theoretical predictions.

Self-avoiding percolation systems represent a more realistic model of gels. The critical elasticity of such systems in not understood, both theoretically and experimentally. In fact, not only that the value of the rigidity exponent f is not known, but it is also unclear whether the onset of rigidity, in self-avoiding systems, occurs at the percolation threshold. The results of extensive numerical studies of two- and three-dimensional systems show that excluded volume interactions have negligible effects both on the value of the exponent f, and on the position of the rigidity threshold.

Frequently Used Notations and Abbreviations

Symbol	Meaning
a	Diameter of hard spheres
$a, a^{\alpha\beta}$	Coefficient of the quartic term in the nearly Gaussian spring energy
b	Maximal extension of tethers
b_0	Nearest-neighbor (lattice) spacing
C_{ijkl}	The tensor of elastic constants
C_{11}	The Voigt notation for the elastic constant C_{xxxx}
C_{12}	The Voigt notation for the elastic constant C_{xxyy}
C_{44}	The Voigt notation for the elastic constant $\frac{1}{2}(C_{xyxy} + C_{xyyx})$
d	Dimensionality
$\tilde{d}$	$= \tilde{\rho} a^2$, reduced density of hard disks
E	Internal energy
$E_0\ (E_1)$	The quadratic (quartic) term in the energy of a nearly Gaussian network
$\vec{E}$	Electric field
E_i	Cartesian component of $\vec{E}$
EV	Excluded volume

F　　　　　Free energy

f　　　　　Free energy density OR critical exponent of elasticity OR force

$\vec{f}^s$　　　　The internal force on surface atom s

$\vec{f}^s_{\text{ext}}$　　　The external force on surface atom s

fc　　　　　Free cluster[1]

FCC　　　　Face-centered cubic

FN　　　　　Fisherman's net[2]

g　　　　　Critical exponent of elastic constants

h　　　　　Critical exponent of $\Delta\mu$

HD　　　　　Hard disk[3]

J　　　　　Jacobian

$\vec{j}$　　　　　Current density

j_i　　　　　Cartesian component of $\vec{j}$

K, $K^{\alpha\beta}$　　Force constants of a Gaussian spring OR conductance of a resistor

k　　　　　Boltzmann constant

L　　　　　Linear size of the system

M_{ij}　　　　Matrix defining a linear transformation [Eq.(2.3)]

MC　　　　　Monte Carlo

N　　　　　Number of atoms

N_I　　　　Number of internal atoms of a cluster

---

[1] Quantities with the superscript "fc" are related to the free clusters (chapter 3).

[2] Quantities with the subscript "FN" are related the fisherman's net (chapter 4).

[3] Quantities with the subscript "HD" are related hard disk systems (chapter 4).

N_0	Number of free clusters
P	External pressure
p	Fraction of bonds in percolation systems
$p\left(R^\alpha, R^\beta\right)$	Probability density of finding atoms α and β at $\vec{R}^\alpha$ and $\vec{R}^\beta$
$\tilde{p}\left(R^\alpha, R^\beta\right)$	$= p\left(R^\alpha, R^\beta\right) \cdot \exp\left(R^{\alpha\beta}/kT\right)$
p_c	Percolation threshold
p_r	Rigidity threshold
PGN	Phantom Gaussian network
PN	Phantom network
PNGN	Phantom nearly Gaussian network
$R,\ R^{\alpha\beta}$	Pair distance in the undeformed system
$\vec{R},\ \vec{R}^{\alpha\beta}$	Pair separation in the undeformed system
$R_i\ (R_i^{\alpha\beta})$	Cartesian component of $\vec{R}\ (\vec{R}^{\alpha\beta})$
$R_0^{\alpha\beta}$	Pair distance at the ground state of a Gaussian network.
$\vec{R}_0^{\alpha\beta}$	Pair separation at the ground state of a Gaussian network
$(R_0^{\alpha\beta})_i$	Cartesian component of $\vec{R}_0^{\alpha\beta}$
$\vec{R}^\alpha$	Position of internal atom α
R_i^α	Cartesian component of $\vec{R}^\alpha$
$\vec{R}^s$	Position of surface atom s
R_i^s	Cartesian component of $\vec{R}^s$
$r,\ r^{\alpha\beta}$	Pair distance

$\vec{r}^{\alpha}$ Position of internal atom α (in the deformed system)

S Entropy

SC   Simple cubic

SCB   Singly connected bond

spc   Spanning cluster[4]

T Temperature

t Conductivity exponent

$V, V(\{0\})$ Volume of the undeformed system

$V(\{\eta\})$ Volume of the deformed system

Z Partition function

Z_C The configurational part of Z

γ The ratio b/b_0 (chapter 4 only)

δ_{ij} Kronecker delta

δ Dirac δ-function OR the ratio b_0/a (chapter 4 only)

$\Delta^{\alpha\beta}$ $= \left[\delta \left(R^{\alpha\beta} - a \right) - \nu^{\alpha\beta} \delta \left(R^{\alpha\beta} - b \right) \right]$ [Eq.(A.3)]

$\Delta\mu$ $= |\mu_1 - \mu_2|$

ϵ Size of a bin

ϵ_n $= (n - 1/2)\epsilon$; $n = 1, 2, \ldots$

η_{ij} Lagrangian strain tensor

---

[4] Quantities with the superscript "spc", are related to the spanning cluster (chapter 3).

$\{\eta\}$ The set of strain variables[5]

$[\eta]$ The matrix with the elements $[\eta]_{ij} = \eta_{ij}$

κ Bulk modulus

μ Shear modulus of isotropic systems

μ_1 $= C_{44} - P$, one of two shear moduli of systems with cubic symmetry

μ_2 $= \frac{1}{2}(C_{11} - C_{12}) - P$, one of two shear moduli of systems with cubic symmetry

ν Correlation length exponent

$\nu^{\alpha\beta}$ 1, if the pair $\langle\alpha\beta\rangle$ is tethered; 0, otherwise

ξ Correlation length

ρ Volume fraction of hard spheres

ρ_0 $= \pi/(3\sqrt{2}) \simeq 0.74$, volume fraction of hard spheres at the close packing density

$\tilde{\rho}$ Number density of hard spheres and hard disks

Σ The conductivity

Σ_{ij} The conductivity tensor

σ The stress $\sigma = -P$

σ_{ij} The stress tensor

$\sigma_{ij}^{\text{conf}}$ The configurational part of the stress tensor

$\sigma_{ij}^{\text{kinetic}}$ The kinetic part of the stress tensor

τ Relaxation time

$\phi(r)$ Pair potential

$\phi'(r)$ Derivative of the pair potential

---

[5] The symbol $\{0\}$ is used to denote the case when all the components of the strain tensor vanish: $\eta_{ij} = 0$.

φ^{α} (φ^{s}) Electric potential at internal (external) node α (s)

$\Omega^{\alpha\beta}$ Solid angle aperture around $\vec{R}^{\alpha\beta}$

1D   One-dimensional

2D   Two-dimensional

3D   Three-dimensional

$\langle\ \rangle$ Thermal average

$\langle\ \rangle_{0}$ Thermal average with Gaussian weights

Contents

Chapter 1

General Introduction

In this thesis I present a new method for calculating the elastic constants of entropy-dominated systems like hard spheres and tethered networks. This chapter discusses subjects related only to the general aspects of the research. An introduction to the physics of the systems whose properties are investigated in this work is given in the relevant chapters. Section 1.1 explains the major differences between the elastic features of energy- and entropy-dominated systems. Section 1.2 deals with purely-entropic systems (such as hard spheres), in which the pair-interactions are approximated by "hard" (zero-or-infinity) potentials. The advantages of using such models to study entropic effects in thermodynamic systems are discussed. A brief summary on elasticity theory of stressed systems is given in section 1.3. Section 1.4 presents the different methods for computing the elastic properties of thermodynamic systems. The discussion focuses on one of the methods, called "fluctuation method", and presents the difficulty in applying this efficient method to systems with hard potentials. It is this problem that the study, presented in this thesis, aims to resolve. The outline of the thesis, including a summary of the main results, is given in section 1.5.

1.1   Entropic Elasticity and Soft Matter

Solids can be broadly classified into *hard matter* and *soft matter*. Hard matter comprises most metals, ceramics and minerals, while soft matter refers to materials like polymers, colloids, membranes and gels. As the titles imply, the distinction between hard and soft materials is related to their very different mechanical features. Soft materials (usually) distort more easily, namely in response to smaller forces, than ordinary crystalline solids. Soft materials are also very flexible and can maintain large strains (tens and even hundreds percents) without failure. Hard materials, on the other hand, break at very small strains, typically less than one percent.

The restoring force invoked in response to a mechanical deformation is related to the increase in the free energy of the system. The free energy F is related to the internal energy E, the entropy S, and the temperature T by $F = E - TS$. Generally speaking, in hard materials the contribution of E to F is much more important than that of S. Hard solids are likely to be found close to their energy ground states, while thermal fluctuations allow only small deviations from these microscopic configurations. When such a system is deformed, a macroscopic number of atoms are shifted from their equilibrium position, and this involves a large energy penalty. This is the origin of their highly rigid and non-flexible nature. In soft matter systems, on the other hand, vastly different microscopic configurations posses very similar internal energies. Energy scales related to translations of atoms and rotations of bonds, in soft materials, are of the order of the thermal energy kT, and therefore tend to be obscured by thermal fluctuations. Strain, applied to such a system, imposes topological restrictions on the allowed microscopic configurations, thus reducing the entropy, which is essentially the (logarithm of the) number of microscopic configurations. The significant response of such systems to a modest shear results from the moderate free energy differences associated with this entropy reduction.

1.2   Hard Potentials

The specific details of inter-atomic interactions are quite unimportant in entropy-dominated systems, due to the minor influence of the internal energy on their thermodynamic properties. In real gases, for instance, the pair potential is frequently sharply repulsive at short distances and weakly attractive at longer separations. If the system is either very dilute or very dense, the attractive part of the potential is hardly felt. In polymer physics, the details of the interactions between neighboring monomers often become irrelevant provided that the molecules are sufficiently long. Similar considerations apply to gels, in particular close to the gel point. One can, therefore, use various ways to describe these interactions provided they capture the essential physical features such as *excluded volume* (EV) effects and *chemical bonding*. Thus, the pair potential $\phi(r)$ used to model the interaction between bonded atoms should increase sharply at $r < a$ and $r > b$, where a and b ($a < b$) represent the typical diameter of atoms and the length of the bonds, respectively. One example of such a pair potential (used by Kremer and Grest in Ref. [1]) is depicted by the solid line in Fig. 1.1. It is a combination of the, so called, purely repulsive 6–12
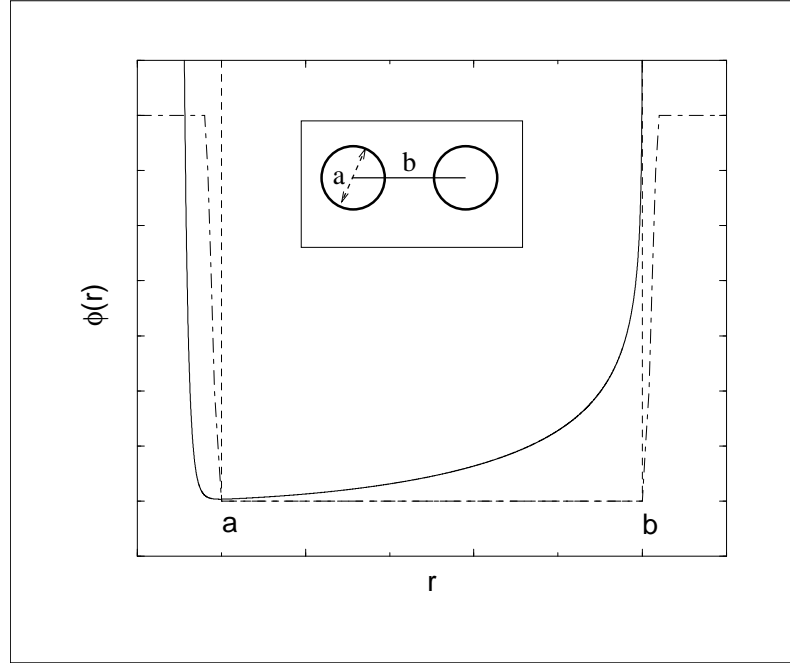
Figure 1.1: Three different potentials used to describe the pair interaction between two bonded atoms. The solid line is the potential $\phi_{\mathrm{LJ}}(r) + \phi_{\mathrm{att}}(r)$ [Eqs. (1.1) and (1.2)] used in Ref. [1]. The dashed line is the hard-spheres-and-tether potential, $\phi_1(r) + \phi_2(r)$ [Eqs. (1.3) and (1.4)]. The dot-dashed line is a smooth approximation to the "hard" potential (see last paragraph in section 2.1). Both axes are in arbitrary units. The inset shows an example of a molecule composed of two spheres of diameter a, bonded by a tether whose maximal length is b.

Lennard-Jones potential,

$$\phi_{\mathrm{LJ}}(r) = \begin{cases} 4\epsilon_0 \left[\left(\frac{a}{r}\right)^{12} - \left(\frac{a}{r}\right)^6 + \frac{1}{4} \right], & \text{for } r < 2^{1/6}a \\ 0, & \text{for } r \geq 2^{1/6}a \end{cases}, \tag{1.1}$$

and the attractive bond potential,

$$\phi_{\mathrm{att}}(r) = \begin{cases} -\frac{1}{2}k b_0^2 \ln\left[1 - \left(\frac{r}{b}\right)^2 \right], & \text{for } r < b \\ \infty, & \text{for } r \geq b \end{cases}. \tag{1.2}$$

An alternative way to describe the inter-atomic interactions, is to use "hard" potentials which take only two values: zero or infinity. EV interactions can be described by the hard sphere potential

$$\phi_1(r) = \begin{cases} \infty, & \text{for } r < a \\ 0, & \text{for } r \geq a \end{cases}. \tag{1.3}$$

Similarly, real chemical bonds can be replaced by inextensible ("tether") bonds [2]

$$\phi_2(r) = \begin{cases} 0, & \text{for } r \leq b \\ \infty, & \text{for } r > b \end{cases}, \tag{1.4}$$

which limit the distance between the bonded atoms to b, but have zero energy at all permitted distances. The sum of "hard" potentials (1.3) and (1.4), i.e. $\phi_1(r) + \phi_2(r)$,

also appears in Fig. 1.1 (dashed line). The similarity of this potential to the other
potentials shown in Fig. 1.1 (as well as to many other "model potentials" used in
other works) is evident and it is, therefore, not surprising that in many cases both
of them can be used to study real systems.[1]

When real potentials are modeled by their "hard analogs", the (potential) en-
ergy of all microscopic configurations is set to the same value — zero (configurations
with infinite energy are non-physical). Such models are called *athermal*. Because the
internal configurational energy is fixed in an athermal system, the Helmholtz free
energy is given by $F = -TS$. The physics of athermal systems is exclusively deter-
mined by entropy considerations. (Throughout this work we omit the kinetic part
of the energy since it is independent of deformation and, hence, does not contribute
to the elastic behavior.) Entropy itself does not depend on the temperature, but
is a function of the geometry of the microscopic structure alone. The temperature
dependence of the free energy is, therefore, trivially linear.

1.3   Basic Definitions in the Theory of Elasticity

The mechanical response of materials to deformations is described in the context
of *elasticity theory*. In the classical *continuum* elasticity theory [4, 5, 6], distortions
are described by the displacement field of the bulk, $\vec{u} = \vec{x}' - \vec{x}$, where $\vec{x}$ denotes the
location of a certain bulk point which, due to the deformation, is shifted to $\vec{x}'$. Born
and Huang (BH) [7] introduced a modern version of microscopic elasticity theory
that explicitly considers the atomic structure of the system and the inter-particle
interactions. The BH theory "defines" an "equilibrium solid" as a solid which has
no stresses in its reference state, and uses the set of quantities $\{\vec{u}_n\}$ to denote the
deviations of the positions of the atoms from their equilibrium values. The classical
elasticity theory can be derived as the continuum limit of the BH theory.

In the BH theory, the elastic properties of the solid are derived from the changes
in the mechanical elastic energy resulting from various deformations. In order
to characterize the elastic behavior of *thermodynamic systems* and, in particular,
entropy-dominated systems, one must use a theory based on thermodynamic po-
tentials (e.g., the free energy), rather than on the mechanical elastic energy which
ignores entropy and temperature. Voigt discussed such a theory for the case of in-
finitesimal strain from a non-stressed configuration [8]. Using a non-stressed config-
uration as a reference state is clearly an approximation since usually in experiments

---

[1]A counter example demonstrating the failure of models with hard potentials to mimic the
behavior of real systems is the gas-liquid phase transition in atomic and colloidal systems. This
transition is not observed in hard sphere systems, but appears only in the presence of additional
attractive interactions [3].

the sample is under initial stress. For hard crystalline solids it is very often justified because the effect of initial stresses on their elastic properties is usually negligible. For soft materials it is usually a poor approximation. Their structures and elastic properties cannot be understood unless the effect of initial stresses is taken into account. It is, therefore, necessary to use a theory for the case of arbitrary initial stress. Such a thermodynamic elasticity theory is presented in Refs. [9, 10], and is briefly summarized bellow.

When a thermodynamic system is deformed, the distance between two atoms which prior to the deformation were separated by $\vec{R}$, becomes

$$r = [R_i R_j (\delta_{ij} + 2\eta_{ij})]^{1/2}, \tag{1.5}$$

where the subscripts denote Cartesian coordinates and summation over repeated indices is implied. The quantities η_{ij} are the components of the *Lagrangian strain tensor*[2], while δ_{ij} is the Kronecker delta. In some special cases, e.g., crystalline solids at zero temperature, η_{ij} is constant in time and space. In soft matter systems, however, this is usually not the case since such systems are often inhomogeneous and, in addition, at a finite temperature their atoms are subject to thermal motion. Therefore, it is convenient to apply a deformation with constant (in time and space) η_{ij} to all *boundary* points, while the positions of the internal atoms are determined by the laws of statistical mechanics. This constant η_{ij} is *defined* as the homogeneous strain applied to such a system.

The mean free energy density, $f = F/V$ (per original, unstrained, unit volume) of a system subjected to a small deformation can be expanded in a power series in the strain variables

$$f(\{\eta\}) = f(\{0\}) + \sigma_{ij}\eta_{ij} + \frac{1}{2}C_{ijkl}\eta_{ij}\eta_{kl} + \ldots \tag{1.6}$$

The coefficients of the linear terms in this expansion are the components of the *stress tensor* (also referred to as Cauchy stress tensor), σ_{ij}, evaluated at the initial configuration. The component σ_{ij} is equal to the mean *internal* force along the ith direction per unit surface area perpendicular to j axis. Mechanical stability requires that internal forces will be balanced by opposite external forces applied on the boundaries of the system. The coefficients of the quadratic terms, C_{ijkl}, are the *elastic constants* of the system (also referred to as the elastic stiffness tensor). As a

---

[2]In the continuum elasticity theory η_{ij} is related to the derivatives of the displacement field $\vec{u}$ with respect to undeformed equilibrium coordinates $\vec{x}$: $\eta_{ij} = \frac{1}{2}\left(\frac{\partial u_i}{\partial x_j} + \frac{\partial u_j}{\partial x_i}\right) + \frac{\partial u_k}{\partial x_i}\frac{\partial u_k}{\partial x_j}$. Note that the definition of η_{ij} includes quadratic terms in the derivatives of the displacement field. The theory in the case of a non-stressed reference state often uses the linear strain whose definition misses the quadratic terms.

fourth rank tensor it has $3^4 = 81$ components in three-dimensional space. Because η_{ij} and σ_{ij} are symmetric second rank tensors, and since

$$C_{ijkl} = \frac{\partial \sigma_{ij}}{\partial \eta_{kl}} \bigg|_{\{\eta\}=\{0\}} \tag{1.7}$$

[see Eq.(1.6)], it follows that the tensor C_{ijkl} has the following symmetries

$$C_{ijkl} = C_{jikl} = C_{ijlk} = C_{klij} = \ldots .$$

Due to these inherent symmetries, only 21 elastic constants can be assigned independent values. This number is further reduced by symmetries present in the reference state of the specific material. For example, systems whose elastic properties posses a cubic symmetry under uniform external pressure P, have a diagonal stress tensor $\sigma_{ij} = -P\delta_{ij}$ and only three *different* non-vanishing elastic constants which in the Voigt (two-index) notation[3] are defined by

$$
\begin{aligned}
C_{11} &\equiv C_{xxxx} = C_{yyyy} = C_{zzzz} \\
C_{12} &\equiv C_{xxyy} = C_{yyzz} = C_{zzxx} = \ldots \\
C_{44} &\equiv \frac{1}{2}(C_{xyxy} + C_{xyyx}) = \frac{1}{2}(C_{yzyz} + C_{yzzy}) = \ldots .
\end{aligned}
$$

In isotropic systems, these three elastic constants obey an additional relation:

$$C_{11} - C_{12} = 2C_{44}, \tag{1.8}$$

which reduces the number of independent elastic constants of isotropic systems to two.

It is customary to dispense with the use of C_{11}, C_{12}, and C_{44} in favor of the elastic moduli κ, μ_1 and μ_2. The quantity κ is called the *bulk modulus*. It is related to the elastic constants by

$$\kappa = \begin{cases} (C_{11} + C_{12})/2, & \text{for two-dimensional systems} \\ (C_{11} + 2C_{12} + P)/3, & \text{for three-dimensional systems} \end{cases}, \tag{1.9}$$

and describes the response to an isotropic bulk deformation which causes a change in the volume of the system but no change in its shape [see Fig. 1.2 (a)]. Deformations which do not change the volume of the system but do modify the shape are called pure shear deformations. Two pure shears are depicted in Fig. 1.2 (b) and (c). The response to these pure shears is described by the *shear moduli* μ_1 and μ_2

$$\mu_1 = C_{44} - P, \tag{1.10}$$

---

[3]Explanation on the Voigt (two–index) notation of elastic constants can be found in any standard textbook of elasticity, e.g., Refs. [9, 10].

and

$$\mu_2 = \frac{1}{2}(C_{11} - C_{22}) - P, \qquad (1.11)$$

which satisfy $\mu_1 = \mu_2$ in the isotropic case [see relation (1.8)]. When the elastic moduli are positive, the system is mechanically stable [11].
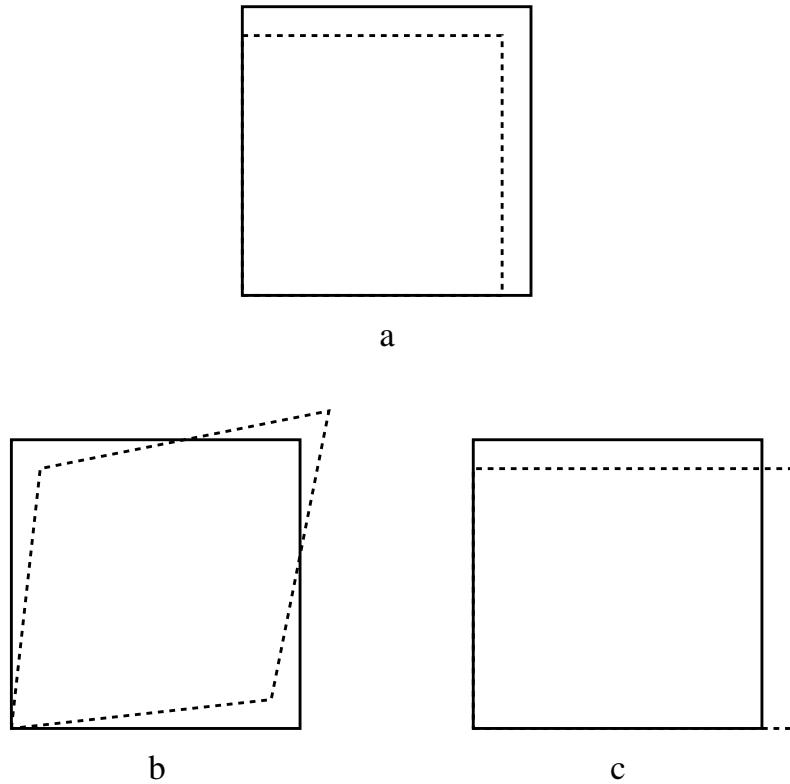
Figure 1.2: A schematic picture of an isotropic bulk deformation (a), and two pure shear deformations (b) and (c). The solid lines show the original (undeformed) shape, while the broken lines depict the deformed state.

1.4 Methods for Determining Elastic Constants

Computational methods for calculation of elastic constants are classified into *strain methods* and *fluctuation methods*. In a strain method calculation, one uses relation (1.7) between the stress, strain and elastic constants, and evaluates the latter by performing a numerical differentiation, i.e., by measuring the (small) stress variations in response to small deformations. This method has been used by Runge and Chester [12], and by Frenkel and Ladd [13], to determine the elastic constants of hard sphere systems. Other examples for the implementation of the strain method in studies of elasticity of polymer networks can be found in Refs. [14, 15]. In the fluctuation method [16], on the other hand, formal expressions for the elastic constants are derived, relating them to the mean squared thermal fluctuation of the

corresponding stress components [17]. These expressions, obtained by differentiating twice the free energy with respect to the strain, can be computed directly from Monte Carlo (MC) or molecular dynamics simulations performed on the unstrained reference system. The fact that simulations are performed in the reference system, with no need to deform the simulation cell, is the major advantage of the fluctuation method over the strain method, which makes it a more efficient and well-controlled technique. Moreover, unlike the strain method where different deformations must be applied in order to compute the different elastic constants, in the fluctuation method they are all computed in a single run.

Squire, Holt and Hoover (SHH) who formulated the original version of the fluctuation method in Ref. [16], used it to measure the elastic constants of solid argon. They used the Lennard-Jones potential to model the inter-atomic interactions. Hard spheres may also be used as a model for systems of noble elements. However, the method of SHH cannot be applied to hard sphere systems, or to any other system with pair-wise "hard" potentials. The origin of the problem lies in the expressions for the elastic constants derived within the fluctuation formalism (which will be presented in Section 2.1). These expressions include the second derivative of the pair potential $\phi(r)$, a quantity which does not exist in the case of "hard" potentials. In the next chapter we derive a fluctuation formalism suitable to model systems that interact via "hard" potentials.

1.5   Outline of the Thesis

In this thesis I present a new method for calculating the elastic constants of systems composed of hard spheres tethered by inextensible bonds. The method extends the fluctuation method which in its standard form cannot be applied to this family of systems.

I begin chapter 2 with an introduction to the original fluctuation method, and derive the expressions for the stress and elastic constants that include derivatives of the pair potential. Then, I present the new version of the method for the case of "hard-spheres-and-tethers" systems. I derive expressions relating the stress and elastic constants to the probability densities of contacts between spheres and the probability densities of having stretched tethers. (The chapter includes a short summary of the derivation, while the detailed mathematical derivation appears in appendix A.) In order to demonstrate the validity, efficiency and accuracy of the method, I present the results of MC simulations which use the new formalism to compute the elastic properties of three-dimensional (3D) hard sphere systems. Hard spheres undergo a first order fluid-solid phase transition upon increasing the density of the

spheres. In the fluid phase I find excellent agreement between the numerical results for the pressure and bulk modulus, and the values predicted by the virial expansion of the equation of state. Moreover, as expected for fluids, the computed shear modulus is vanishingly small. At the solid phase, I measure the elastic constants near the close-packing density, a regime which was not investigated numerically before. The numerical results are compared with the asymptotic expressions derived by the "free-volume" approximation and, again, a very good agreement is found between the theory and the numerical results. Some important technical aspects of the simulations are discussed in appendix B.

Chapters 3–5 deal with elasticity of *phantom* polymeric networks, i.e., networks without entanglements and EV interactions. In chapter 3 I study the elastic properties of networks of *Gaussian* springs. A Gaussian spring is a spring whose energy, $E = \frac{1}{2}Kr^2$, is proportional to its squared end-to-end distance, r^2. I show that Gaussian networks (of arbitrary topology) have a special characteristic feature — their elastic constants vanish. I also demonstrate that the stress tensor of a Gaussian network coincides with the conductivity tensor of an equivalent resistor network, in which each spring with force constant K is replaced by a resistor of conductance K. (A detailed proof of the equality between the two tensors is given in appendix C.) Corrections to Gaussian behavior are studied by considering a phantom *nearly Gaussian* network, in which the spring's energy includes an additional small term equal to $\frac{1}{4}ar^4$. Perturbative analysis is used in order to derive an expression for the elastic constants of such networks.

In chapter 4 I consider a "toy model" consisting of a two-dimensional (2D) triangular net of point-like atom, each of which is connected to its six neighbors by tethers. When the net is not very stretched it behaves like a Gaussian net and has elastic constants that are practically zero. The non-Gaussian nature of the pair-potential is observed near full extension, when the stress and elastic constants increase dramatically. I present a transformation which maps the highly-extended net into a 2D hard sphere (hard disk) solid near close packing. I use this mapping and expressions for the elastic constants of hard disk solids, to predict the elastic constants of the net close to full extension. Numerical results confirm these predictions.

Chapter 5 discusses the entropic elasticity of phantom percolation networks, in which only a fraction p of the neighbors are connected. I address the question of the critical elastic behavior just above the percolation threshold p_c, where the shear modulus behaves as $(p - p_c)^f$. In the Gaussian case, the relation between the stress of Gaussian networks and the conductivity of resistor networks (discussed in chapter 3) leads to the conclusion that the *rigidity exponent f* is equal to the

conductivity exponent in random resistor networks. In the nearly Gaussian case, I use the expression for the elastic constants to show that they also have power law dependence on $(p - p_c)$. I derive bounds on the value of the critical critical exponent of the elastic constants. Finally, I present numerical results for tethered percolation networks and show that they agree with the predictions of the Gaussian and the nearly Gaussian models.

Entropic elasticity of percolation systems with EV interactions is studied in chapter 6. The behavior of these systems is *not* described by the phantom Gaussian model, and therefore it is not clear if the rigidity and conductivity exponents are equal. Moreover, in the presence of EV interactions it is not self-evident that the onset of rigidity occurs at p_c. The possibility that the rigidity threshold is shifted below p_c arises because percolation systems of hard spheres and tethers solidifies both as a result of increasing the diameter of the spheres and also by increasing the fraction of present bonds. In chapter 6 I report the results of an extensive numerical study of the elastic behavior of 2D and 3D percolation systems. It is shown that over a broad range of hard spheres diameters a the rigidity threshold is insensitive to a and indistinguishable from p_c. Close to p_c, the shear modulus behaves as $(p - p_c)^f$, where the exponent $f \simeq 1.3$ and $f \simeq 2.0$ for 2D and 3D systems, respectively. These values are similar to the corresponding values of the conductivity exponent in random resistor networks.

Chapter 7 summarizes the thesis. It also includes a short discussion at other possible applications of the method.

Chapter 2

The Fluctuation Formalism for Elasticity of Hard-Spheres-and-Tethers Systems

This following chapter deals with the fluctuation method for calculating the elastic constants of thermodynamic systems. The major details of the derivation of the *original* formalism, which can be applied to systems with smooth potentials only, are given in section 2.1. The new formalism [18] is presented in section 2.2, where a short summary of the derivation of the method and the expressions for the stress and elastic constants are given. The detailed mathematical derivation of the formalism is relegated to appendix A. A relation is found between the components of the elastic tensor and the probability densities of contact between spheres and the probability densities of having stretched bonds. In section 2.3 we demonstrate the validity, efficiency and accuracy of the method by using the new formalism in MC simulations of hard sphere systems [18]. Section 2.4 summarizes the main results in this chapter.

2.1 The Original Formalism

The fluctuations of thermodynamic quantities like the energy or magnetization, *at equilibrium*, can be related to "generalized susceptibilities" which measure the variation of these quantities in response to small changes of corresponding external fields. In the case of energy fluctuations the relevant susceptibility is the heat capacity at constant volume C_V, while the appropriate external field is the temperature T. The former, defined by $C_V \equiv \partial E / \partial T$, is related to the equilibrium energy fluctuations by: $C_V = (kT)^2 [\langle E^2 \rangle - \langle E \rangle^2]$, where $\langle \ \rangle$ denotes a thermal average [19]. A similar relation exists between the fluctuation of the magnetization M and the magnetic susceptibility $\chi \equiv \partial M / \partial H$: $\chi = kT [\langle M^2 \rangle - \langle M \rangle^2]$, where H in the definition of χ is the external magnetic field [19]. Elastic constants describe the stress variation in

response to small strain [see Eq.(1.7)]. Therefore, we should not be surprised to find expressions relating them to stress fluctuations. These expressions, however, are not as simple as the above "fluctuation" expressions for C_V and χ and, moreover, their derivation is less trivial. In the following, we present the major steps in the derivation of the "fluctuation" method for elastic constants, devised by Squire *et al.* [16] about thirty years ago.

Consider a classical central force system in which the internal energy is the sum of pair interactions

$$E = \sum_{\alpha \neq \beta} \phi\left(r^{\alpha\beta}\right),$$

where $r^{\alpha\beta}$ is the distance between atoms α and β.[1] The corresponding canonical partition function is

$$Z = \frac{(2\pi m k T)^{3N/2}}{h^{3N}} \int_{V(\{\eta\})} \prod_{\gamma=1}^{N} d\vec{r}^{\gamma} \, \exp\left(-\sum_{\langle\alpha\beta\rangle} \phi\left(r^{\alpha\beta}\right)/kT\right) = \frac{(2\pi m k T)^{3N/2}}{h^{3N}} Z_C,$$

(2.1)

where N is the number of atoms, m the mass of an atom, T the temperature, k the Boltzmann constant and h is the Planck constant. The integration volume, $V(\{\eta\})$, is the volume in space occupied by the deformed system. The function Z_C is the configurational part of the partition function. The prefactor is associated with the momentum degrees of freedom, and since they are unaffected by the deformation of the system, it will be omitted hereafter. The (elastic part of the) free energy is related to Z_C by

$$F = -kT \ln(Z_C).$$

(2.2)

In a canonical ensemble calculation only the surface of the system, not the entire volume, deforms homogeneously. The surface of the system, $S(\{\eta\})$, defines the boundaries of integration volume, $V(\{\eta\})$. The surface $S(\{\eta\})$ of the strained volume and the surface $S(\{0\})$ of the unstrained one, are related by a *linear* transformation,

$$r_i = M_{ij} R_j,$$

(2.3)

which maps every point $\vec{R}$ on $S(\{0\})$ to its strained spatial position $\vec{r}$ on $S(\{\eta\})$. In Eq.(2.1) we note that the partition function depends on the strain variables $\{\eta\}$ only through the integration volume, $V(\{\eta\})$, and not through the integrand. The idea of the fluctuation formalism is to change the integration variables from r_i to R_i, and

---

[1]The interactions between various pairs of atoms do not have to be identical. Thus, we should denote the pair potential as $\phi_{\alpha\beta}(r^{\alpha\beta})$. However, for brevity we will omit the subscripts of the potential and the indices of the argument $r^{\alpha\beta}$ will serve as an indicator of the specific potential.

replace the strain-dependence of the boundaries of integration by strain-dependence of the integrand:

$$Z_C = e^{-F/kT} = \int_{V(\{0\})} \prod_{\gamma=1}^{N} d\vec{R}^\gamma \, J(\{\eta\}) \exp\left(-\sum_{\langle\alpha\beta\rangle} \phi\left(\left[R_i^{\alpha\beta} R_j^{\alpha\beta}(\delta_{ij} + 2\eta_{ij})\right]^{1/2}\right)/kT\right),$$
(2.4)

where J is the Jacobian of the linear transformation (2.3). To find the dependence of J on $\{\eta\}$ we note that the above linear transformation gives

$$|r|^2 = r_i r_i = R_i R_j M_{ik} M_{jk} = R_i R_j M_{ik} M_{kj}^t,$$

where M^t is the transpose of M. When this equation is compared with Eq.(1.5), we readily see that

$$[MM^t]_{ij} = 2\eta_{ij} + \delta_{ij}.$$

For a system of N particles

$$J = [\det(M)]^N = \left\{[\det(M)]^2\right\}^{N/2} = \left\{\det\left(2[\eta] + [I]\right)\right\}^{N/2},$$
(2.5)

where $[\eta]$ is the matrix with the elements $[\eta]_{ij} = \eta_{ij}$ and $[I]$ is the identity matrix. With this identity, substituted into Eq.(2.4) and then into Eq.(2.2), we have a formal expression for the free energy as a function of the strain. When we differentiate the free energy with respect to the strain variables, we easily derive the following expressions for the stress tensor σ_{ij}, and the tensor of elastic constants C_{ijkl} (which are the coefficients of the free energy density expansion in strain components [Eq.(1.6)]):

$$\sigma_{ij} = \frac{1}{V}\frac{\partial F}{\partial\eta_{ij}}\bigg|_{\{\eta\}=\{0\}} = \frac{1}{V}\left\langle\sum_{\langle\alpha\beta\rangle}\phi'\left(R^{\alpha\beta}\right)\frac{R_i^{\alpha\beta} R_j^{\alpha\beta}}{R^{\alpha\beta}}\right\rangle - \frac{NkT\delta_{ij}}{V},$$
(2.6)

and

$$\begin{aligned}
C_{ijkl} &= \frac{1}{V}\frac{\partial^2 F}{\partial\eta_{ij}\partial\eta_{kl}}\bigg|_{\{\eta\}=\{0\}} \\
&= \frac{1}{VkT}\left\{\left\langle\sum_{\langle\alpha\beta\rangle}\phi'\left(R^{\alpha\beta}\right)\frac{R_i^{\alpha\beta} R_j^{\alpha\beta}}{R^{\alpha\beta}}\right\rangle\left\langle\sum_{\langle\alpha\beta\rangle}\phi'\left(R^{\alpha\beta}\right)\frac{R_k^{\alpha\beta} R_l^{\alpha\beta}}{R^{\alpha\beta}}\right\rangle\right. \\
&\quad \left. - \left\langle\left[\sum_{\langle\alpha\beta\rangle}\phi'\left(R^{\alpha\beta}\right)\frac{R_i^{\alpha\beta} R_j^{\alpha\beta}}{R^{\alpha\beta}}\right]\left[\sum_{\langle\alpha\beta\rangle}\phi'\left(R^{\alpha\beta}\right)\frac{R_k^{\alpha\beta} R_l^{\alpha\beta}}{R^{\alpha\beta}}\right]\right\rangle\right\} \\
&\quad + \frac{1}{V}\left\langle\sum_{\langle\alpha\beta\rangle}\phi''\left(R^{\alpha\beta}\right)\frac{R_i^{\alpha\beta} R_j^{\alpha\beta} R_k^{\alpha\beta} R_l^{\alpha\beta}}{(R^{\alpha\beta})^2}\right\rangle \\
&\quad - \frac{1}{V}\left\langle\sum_{\langle\alpha\beta\rangle}\phi'\left(R^{\alpha\beta}\right)\frac{R_i^{\alpha\beta} R_j^{\alpha\beta} R_k^{\alpha\beta} R_l^{\alpha\beta}}{(R^{\alpha\beta})^3}\right\rangle + \frac{2NkT\delta_{il}\delta_{jk}}{V}.
\end{aligned}$$
(2.7)

In the above expressions summation over all distinct pairs of atoms $\langle \alpha\beta \rangle$, is performed. $R^{\alpha\beta}$ is the inter-particle distance of the pair under consideration and $R_i^{\alpha\beta}$ denotes the i-th Cartesian component of the vector $\vec{R}^{\alpha\beta} \equiv \vec{R}^{\alpha} - \vec{R}^{\beta}$. The symbol $\langle \; \rangle$ denotes a thermal average. The term in braces in Eq.(2.7) is the "fluctuation term", while the following two terms form the "Born term". The terms $-NkT\delta_{ij}/V$ and $2NkT\delta_{il}\delta_{jk}/V$ in Eqs.(2.6) and (2.7), respectively, are the "kinetic" contributions to the stress and the elastic tensors. They are related to terms appearing when J [Eq.(2.5)] is differentiated with respect to $\{\eta\}$.

The fluctuation formalism cannot be trivially used to measure the elastic constants of systems interacting via "hard" potentials, because these potentials are non-differentiable while the derivatives of the pair potential are needed in expression (2.7). Inserting "hard" potentials directly into the formal expressions for the elastic constants leads to what looks like infinite terms or terms involving products of discontinuous functions with δ-functions centered at discontinuity, and many other ambiguities and divergences. It is, therefore, convenient to use smooth approximations of these "hard" potentials, $\phi_1(r)$ and $\phi_2(r)$ [(1.3) and (1.4)], for which the averages in expression (2.6) and (2.7) can, in principle, be determined. An example for such a potential, $\phi(r)$, is sketched in Fig. 1.1. This potential, which resembles the "hard" potential $\phi_1(r) + \phi_2(r)$, has the following features:

1. $\phi\left(r^{\alpha\beta}\right)/kT \ll 1$, for $a + \varepsilon < r < b - \varepsilon$.

2. $\phi\left(r^{\alpha\beta}\right)/kT \gg 1$, for $r < a - \varepsilon$.

3. If the pair of atoms α and β is tethered then $\phi\left(r^{\alpha\beta}\right)/kT \gg 1$, for $r > b + \varepsilon$; otherwise $\phi\left(r^{\alpha\beta}\right)/kT \ll 1$, for $r > b + \varepsilon$.

4. In the small intervals $a - \varepsilon < r < a + \varepsilon$ and $b - \varepsilon < r < b + \varepsilon$ between the above regimes, $\phi\left(r^{\alpha\beta}\right)/kT$ increases (or decreases) sharply. Nevertheless, we assume that along these intervals, $\phi(r)$ is interpolated in a smooth way.

After defining these properties of the potential $\phi(r)$, we substitute it in expressions (2.6) and (2.7) for the stress and elastic constants. We then look for what we call the "athermal limit" of these expressions, namely the limiting expressions obtained when we set the size of the interpolation interval, ε, to zero, while at the same time the potential difference between the regimes $r < a$ and $r > a$ tends to infinity. In the "athermal limit", $\phi(r)$ becomes a "hard" potential. The "athermal limit" of expressions (2.6) and (2.7) can be regarded as the fluctuation expressions of hard-spheres-and-tethers systems. The "athermal" limit of expression (2.6) for σ_{ij} is easily

derived.[2] In the derivation of the "athermal" limit of expression (2.7) for C_{ijkl} it is necessary to consider the sum of the terms appearing in expression (2.7) since some of the individual terms diverge. The combination of these terms does have a meaningful limit which does not depend on the exact form of the approximating potential $\phi(r)$.

2.2 The New Formalism

In this section we introduce the fluctuation expression for the elastic constants of hard-spheres-and-tethers systems. Since the mathematical derivation of the expression is rather lengthy, we will not present it here in detail. We leave the detailed mathematical formulation of the method to appendix A, while here we restrict ourselves to a short description of the major points in the derivation. We will introduce the expressions obtained for the stress and elastic constants and discuss shortly their "physical" meaning. A demonstration of the applicability of the method is found in the next section, where we present numerical results obtained for hard sphere systems.

Expression (2.6) for the stress tensor, σ_{ij}, suggests that the stress is the thermal-volume average of quantities related to the local forces applied to the atoms. For the present discussion, let us assume that we deal with a central force system in which the pair interactions are described by a certain approximating potential, $\phi(R)$ (see previous section). For such a potential we note that the force $f_{\alpha\beta} = -\phi'\left(R^{\alpha\beta}\right)$ acting between the pair of atoms $\langle\alpha\beta\rangle$ almost always vanishes, except for very short instances of time (in a statistical ensemble language — only in a small portion of the configurations phase space), when $R^{\alpha\beta} \sim a$, or (if the two atoms are tethered) $R^{\alpha\beta} \sim b$. Hard-spheres-and-tethers models can be regarded as limiting cases in which these pair-forces become infinitely large for time intervals which become vanishingly small, keeping the rate of momentum exchange between atoms fixed. From the mathematical point of view it is important to note that what we actually have in the integral expressions for σ_{ij} (2.6) are the derivatives of the Boltzmann factor, $\left[\exp\left(-\phi\left(R^{\alpha\beta}\right)/kT\right)\right]' = \left[-\phi'\left(R^{\alpha\beta}\right)/kT\right]\exp\left(-\phi\left(R^{\alpha\beta}\right)/kT\right)$. In the "athermal limit" the Boltzmann factor converges to a step function where the discontinuity (from zero to unity) occurs at $R^{\alpha\beta} = a$, and an opposite discontinuity (from unity to zero) occurs at $R^{\alpha\beta} = b$, if the pair $\langle\alpha\beta\rangle$ is tethered. The derivative of a step function is just the Dirac δ-function. We thus find that in order to recover the

---

[2]In fact, slightly different versions of the expression for the stress in systems with "hard" potentials were known prior to this work, and had been used in simulations of hard sphere systems. See, e.g., Runge and Chester [12], and Barker and Henderson [20].

"athermal limit" of σ_{ij}, we only need to perform the simple transformation

$$\phi'\left(R^{\alpha\beta}\right) \longrightarrow -kT\Delta^{\alpha\beta} \equiv -kT\left[\delta\left(R^{\alpha\beta} - a\right) - \nu^{\alpha\beta}\delta\left(R^{\alpha\beta} - b\right)\right], \qquad (2.8)$$

where $\nu^{\alpha\beta}$, the "topology variable", takes the value 1 if the pair $\langle\alpha\beta\rangle$ is tethered, and 0 otherwise. This gives the known result [12, 20]

$$\sigma_{ij} = -\frac{kT}{V}\left\{\sum_{\langle\alpha\beta\rangle}\left\langle\frac{R_i^{\alpha\beta}R_j^{\alpha\beta}}{R^{\alpha\beta}}\Delta^{\alpha\beta}\right\rangle + N\delta_{ij}\right\}, \qquad (2.9)$$

for the components of the stress tensor. Note that the thermal average of $\Delta^{\alpha\beta}$ is just the difference between the probability density of contact between the pair of spheres $\langle\alpha\beta\rangle$, $p\left(R^{\alpha\beta} = a+\right)$, and the probability density, $p\left(R^{\alpha\beta} = b-\right)$, of finding the tether connecting them stretched to its maximal length. If a tether between them does not exist ($\nu^{\alpha\beta} = 0$), we ignore this second probability density.[3]

The above transformation (2.8) is also useful in obtaining the "athermal limit" of many of the terms appearing in expression (2.7) for the components of the tensor of elastic constants. More specifically, it should be applied in all the terms which contain the first derivative, $\phi'\left(R^{\alpha\beta}\right)$, or the products, $\phi'\left(R^{\alpha\beta}\right)\phi'\left(R^{\gamma\delta}\right)$, corresponding to two distinct pair of atoms $\langle\alpha\beta\rangle \neq \langle\gamma\delta\rangle$. [This product should be simply replaced by $(kT)^2\Delta^{\alpha\beta}\Delta^{\gamma\delta}$.] This leaves us with only two types of terms, containing the squares of the first derivatives, $\phi'^2\left(R^{\alpha\beta}\right)$, and the second derivatives, $\phi''\left(R^{\alpha\beta}\right)$. Finding the "athermal limit" of both terms is the "missing piece in the puzzle" in the formulation of the method. When we substitute an approximating potential into these terms, it is not difficult to find that neither of them has a definite "athermal limit". Only if we combine them into a single term, we do manage to find an appropriate limit, which can be also expressed in terms of the quantities $\Delta^{\alpha\beta}$. A major part of the derivation, which appears in appendix A, is devoted to the mathematical treatment of this combined term. Here we just quote the final expression for the elastic constants:

$$
\begin{aligned}
C_{ijkl} &= \frac{2NkT}{V}\delta_{il}\delta_{jk} + \frac{kT}{V}\left\{(d+2)\sum_{\langle\alpha\beta\rangle}\left\langle\frac{R_i^{\alpha\beta}R_j^{\alpha\beta}R_k^{\alpha\beta}R_l^{\alpha\beta}}{\left(R^{\alpha\beta}\right)^3}\Delta^{\alpha\beta}\right\rangle\right. \\
&\quad - \frac{1}{2}\sum_{\langle\alpha\beta\rangle}\sum_{\gamma\neq\alpha,\beta}\left\langle\left[\frac{R_i^{\alpha\beta}R_j^{\alpha\beta}R_k^{\alpha\beta}R_l^{\alpha\beta}}{\left(R^{\alpha\beta}\right)^2}\Delta^{\alpha\beta}\left(\frac{\vec{R}^{\alpha\beta}\cdot\vec{R}^{\alpha\gamma}}{R^{\alpha\beta}R^{\alpha\gamma}}\Delta^{\alpha\gamma} + \frac{\vec{R}^{\alpha\beta}\cdot\vec{R}^{\gamma\beta}}{R^{\alpha\beta}R^{\gamma\beta}}\Delta^{\beta\gamma}\right)\right]\right\rangle \\
&\quad + \left.\left[\sum_{\langle\alpha\beta\rangle}\left\langle\frac{R_i^{\alpha\beta}R_j^{\alpha\beta}}{R^{\alpha\beta}}\Delta^{\alpha\beta}\right\rangle\right]\left[\sum_{\langle\alpha\beta\rangle}\left\langle\frac{R_k^{\alpha\beta}R_l^{\alpha\beta}}{R^{\alpha\beta}}\Delta^{\alpha\beta}\right\rangle\right]\right.
\end{aligned}
$$

---

[3]For the clarity of the discussion we assume that all pair interactions include the hard sphere part $[\phi_1(r)$, Eq.(1.3)]. In later chapters we will also consider systems without EV interactions. For such systems one should simply define $\Delta^{\alpha\beta} \equiv kT\nu^{\alpha\beta}\delta\left(R^{\alpha\beta} - b\right)$.

$$- \sum_{\langle \alpha\beta \rangle} \sum_{\langle \gamma\delta \rangle \neq \langle \alpha\beta \rangle} \left\langle \frac{R_i^{\alpha\beta} R_j^{\alpha\beta} R_k^{\gamma\delta} R_l^{\gamma\delta}}{R^{\alpha\beta} R^{\gamma\delta}} \Delta^{\alpha\beta} \Delta^{\gamma\delta} \right\rangle \Bigg\} . \tag{2.10}$$

In the above expression we distinguish between the different sums: $\sum_{\langle \alpha\beta \rangle}$ denotes summation over all pairs $\langle \alpha\beta \rangle$, $\sum_{\langle \gamma\delta \rangle \neq \langle \alpha\beta \rangle}$ denotes summation over the rest of the *pairs*, $\langle \gamma\delta \rangle$, while $\sum_{\gamma \neq \alpha,\beta}$ denotes summation over the rest of the *atoms*, γ (distinct from α and β). d is the dimensionality of the system.

Expressions (2.9) and (2.10) relate the stress and elastic constants of hard-spheres-and-tethers systems to the thermal averages of certain geometrical quantities. We see that except for the kinetic terms, originating in the change of the volume of the system caused by the deformation, contributions to the stress and elastic constants are due to pairs of atoms touching each other or due to bonds that are stretched to their maximal length. These are indeed the mechanisms through which tethered hard spheres exchange momentum with each other. Alternatively, expressions (2.9) and (2.10) can be understood as follows: In hard-spheres-and-tethers systems entropy measures the extent of configurations phase space. Changes in entropy (to which the stress and elastic constants correspond) are related to the exclusion and inclusion of configurations. When an unstrained configuration is infinitesimally transformed to its deformed correspondent, it may become physically forbidden (or vice versa, a physically forbidden configuration may become allowed), only when there exist at least one pair of spheres in contact or when one bond is in maximal stretching. The elastic properties of these systems must be, therefore, related to such events.

2.3 Numerical Example — Hard Spheres

2.3.1 The Phase Behavior of Hard Spheres

Hard sphere systems have been the subject of an intensive research for already several decades [21]. They were, in fact, the first systems for which Metropolis *et al.* performed the first MC simulations in 1953 [22]. Hard spheres serve as the simplest model for real fluids, glasses and colloids. Moreover, many perturbation theories use them as reference systems for more realistic models including attractive interactions (see earlier, section 1.2). The phase diagram of hard spheres, shown in Fig. 2.1, is a function of one parameter only — the volume fraction ρ occupied by the spheres. The most remarkable feature of this phase diagram is the occurrence of a first order phase transition from low density isotropic fluid to a high density crystal. The possibility that systems of particles interacting via repulsive potentials can undergo such an entropy-driven phase transition had been speculated upon by Kirckwood in 1939

[23]. This prediction was quite controversial at that time since entropy is usually associated with disorder. Indeed, the transition from isotropic fluid into a periodic solid involves loss of *orientational* entropy. However, this entropy loss is compensated by the gain of *transitional* entropy, i.e., the increase in the volume available to each sphere. The phase transition in hard sphere systems was first observed in 1957 through computer simulations performed by Alder and Wainwright [24] and Wood and Jacobson [25]. The volume fractions ρ_{freezing} and ρ_{melting} between which the fluid and crystal coexist were determined in 1968 by Hoover and co-workers [26]. They found $\rho_{\text{freezing}} = 0.494$ and $\rho_{\text{melting}} = 0.545$. The solid formed above ρ_{melting} can be further compressed up to the close-packing density $\rho_0 = \pi/(3\sqrt{2}) \simeq 0.74$ into either the face-centered cubic (FCC) or the hexagonal closed-packed crystalline arrangements. Recent numerical simulations indicated a preference for the FCC crystals, but the free energy differences between the two structures are extremely small, about $10^{-3}kT$ per particle [27, 28].
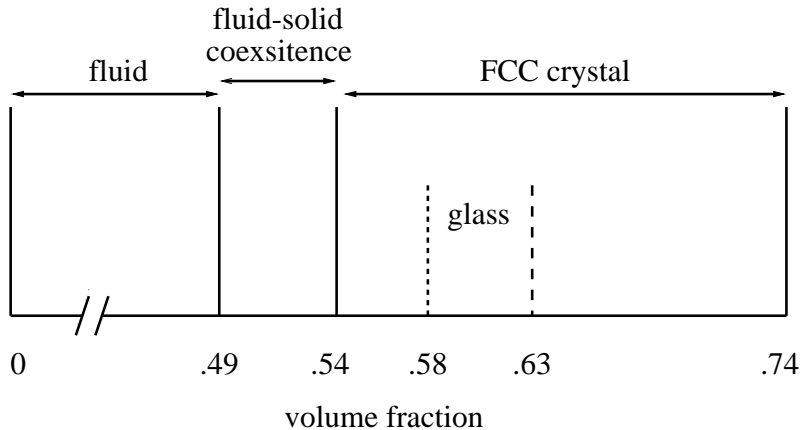
Figure 2.1: The equilibrium phase diagram of hard sphere systems. The "glass" phase is a metastable state which does not exist under microgravity conditions.

The experimental verification that hard sphere systems follow the above phase diagram was made by Pusey and van Megen [29] who studied sterically stabilized PMMA colloidal suspensions. In addition to the fluid-crystal transition, they reported the existence of a glassy metastable phase at volume fractions between $\rho \sim 0.58$ and $\rho \sim 0.63$ corresponding, respectively, to the random loose and random close packing densities. In the glass regime, the diffusion of spheres is limited by sedimentation. Chaikin and co-workers demonstrated that glassy samples crystallize under microgravity conditions [30].

2.3.2   Elasticity of Hard Spheres Systems

In the following section we present numerical results obtained by MC simulations using the new formalism for elastic constants. Several numerical [12, 13] and ana-

lytical [31] works were dedicated to *elasticity of* hard sphere systems. Nevertheless, the accuracy of the values of the elastic constants still leaves much to be desired. Therefore, although the main purpose of this section is to demonstrate the validity and applicability of the formalism, the numerical results have their own physical usefulness. Before we reach the results, I would like to turn the reader's attention to a problem arising due to the appearance of Dirac δ-functions in expressions (2.9) and (2.10). The delta function $\delta(R - a)$ cannot be averaged directly from MC configurations since the measure of the part of the configurations phase space at which $R = a$, vanish. Therefore, we approximate the delta function $\delta(R - a)$ by the distribution function

$$h_n(R) = \begin{cases} 1/\epsilon, & \text{for } a + (n-1)\epsilon \leq R < a + n\epsilon \\ 0, & \text{otherwise} \end{cases},$$

which makes the averages using the configurations where the pair separation R is found inside the small interval ("bin"), $a + (n - 1)\epsilon \leq R < a + n\epsilon$. We perform a set of such approximations with bins corresponding to $n = 1, 2, 3, \ldots$, and then extrapolate the set of "bin averages" to $n \to 0$ in order to obtain our estimates of the correct averages. This technique, which has been applied in the simulations, is discussed in more detailed in appendix B.

The simulations were performed on systems consisting of 13500 spheres with periodic boundary conditions. Subsequent MC configurations were *not* generated by conventional Metropolis single atom steps, but rather using collective steps of chains of atoms, as recently suggested by Jaster [32]. The MC time unit is defined as the time (measured in number of MC configurations) in which, on the average, we attempt to start one "chain move" from every particle. The acceptance probability of these moves was approximately half. The simulations were extended over $9 \cdot 10^5$ MC time units. This time is substantially larger than the relaxation time which was estimated from the auto-correlation function of the amplitude of the longest wavelength phonon in the system, and which for all densities [that ranged from the melting density ($\rho/\rho_0 = 0.736$) up to almost the close packing density ($\rho/\rho_0 = 0.99$)] was found to be less than 3000 MC time units. The relevant quantities were evaluated every 3 MC time units. The error estimates which appear in graphs presenting the results, represent one standard deviation in the estimates of the corresponding averages.

The FCC solid has a cubic symmetry, and therefore its elastic properties are described by the pressure P and three elastic constants C_{11}, C_{12}, C_{44} (see section 1.3). The results for P, the bulk modulus $\kappa = \frac{1}{3}(C_{11} + 2C_{12} + P)$, and for C_{12} and C_{44} of hard sphere FCC solids, are presented in Figs. 2.2–2.5, respectively (solid circles). Note that each of the elastic constants was estimated by the average
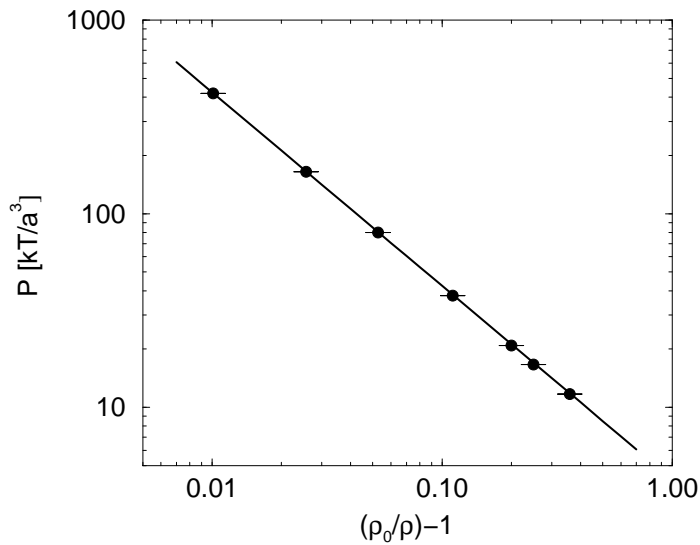
Figure 2.2: The pressure, P, in units of kT/a^3, as function of the inverse reduced density, ρ_0/ρ. The circles mark numerical results, while the solid line depicts the free volume approximation for the pressure [Eq.(2.11)].

of the corresponding three different components of the tensor C_{ijkl} [for instance, $C_{12} = \frac{1}{3}(C_{xxyy} + C_{yyzz} + C_{zzxx})$]. The solid curves in Figs. 2.2–2.5 depict expressions, suggested by Stillinger and Salsburg [33], for the *asymptotic* behavior of these quantities, at the limit of the close-packing density, ρ_0. These authors have shown that the free volume approximation gives the *correct* asymptotic results for the pressure and bulk modulus:

$$P = \frac{3\sqrt{2}}{\rho_0/\rho - 1} \frac{kT}{a^3},$$
(2.11)

and

$$\kappa = \frac{C_{11} + 2C_{12} + P}{3} = \frac{3\sqrt{2}}{(\rho_0/\rho - 1)^2} \frac{kT}{a^3}.$$
(2.12)

For the elastic constants C_{12} and C_{44}, it has been conjectured in Ref. [33] that close to ρ_0 their density dependencies have also a free volume functional form:

$$C_{12} = \frac{A_1}{(\rho_0/\rho - 1)^2} \frac{kT}{a^3},$$
(2.13)

and

$$C_{44} = \frac{A_2}{(\rho_0/\rho - 1)^2} \frac{kT}{a^3},$$
(2.14)

but with constants A_1 and A_2 which have not been accurately determined. Our numerical results confirm the validity of these asymptotic expressions. Most of the data points fall on the solid curves. This shows that the asymptotic expressions provide rather good estimates for the stress and elastic constants, even for densities
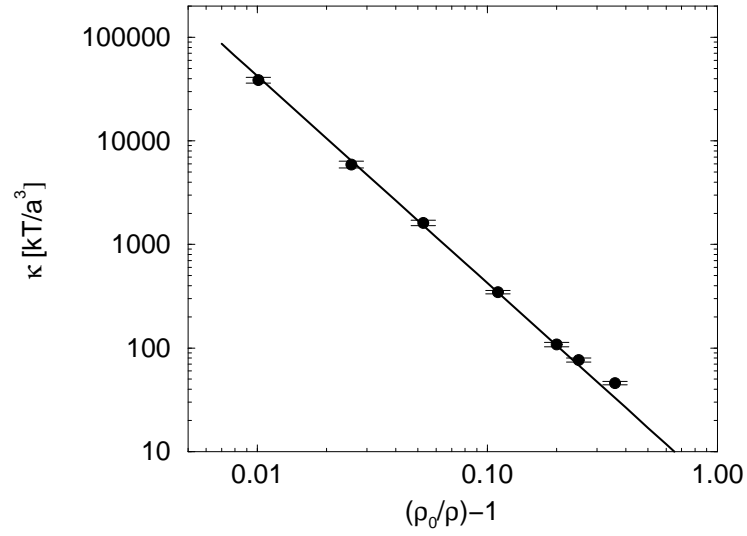
Figure 2.3: The bulk modulus, κ, in units of kT/a^3, as a function of the inverse reduced density, ρ_0/ρ. The circles mark numerical results, while the solid line depicts the free volume approximation for the bulk modulus [Eq.(2.12)].
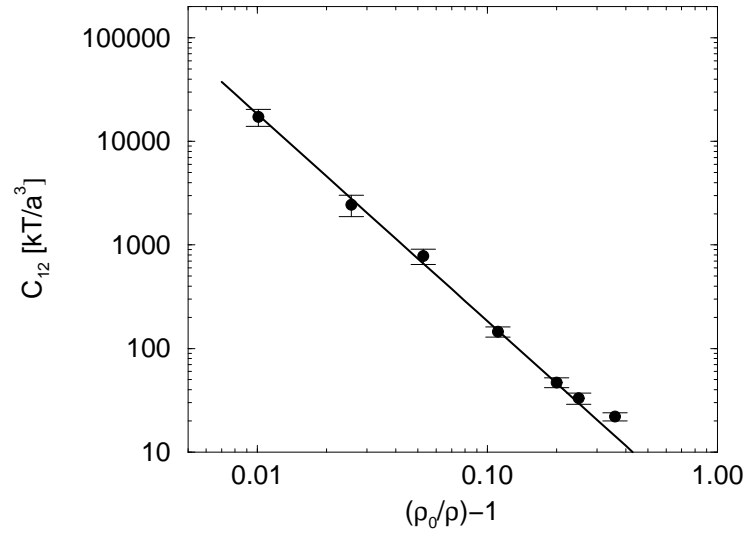
Figure 2.4: The elastic constant C_{12} in units of kT/a^3, as a function of the inverse reduced density, ρ_0/ρ. The circles mark numerical results, while the solid line depicts Eq.(2.13) with $A_1 = 1.84$.

which are close to the melting density. The curves in Figs. 2.4 and 2.5 correspond to expressions (2.13) and (2.14) with the coefficients $A_1 = 1.84 \pm 0.14$ and $A_2 = 5.86 \pm 0.11$. These values were obtained by fitting the numerical results for the four largest densities ($\rho/\rho_0 = 0.99$, 0.975, 0.95, 0.9) to expressions (2.13) and (2.14).
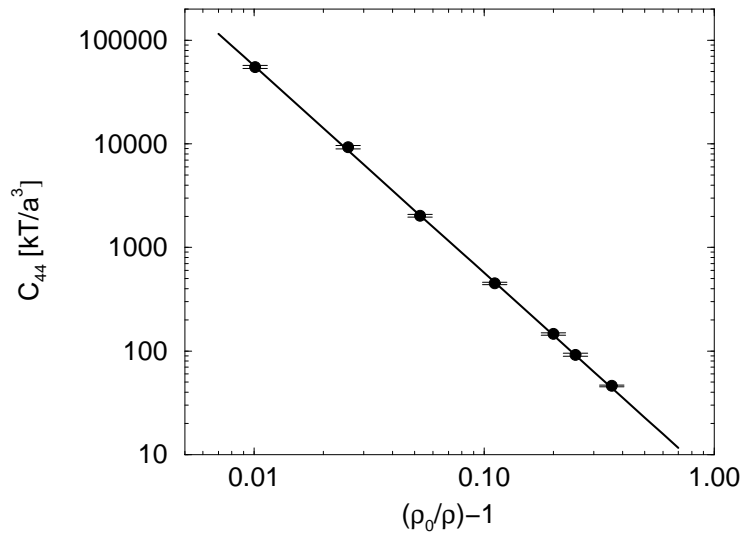
Figure 2.5: The elastic constant C_{44} in units of kT/a^3, as a function of the inverse reduced density, ρ_0/ρ. The circles mark numerical results, while the solid line depicts Eq.(2.14) with $A_2 = 5.86$.

The numerical results presented in Figs. 2.2–2.5 improve the existing numerical data published by Frenkel and Ladd [13]. They used the strain method technique (see section 1.4) and performed simulations on smaller systems of 108 spheres. At the smaller densities their results are in a very good agreement with the numerical results presented in this work. At a larger density $(\rho/\rho_0 = 0.9)$, however, there is a considerable disagreement, where our results seem to be more consistent with the asymptotic expressions of Stillinger and Salsburg. This inconsistency with the results in Ref. [13] is partially explained by finite size effects, but partially it is also due to the difficulties in using the strain method in systems at high pressure. In such systems, small deformations invoke relatively large pressure changes, and therefore in order to achieve a good estimate for the numerical derivatives one must use extremely small strains and measure the stress components with a very high accuracy. In our fluctuation method simulations this problem is not raised.

Finally, we present results obtained for hard sphere fluid systems (Fig. 2.6). In the fluid phase the system is isotropic, and therefore characterized by the pressure and two elastic moduli (section 1.3). The shear modulus vanishes, while the pressure and the bulk modulus can be accurately calculated from the virial expansion of the equation of state. (The curves appearing in Fig. 2.6 were derived using the first 7 terms of the virial expansion [34].) We measured the elastic moduli at 4 different volume fractions $\rho = 0.1$, 0.2, 0.3 and 0.4. The simulations were performed on systems of 8000 spheres over a total time of $1.35 \cdot 10^6$ MC time units. The rest of

the technical details are identical to these applied in the solid phase simulations (see text, earlier in this section). The good agreement of the numerical results with the analytical predictions is, again, evident.

2.4 Summary

The fluctuation formalism for calculations of the elastic constants, originally devised for conventional potentials, was extended to apply to "hard" potentials. We found expressions relating the components of the tensor of elastic constants to the (two-, three- and four-point) probability densities of contact between hard spheres and the probability densities of stretching tether bonds, which are the mechanisms through which atoms exchange momentum with each other in such systems. The new formalism is not restricted to certain topologies, but is general to all "hard-spheres-and-tethers" systems. In this chapter we applied it to hard sphere systems both in the fluid and the solid phases. The numerical results, which agree well with analytical predictions, demonstrate the efficiency and accuracy of the method. Implementing the method in numerical simulations is, generally speaking, quite straightforward. The only non-trivial point is the fact that Dirac δ-functions appear in the expressions for the stress and elastic constants. Therefore, the thermal averages in these expressions cannot be evaluated directly. The "bins" technique (discussed in details in appendix B) helps us to overcome this problem.
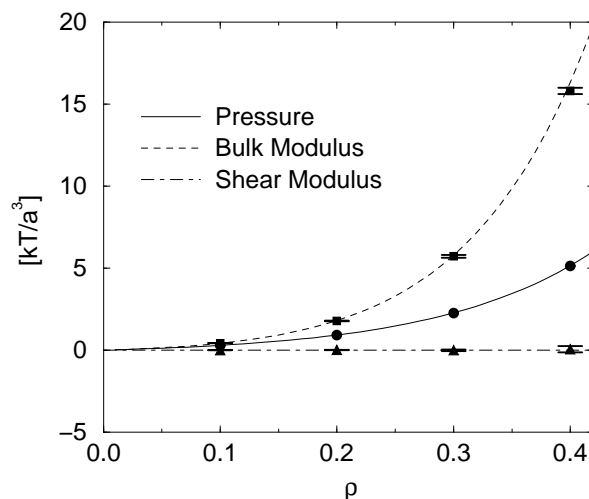
Figure 2.6: The pressure and two elastic moduli of a hard sphere system in the fluid phase as function of the volume fraction occupied by the spheres, ρ. The shear modulus vanishes at the fluid phase. Curves depicting the pressure and the bulk modulus were calculated using the first 7 terms of the virial expansion (see Ref. [34]). The circles, triangles and squares mark numerical results obtained for densities, $\rho = 0.1, 0.2, 0.3, 0.4$.

Chapter 3

Elasticity of Gaussian and Nearly Gaussian Phantom Networks

Rubber and *gels* are macroscopically large polymeric solid networks formed when polymers or monomers in fluid solutions are randomly cross-linked by permanent bonds. This process is called *vulcanization* or *gelation*, when the latter term usually applies to cross-linking of monomers or very short polymers — gels; while the former term usually describes the formation of dense networks of long polymers — rubber. Polymer networks are frequently used in daily life. Simple examples are car tires, thermosets, coatings, adhesives, plasticized PVC and gelatin puddings. Sophisticated applications include micro filtration, controlled drug delivery and plant growth control. Nature uses polymer networks, as well. The cytoskeleton, for instance, is supported by a network of actin, which is a semi-flexible polymer with globular proteins as monomer units.

The bonds forming a polymer network can be either chemical or physical. Chemical crosslinking is obtained by covalent bonds joining segments in already formed chains. Active linking agents (such as sulfur or peroxide cures) and ionizing irradiation are the most common methods to establish such bonds. Physical crosslinking, on the other hand, involves non-covalent interactions (e.g., Coulombic, van der Waals, hydrophobic and hydrogen bonds interactions) which lead to the association between certain parts of different chains. Physical crosslinkings are, in general, not permanent, and may disappear by applied mechanical deformations or increase in temperature. Therefore, physical gels are sometimes called *thermoreversible*. In the present work we do not consider physical networks, but only chemical ones in which the connectivity can be assumed to be fixed.

Clearly, the most remarkable feature of rubber and gels is the property of *high elasticity*, namely the ability to deform considerably on application of small external forces and, yet, to remain elastic (i.e, to recover the undeformed size and shape on release of external load) even in response to deformations increasing their dimensions

far beyond their original, unstrained, size. This elastic behavior is attributed to the network structure of these materials, and to the fact that the elastic restoring forces are of entropic, rather than energetic, origin. The simplest theory of *rubber elasticity* which captures these essential physical features, is the classical "phantom network" (PN) theory which was independently introduced in the 1940s by several authors [35, 36]. The PN model assumes that the configurations of the different polymer chains are independent of each other, and neglects the EV interactions between the monomers. With these simplifying assumptions one can treat each polymer chain in the network as an ideal one. By averaging over the positions of the monomers one finds that the probability density of finding chain ends separated by $\vec{r}$, takes a Gaussian form $\sim \exp\left[-\frac{1}{2}Br^2\right]$, where B usually depends on the temperature T. The free energy of the chain is proportional to (minus) the logarithm of this probability density and, therefore, proportional to r^2, as if it is a linear spring of vanishing equilibrium length, which will be called *Gaussian spring.* In the PN model, the thermal averages of some quantities can be calculated analytically due to the Gaussian form of the statistical weights [10], and this makes it an excellent starting point for more advanced models with EV interactions and entanglements [37].

The problem of *gel elasticity* introduces an additional complication already at the level of the PN model. In gels the network strands are very short and do not necessarily resemble Gaussian springs. Nevertheless, one may still construct a Gaussian model of gel elasticity, simply by replacing each bond of the gel by a Gaussian spring. In the absence of EV interactions, the validity of this model is justified by the fact that even if the elementary pair potential between bonded atoms is very different from that of a Gaussian spring, the *effective* interaction between somewhat more distant atoms is, almost always, quadratic. This is a well known feature of long polymer chains [38], which follows from the central limit theorem. For topologically simple 2D regular (non-random) nets, this property was demonstrated by Kantor *et al.* [2] (see more details in the next chapter of the thesis).

One of the more famous conjectures about the elastic behavior of Gaussian networks was made by de Gennes some years ago [39]. He used an analogy between elasticity of networks of Gaussian springs and conductivity of resistor networks and argued that rigidity, just like conductivity, appears at the connectivity threshold, when a macroscopically large network spans the system. He further argued that at the phase transition the shear modulus and the conductivity should have the same dependence on the distance of the system from the connectivity threshold. One of the aims of the present chapter is to prove this equivalence.

This chapter discusses the elastic properties of phantom networks of Gaussian and nearly Gaussian springs [40]. In section 3.1 we derive exact results for the stress

and elastic constants of Gaussian networks. We show that the stress *tensor* of a Gaussian elastic network is *equal* to the conductivity *tensor* of an equivalent resistor network. This equality, whose detailed proof is given in appendix C, quantifies the somewhat vague statement of de Gennes about an analogy between elasticity of Gaussian networks to conductivity of resistor networks. It is also shown that the elastic constants of a system consisting of a single spanning cluster of Gaussian springs *vanish*. We discuss the effect of the finite clusters which model the small molecules formed in the process of crosslinking and show that they play a crucial role in stabilizing the system. In section 3.2 we investigate the elastic behavior of phantom networks of nearly Gaussian springs, whose energy dependence on their extension includes a small quartic term additional to the quadratic one. A perturbative analysis yields an expression for the elastic constants of such networks. Section 3.3 includes a short summary and discussion of the main results.

3.1 Elasticity of Gaussian Networks — Exact Results

Consider a d-dimensional system shown schematically in Fig. 3.1. The black circles in Fig. 3.1 represent atoms while the zigzag lines indicate the bonds, attractive pair-potentials, which connect them in a certain fixed (quenched) topology. Atoms which are found inside the volume of the systems are called *internal* atoms. *Surface* atoms have fixed coordinates on the boundaries of the system. The bonds connect atoms into clusters. Clusters containing only internal atoms are *free* to move in the entire volume. Cluster with both internal and surface atoms are non-free. Among them, one (and, in some cases, several) may extend from one side of the system to the opposite side. This is the "spanning" cluster.

The system whose elastic properties are studied in this section consists of point-like atoms connected by Gaussian springs. The energy of each Gaussian spring is given by

$$\phi_{\alpha\beta}\left(\vec{R}^{\alpha} - \vec{R}^{\beta}\right) = \frac{1}{2}K^{\alpha\beta}\left(\vec{R}^{\alpha} - \vec{R}^{\beta}\right)^{2} = \frac{1}{2}K^{\alpha\beta}\left(R^{\alpha\beta}\right)^{2}, \qquad (3.1)$$

where $\vec{R}^{\alpha}$ and $\vec{R}^{\beta}$ denote the positions of atoms α and β, and $R^{\alpha\beta}$ is the distance between these atoms. The spring constant $K^{\alpha\beta}$ is assumed to have a fixed, *temperature-independent*, value.[1] The total elastic energy is given by the sum over

---

[1]It should be noted that usually the force constants in entropic systems strongly depend on T. The choice of temperature-independent force constants in this section is made for the purpose of convenience of the derivation of the mathematical theorems.
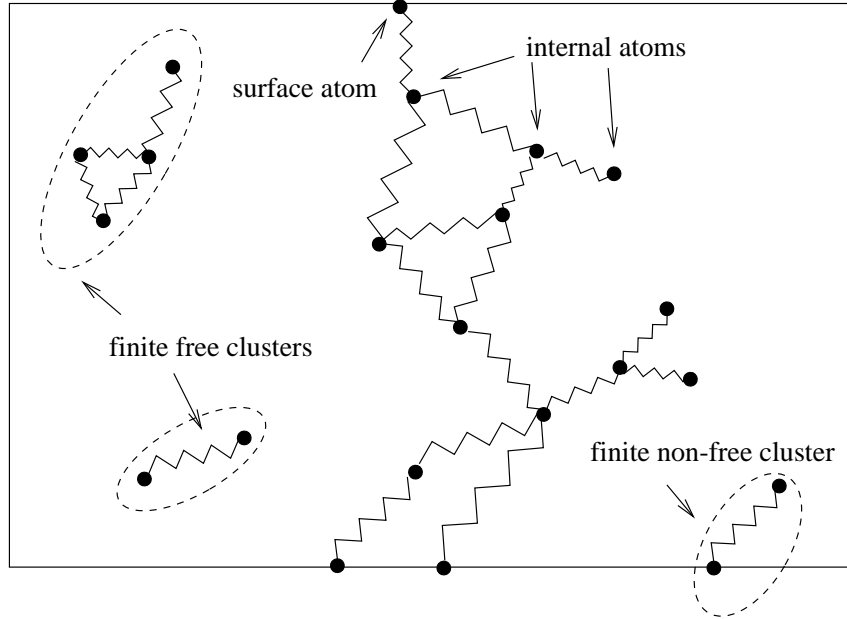
Figure 3.1: A schematic picture of a network of springs. The system includes a spanning elastic network as well as some finite clusters. Atoms can be either internal, i.e., free to move inside the volume, or external, i.e., attached to permanent positions on the boundaries. Non-free clusters have at least one external atom.

the energies of all the springs

$$E = \sum_{\langle \alpha\beta \rangle} \phi_{\alpha\beta} = \sum_{\langle \alpha\beta \rangle} \frac{1}{2} K^{\alpha\beta} \left(R^{\alpha\beta} \right)^2 .$$

The components of the stress tensor of our system are related to the pair-potentials, $\phi_{\alpha\beta}(R^{\alpha\beta})$, via expression (2.6) which in the case of potential (3.1) reduces to

$$\sigma_{ij} = \frac{1}{V} \left\langle \sum_{\langle \alpha\beta \rangle} K^{\alpha\beta} R_i^{\alpha\beta} R_j^{\alpha\beta} \right\rangle - \frac{NkT}{V} \delta_{ij}. \qquad (3.2)$$

In this expression the sum is performed over all the *connected* pair.

The two terms in the expression (3.2) are called the configurational and kinetic terms, respectively. The configurational term can be divided into terms, each one including the sum over the bonds of one distinct cluster. Since there are no EV interactions, these terms are independent of each other (the clusters do not interact with each other), and the contributions of the different clusters to the stress are additive. We identify the stress applied by each cluster as

$$\sigma_{ij}^{\text{cluster}} = \frac{1}{V} \left\langle \sum_{\langle \alpha\beta \rangle \,\in\, \text{cluster}} K^{\alpha\beta} R_i^{\alpha\beta} R_j^{\alpha\beta} \right\rangle - \frac{N_I kT}{V} \delta_{ij}, \qquad (3.3)$$

where N_I is the number of internal atoms of the cluster.

3.1.1   The Contribution of the Free Clusters

The gas of free clusters is an ideal gas. Since the different clusters do not "feel" each other, it is intuitively clear that the contribution to the stress of each free cluster should be as of a point-like atom. To prove this result (which is general to phantom systems and does not depend on the particular form of the pair-potential), we use the fact that for a free cluster (fc), one can integrate out d degrees of freedom (of say, $\vec{R}^1$) in Eq.(3.3), and express the terms appearing in it in the relative coordinates $R_i^{\alpha 1} = R_i^{\alpha} - R_i^1$ $\{\alpha = 2, \ldots, N_I\}$. (This statement is correct only in the thermodynamic limit, when the linear size of the system becomes much larger than the radius of gyration of the free cluster.) One can easily verify that in the relative coordinates Eq.(3.3) may also be written in the following way

$$\sigma_{ij} = \frac{1}{V} \left\langle \sum_{\alpha=2}^{N_I} R_i^{\alpha 1} \frac{\partial E}{\partial R_j^{\alpha 1}} \right\rangle - \frac{N_I kT}{V} \delta_{ij},$$

which from the equipartition theorem gives $\sigma_{ij} = -(kT/V)\delta_{ij}$. The stress applied by *all* the free clusters is simply

$$\sigma_{ij}^{\text{fc}} = -\frac{N_0 kT}{V} \delta_{ij}, \tag{3.4}$$

where N_0 is the total number of free clusters. Similarly, the contribution of the free clusters to the elastic constants is also as of an ideal gas, given by the kinetic term [16]

$$C_{ijkl}^{\text{fc}} = \frac{2N_0 kT}{V} \delta_{il}\delta_{jk}. \tag{3.5}$$

3.1.2   Elasticity of the Spanning Cluster

The stress and elastic constants of the spanning network of Gaussian springs with temperature-independent force constants, are temperature-independent. The free energy F of the spanning network is a function of the temperature T and the positions of the surface atoms $\{\vec{R}^s\}$. If the values of these variables change quasi-statically, then

$$dF = -SdT + \sum_s \vec{f}_{\text{ext}}^s \cdot d\vec{R}^s, \tag{3.6}$$

where S is the entropy, $\vec{f}_{\text{ext}}^s$ is the external force which drags the surface atom s, and summation is made over all the surface atoms. In a quasi-static process, the force $\vec{f}_{\text{ext}}^s$ is balanced by the force $\vec{f}^s$ applied by the network on atom s, namely

$$-\vec{f}_{\text{ext}}^s = \vec{f}^s = \left\langle \sum_{\alpha} K^{\alpha s} \left(\vec{R}^{\alpha} - \vec{R}^s \right) \right\rangle, \tag{3.7}$$

where summation is over all atoms α connected to atom s. The terms appearing in the thermal average in Eq.(3.7) are linear in the coordinates $\vec{R}^\alpha$. Since the Boltzmann weight is a Gaussian, i.e., an exponent of a quadratic form of the coordinates, these averages coincide with the most probable values, namely their values at the energetic ground state, and therefore do not depend on the temperature. We thus conclude that $\vec{f}^s$ is a temperature-independent quantity, and from Eqs.(3.6) and (3.7) we readily find that

$$\frac{\partial^2 F}{\partial T \partial \vec{R}^s} = -\frac{\partial \vec{f}^s}{\partial T} = 0.$$

The last result implies that F can be decomposed into two parts

$$F(T, \{\vec{R}^s\}) = F_1(T) + F_2(\{\vec{R}^s\}).$$

If we consider homogeneous deformations we may define a reference system and use the strain variables $\{\eta_{ij}\}$, instead of $\{\vec{R}^s\}$

$$F = F_1(T) + F_2(\{\eta_{ij}\}).$$

The stress and elastic constants are the coefficients in the $\{\eta\}$-expansion of F_2 [see Eq.(1.6)]. Therefore, they do not depend on the temperature.

  The stress applied by the spanning network is equal to the conductivity of a resistor network with the same topology. The stress of the spanning cluster (spc) [Eq.(3.3)]

$$\sigma_{ij}^{\mathrm{spc}} = \frac{1}{V} \left\langle \sum_{\langle \alpha\beta \rangle \, \in \, \mathrm{spc}} K^{\alpha\beta} R_i^{\alpha\beta} R_j^{\alpha\beta} \right\rangle - \frac{N_I kT}{V} \delta_{ij},$$

can be rewritten in the form

$$\sigma_{ij}^{\mathrm{spc}} = \frac{1}{V} \left\{ \left\langle \sum_{\alpha=1}^{N_I} R_i^\alpha \frac{\partial E}{\partial R_j^\alpha} \right\rangle + \left\langle \sum_{\langle \alpha s \rangle \, \in \, \mathrm{spc}} K^{\alpha s} R_i^s R_j^{s\alpha} \right\rangle \right\} - \frac{N_I kT}{V} \delta_{ij}, \qquad (3.8)$$

where the first sum is over all the internal atoms, while the second sum is over all the bonds connecting internal and surface atoms. (The subscripts s and α denote surface and internal atoms, respectively.) In the thermodynamic limit we deduce from the equipartition theorem that the first and the third (kinetic) terms in Eq.(3.8) cancel each other. We are thus left only with the second term

$$\sigma_{ij}^{\mathrm{spc}} = \frac{1}{V} \left[\sum_{\langle \alpha s \rangle \, \in \, \mathrm{spc}} K^{\alpha s} R_i^s \left\langle R_j^{s\alpha} \right\rangle \right]. \qquad (3.9)$$

The thermal averages in Eq.(3.9) are of quantities which are linear in the co-ordinates of the internal atoms and, therefore, may be replaced by the equilibrium values of these quantities (see earlier in this subsection). The equilibrium values of $\vec{R}^\alpha$ minimize the energy of the spanning cluster

$$
E^{\text{spc}} = \sum_{\langle\alpha\beta\rangle \,\in\, \text{spc}} \frac{1}{2} K^{\alpha\beta} \left(\vec{R}^\alpha - \vec{R}^\beta \right)^2 \;=\; \sum_{j=1}^{d} \left[\sum_{\langle\alpha\beta\rangle \,\in\, \text{spc}} \frac{1}{2} K^{\alpha\beta} \left(R_j^\alpha - R_j^\beta \right)^2 \right]
$$

$$
\equiv \; \sum_{j=1}^{d} E_j{}^{\text{spc}}. \tag{3.10}
$$

The dependence of E^{spc} on the components R_j^α corresponding to one Cartesian direction, j, is included in the term E_j^{spc}. The problem of finding the equilibrium values of $\vec{R}^\alpha$ decouples into d scalar problems of finding the equilibrium values of R_j^α. In order to calculate these values we need to solve d sets of linear equation (one set for each Cartesian component):

$$
\sum_\beta K^{\alpha\beta} \left(R_j^\alpha - R_j^\beta \right) = 0, \tag{3.11}
$$

corresponding to the vanishing of the jth component of the force acting on each internal atom. (For each atom α, summation in the relevant equation is over all atoms β connected to it.)

Let us define a resistor network with the same connectivity as the elastic network, in which each spring is replaced by a resistor with conductance $K^{\alpha\beta}$. The values of the electric potential at the internal nodes, $\{\varphi^\alpha\}$, are obtained by minimization of the heat power produced in the network, $\mathcal{P} = \sum_{\langle\alpha\beta\rangle} K^{\alpha\beta}(\varphi^\alpha - \varphi^\beta)^2$. Except for a prefactor of $\frac{1}{2}$, $\mathcal{P}$ is identical with $E_j{}^{\text{spc}}$ [Eq.(3.10)], where φ^α plays the role of R_j^α. If we replace R_j^α by φ^α in the force equations (3.11), we obtain the set of Kirchoff equations enforcing the vanishing of the sum of currents entering the internal nodes of the network. By replacing R_j^α by φ^α, we define a mapping of the mechanical problem to an electrostatic one. In fact, we have d different electrostatic problems corresponding to each Cartesian component of the mechanical problem. They differ from each other in their boundary conditions, namely the values of the electric potential on the surface nodes, $\{\varphi^s\}$. In the jth electrostatic problem, we set φ^s equal to R_j^s, i.e., we assume that the electric potential at each boundary point is equal to the jth Cartesian coordinate of the point.

The interesting question now is what is the analog of the stress tensor in the electrostatic problem. This appears to be the conductivity tensor Σ_{ij} defined by

$$
\langle j_i \rangle = \Sigma_{ij} \langle E_j \rangle,
$$

where $\langle \vec{j} \rangle$ and $\langle \vec{E} \rangle$ are the *volume averages* of the current density and the electric field, respectively. More precisely, if we follow the mapping defined above we have the *exact* equality

$$\sigma_{ij} = \Sigma_{ij}. \qquad (3.12)$$

A detailed proof of this equality is given in appendix C. Here we just note that the proof consists of two steps: The first step shows that in the jth electrostatic problem, because of the choice of boundary conditions, $\langle \vec{E} \rangle$ is a unity electric field pointing in the $(-j)$th direction. In the presence of such an electric field $\langle j_i \rangle = -\Sigma_{ij}$. The second step of the proof shows that $-\langle j_i \rangle$, and therefore Σ_{ij} are given by the electrostatic equivalent of Eq.(3.9)

$$\Sigma_{ij}^{\mathrm{spc}} = \frac{1}{V} \left[\sum_{\langle \alpha s \rangle \, \in \, \mathrm{spc}} K^{\alpha s} R_i^s \left(\varphi^s - \varphi^\alpha \right) \right], \qquad (3.13)$$

and therefore Eq.(3.12) is valid.

The elastic constants of the spanning network vanish. It has already been shown that C_{ijkl}, the elastic constants of the spanning cluster of Gaussian springs with temperature-independent force constants, are temperature-independent. Therefore, we may calculate them at any temperature, and in particular at $T = 0$. At zero temperature the free energy coincides with the internal energy, given by Eq.(3.10), where $\{ \vec{R}^\alpha \}$, the positions of the internal nodes, take their equilibrium values. Suppose now that the system is homogeneously strained. The positions of the surface nodes, $\{ \vec{R}^s \}$, change according to the linear transformation (2.3), with a constant matrix M_{ij}. In order to find the new equilibrium positions of the internal atoms, in the strained system, we need to solve the set of equation (3.11) with the new boundary conditions. Since both the equations and the transformation of the boundary conditions are linear, the new solution is given by $r_i^\alpha = M_{ij} R_j^\alpha$. The elastic energy of the strained spanning cluster is given by [see Eqs.(1.5) and (3.10)]

$$
\begin{aligned}
E^{\mathrm{spc}} = \frac{1}{2} \sum_{\langle \alpha \beta \rangle \, \in \, \mathrm{spc}} K^{\alpha \beta} (r^{\alpha \beta})^2 &= \frac{1}{2} \sum_{\langle \alpha \beta \rangle \, \in \, \mathrm{spc}} K^{\alpha \beta} \left[(M^t M)_{ij} R_i^{\alpha \beta} R_j^{\alpha \beta} \right] \\
&= \frac{1}{2} \sum_{\langle \alpha \beta \rangle \, \in \, \mathrm{spc}} K^{\alpha \beta} \left[(2 \eta_{ij} + \delta_{ij}) R_i^{\alpha \beta} R_j^{\alpha \beta} \right].
\end{aligned}
$$

This gives the dependence of E on the strain variables, which includes only linear terms in η_{ij}. Since the elastic constants are the coefficients of the quadratic terms in the $\{\eta\}$-expansion of the free energy [Eq.(1.6)], we conclude that

$$C_{ijkl}^{\mathrm{spc}} \equiv 0. \qquad (3.14)$$

3.1.3   The Stability of Systems of Gaussian springs

Stable solid thermodynamic systems have positive bulk and shear moduli, κ, μ_1 and μ_2 [Eqs.(1.9), (1.10) and (1.11)]. In phantom systems, the contributions of the spanning cluster and the ensemble of free clusters to κ, μ_1 and μ_2 are additive. Due to the vanishing of the elastic constants of the spanning cluster (3.14), we find that its contribution to the elastic moduli is: $\mu_1^{\mathrm{spc}} = \mu_2^{\mathrm{spc}} = -P^{\mathrm{spc}} > 0$,[2] and $\kappa^{\mathrm{spc}} = 0$ (two-dimensions) or $\kappa^{\mathrm{spc}} = P^{\mathrm{spc}}/3 < 0$ (three-dimensions) [$P^{\mathrm{spc}} < 0$ is the negative (stretching) pressure applied by the spanning cluster]. The fact that κ^{spc} is not positive means that the spanning cluster alone is not stable against homogeneous volume fluctuations. The contribution of the free clusters to the elastic moduli is as of an ideal gas, given by: $\mu_1^{\mathrm{fc}} = \mu_2^{\mathrm{fc}} = 0$, and $\kappa^{\mathrm{fc}} = N_0 kT/V$ [see Eqs.(1.9), (1.10), (1.11) , (3.4) and (3.5)]. The vanishing of the of the shear moduli μ_1^{fc} and μ_2^{fc} simply indicates that the collection of free clusters is a fluid. The positive contribution of the free clusters to the bulk modulus is crucial for the stability of the system. Two-dimensional Gaussian networks are stabilized in the presence of free clusters since $\kappa = \kappa^{\mathrm{spc}} + \kappa^{\mathrm{fc}} = \kappa^{\mathrm{fc}} > 0$. Three-dimensional systems are stabilized provided that the positive contribution of the free clusters to κ overcomes the negative contribution of the spanning cluster.

In real gels, it is possible to wash out the finite clusters (or most of them) and obtain a, so called, dry gel. Within the Gaussian model such a system is expected to be unstable. This contradicts experimental observations and demonstrates the importance of EV and entanglements effects. In the presence of EV interactions, the polymer chains forming the network cannot be treated as Gaussian springs. Therefore, the elastic constants of such networks do not vanish, and consequently, there is no simple relation between the pressure and the elastic moduli. Moreover, EV interactions make a positive contribution to the pressure which may, therefore, be both positive or negative. In dense systems, EV interactions may effectively cancel out [38]. However, dense systems can only be achieved in the presence of the finite clusters. In that case the different clusters interact with each other, and their contributions to the pressure and elastic moduli are not additive. In the following section we consider a different correction to the Gaussian model: without EV interactions, but with a non-Gaussian pair potential.

---

[2]Note the remarkable feature that $\mu_1 = \mu_2$ for *all* Gaussian networks, and not only for isotropic ones.

3.2 Elasticity of Nearly Gaussian Networks

The elastic response of phantom polymer chains and polymeric networks is as of systems of Gaussian springs only in the first approximation. It always includes a non-linear part, which becomes significant when the network is sufficiently stretched, much beyond its characteristic thermal length [36, 41]. In order to study the nature of this correction, we consider networks of springs having the spring energies

$$\phi_{\alpha\beta}\left(R^{\alpha\beta}\right) = \frac{1}{2}K^{\alpha\beta}\left(R^{\alpha\beta}\right)^2 + \frac{1}{4}a^{\alpha\beta}\left(R^{\alpha\beta}\right)^4. \tag{3.15}$$

Our choice for the spring energy is inspired by the free energy of a finite long polymer chain [36], where the leading correction to the linear relation between the force and the chain end-to-end vector $\vec{f} = -K\vec{R}$, is a term proportional to $R^2\vec{R}$. The elastic energy of the system is given, again, by the sum of all springs energies

$$E = \sum_{\langle\alpha\beta\rangle} \phi_{\alpha\beta} = \sum_{\langle\alpha\beta\rangle}\left[\frac{1}{2}K^{\alpha\beta}\left(R^{\alpha\beta}\right)^2 + \frac{1}{4}a^{\alpha\beta}\left(R^{\alpha\beta}\right)^4\right] \equiv E_0 + E_1. \tag{3.16}$$

In the following derivation we assume that $E_1 \ll E_0$, and treat the quartic term perturbatively. In fact, we will make a more restrictive assumption that for each bond $a^{\alpha\beta}\left(R^{\alpha\beta}\right)^4 \ll K^{\alpha\beta}\left(R^{\alpha\beta}\right)^2$. Since the quadratic term E_0 does not make any contribution to the elastic constants, we will focus on the contribution of the perturbation term, E_1, to them.

In the lowest order of a perturbation theory, the elastic constants of the network [defined by Eq.(3.16) with temperature-independent constants $K^{\alpha\beta}$ and $a^{\alpha\beta}$] are temperature independent. Substituting the pair potential (3.16) into expression (2.6) for the stress tensor, and expanding this expression to the first order in $a^{\alpha\beta}$, yields

$$\sigma_{ij} = \sigma_{ij}^0 + \frac{1}{V}\left\langle \sum_{\langle\alpha\beta\rangle} a^{\alpha\beta}\left(R^{\alpha\beta}\right)^2 R_i^{\alpha\beta}R_j^{\alpha\beta}\right\rangle_0$$
$$- \frac{1}{VkT}\left\langle \delta\left(\sum_{\langle\alpha\beta\rangle} K^{\alpha\beta}R_i^{\alpha\beta}R_j^{\alpha\beta}\right)\delta E_1\right\rangle_0, \tag{3.17}$$

where $\delta A \equiv A - \langle A\rangle_0$ denotes a thermal fluctuation of the quantity A, and $\langle\ \rangle_0$ denotes a thermal average with the (unperturbed) Gaussian Boltzmann weight $\exp(-E_0/kT)$. σ_{ij}^0 is the stress tensor of the corresponding Gaussian network (where $a^{\alpha\beta} \equiv 0$), given by Eq.(3.2), which can be also expressed by its value at $T = 0$

$$\sigma_{ij}^0 = \frac{1}{V}\sum_{\langle\alpha\beta\rangle}\left[K^{\alpha\beta}\left(R_0^{\alpha\beta}\right)_i\left(R_0^{\alpha\beta}\right)_j\right]. \tag{3.18}$$

In the above expression $\left(R_0^{\alpha\beta}\right)_i$ is the ith Cartesian component of the bond vector $\vec{R}_0^{\alpha\beta}$, defined as the pair separation $\vec{R}^{\alpha\beta}$ at the ground state of the unperturbed Gaussian network.

The next step is to substitute the pair potential (3.16) into the expression for the elastic constants [Eq.(2.7)]. By expanding this expression to the first order in $\{a^{\alpha\beta}\}$, and using the fact that for the Gaussian network $C_{ijkl} = 0$ [Eq.(3.14)], we find that

$$C_{ijkl} = \frac{2}{V}\left\langle \sum_{\langle\alpha\beta\rangle} a^{\alpha\beta} R_i^{\alpha\beta} R_j^{\alpha\beta} R_k^{\alpha\beta} R_l^{\alpha\beta} \right\rangle_0 + \langle X \rangle_0 ,$$

where X is a combination of terms, each of which includes the thermal fluctuations of some quantities. Since at $T = 0$ there are no thermal fluctuations, that term vanishes and we readily find that

$$\begin{aligned}
C_{ijkl}(T = 0) &= \frac{2}{V}\left\langle \sum_{\langle\alpha\beta\rangle} a^{\alpha\beta} R_i^{\alpha\beta} R_j^{\alpha\beta} R_k^{\alpha\beta} R_l^{\alpha\beta} \right\rangle_0 \\
&= \frac{2}{V} \sum_{\langle\alpha\beta\rangle} \left[a^{\alpha\beta} \left(R_0^{\alpha\beta}\right)_i \left(R_0^{\alpha\beta}\right)_j \left(R_0^{\alpha\beta}\right)_k \left(R_0^{\alpha\beta}\right)_l \right] .
\end{aligned} \quad (3.19)$$

The second equality in the above equation is obtained by equating the expression inside $\langle\ \rangle_0$ to its value at equilibrium (at zero temperature the thermal average coincides with this value).

At a finite temperature we may write the elastic constants as the product of $C_{ijkl}(T = 0)$, and a dimensionless function, which may depend only on terms of the form $(kT\, a^{\alpha\beta})/(K^{\gamma\delta} K^{\epsilon\zeta})$. Expanding the function into power series in these variables yields

$$C_{ijkl} = C_{ijkl}(T = 0) \left[1 + \left(\text{linear terms in } \left\{ \frac{kT\, a^{\alpha\beta}}{K^{\gamma\delta} K^{\epsilon\zeta}} \right\} \right) + \dots \right] .$$

Since $C_{ijkl}(T = 0)$ is a linear function in the quantities $a^{\alpha\beta}$, and since we are interested only in the first order correction due to the perturbation (namely, in terms linear in $a^{\alpha\beta}$), we conclude that to the lowest order in $a^{\alpha\beta}$, C_{ijkl} are temperature independent, and therefore given by the above expression (3.19).

3.3   Summary

In this chapter we investigated the elastic properties of phantom Gaussian and nearly Gaussian networks. For Gaussian networks, the stress and elastic constants were calculated exactly. A characteristic feature of Gaussian networks is the vanishing

of their elastic constants. This feature does not depend neither on the temperature nor on topology of the networks. Another interesting result was a proof for the equality between the stress tensor of a Gaussian elastic network and the conductivity tensor of a resistor network, in which the conductance of each resistor is equal to the corresponding spring constant $K^{\alpha\beta}$. This result quantifies de Gennes' statement about an analogy between elasticity of Gaussian networks and conductivity of resistor networks.

We have also investigated the non-linear correction to the elastic behavior, by studying the properties of networks of springs whose energies include small quartic terms, additional to the leading quadratic (Gaussian) terms. While the stress tensor is still dominated by the contribution of the quadratic term, the elastic constants (which vanish in the Gaussian case) are solely due to the non-Gaussian correction. The elastic constants of such networks were calculated to the first order in perturbation theory.

Chapter 4

The Fisherman's Net Model

The present chapter deals with the entropic elasticity of 2D tethered networks. Such networks have been investigated as models of polymerized membranes [42]. Membranes are commonly found in biological and physical systems. The human red blood cell is an example for a biological liquid bilayer membrane of amphiphillic molecules each with one or more hydrophobic hydrocarbon tails and a polar head group. This membrane also consists of a "spectrin network" which is attached to the inner layer through proteins. This protein network (which forms the skeleton of the red blood cell) is an example of a solid monolayer membrane. Solid membranes can also be synthesized by cross-polymerization of lipid bilayers [43]. Another group of relevant systems includes certain, thin, nanostructured C_6-symmetric sheets [44].

We consider a "toy model" called the *fisherman's net* (FN), consisting of a 2D solid triangular network of point-like atoms each of which is connected to six nearest neighbors by tethers of maximal length b [41]. The FN can be regarded as a 2D generalization of a phantom polymer chain of tethers. The elastic behavior of the latter is well understood [36]: When the chain is weakly stretched it behaves as a Gaussian spring and exhibits a linear relation between the force and the end-to-end distance. Corrections to the linear force-extension relation become notable when the end-to-end separation becomes an appreciable fraction of the fully extended chain's length. The present chapter reveals a similar behavior for 2D nets. Loose nets are Gaussian and have vanishing elastic constants. Highly stretched nets show deviation from Gaussian behavior. In the asymptotic limit of full extension, the elastic properties of the FN coincides with the properties of 2D hard sphere (hard disk) systems.

The chapter is organized in the following way: The model is presented and the details of the simulation are discussed in section 4.1. Sections 4.2 and 4.3 deal, respectively, with the behavior of highly stretched and weakly stretched nets. The main results are summarized in section 4.4.

4.1 Details of the Model and the Simulations

The FN model consists of a 2D network of point-like atoms, i.e., it is a phantom net without EV interactions. The topology of the net is such that the mean positions of the atoms form a regular triangular lattice with lattice spacing b_0, while each pair of nearest neighbor atoms is connected by a tether whose maximal extension is $b \geq b_0$. In the simulations we used nets consisting of 1600 atoms. Periodic boundary conditions, which fixed the volume and prevented the net from collapsing, were applied. Fig. 4.1 depicts typical equilibrium configurations corresponding to two different values of $\gamma \equiv b/b_0$, the ratio between the maximal and actual extensions of the net. The MC configurations were generated using the Jaster scheme [32] for collective steps of chains of atoms. 1600 move attempts (with acceptance probability ~ 0.7) were made at each MC time unit, where at each attempt a new atom was selected randomly. (On the average, each atom was chosen once in a MC time unit.) Correlations between subsequent configurations were estimated from the auto-correlation function of the amplitude of the longest-wavelength phonon in the systems (both longitudinal and transverse phonons were checked). For all γ values, it was found that after less than 1000 MC time units, the memory of the initial configuration is completely lost. The stress and elastic constants were measured [using expressions (2.9) and (2.10)] for many values of γ. For each γ, the relevant quantities were averaged over a set of $1.5 \cdot 10^7$ configurations separated from each other by 3 MC time units. The standard deviations of the averages were also evaluated. The error bars appearing in the graphs which present our numerical results correspond to one standard deviation.

The FN is six-fold symmetric when it is equally stretched along all the spatial directions. Its elastic properties in this reference state should be as of an isotropic system (see p.35, discussion on hexagonal systems, in Ref. [6]), namely characterized by the negative externally applied pressure P (stretching) needed in order to fix the size of the net (or, equivalently, by the positive stress $\sigma = -P$), and by two elastic moduli or elastic constants.[1] Some of the elastic properties of the system have been studied by Boal *et al.* [45]. (Some extensions of that work can be found in Ref. [46].) In Ref. [45] fixed pressure ensemble has been used, and the elastic moduli have been extracted from the fluctuations of the linear size of a rectangular cell. The simulations presented in this chapter applies to the fixed volume case, uses significantly larger systems and a wider range of stresses. Whenever comparison is possible, our results are in good agreement with Ref. [45].

---

[1] If the net is not confined in two dimensions but rather allowed to explore the third dimension, a third parameter describing bending rigidity comes into play.
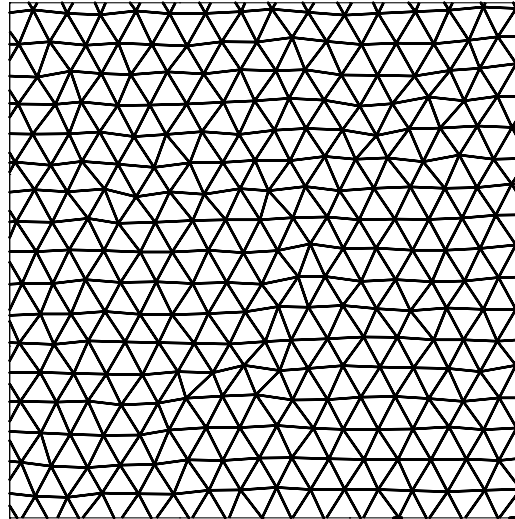
(a)
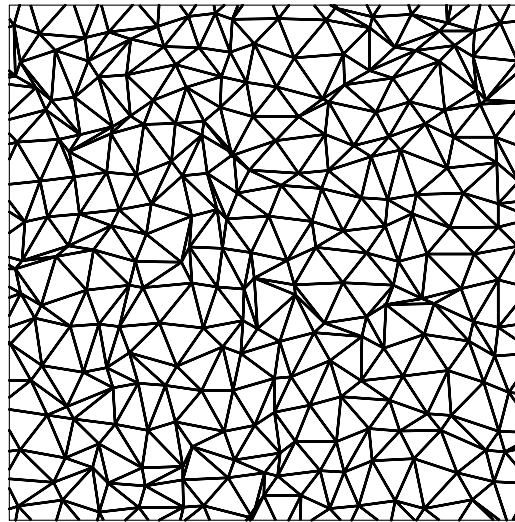
(b)

Figure 4.1: Configurations corresponding to different values of the ratio γ between the maximal and actual extensions of the net: (a) $\gamma = 1.1$, (b) $\gamma = 1.5$. Only part of the net is shown in the figures.

4.2   The FN Near Full-Extension

When the net is fully extended ($\gamma = 1$), atoms cannot leave their mean lattice positions. Entropy, therefore, vanishes, while the stress and elastic constants diverge. For slightly larger values of γ, atoms are restricted to small thermal fluctuations around their lattice positions, as in Fig. 4.1 (a).   A similar atomic-level picture appears in hard disk (HD) solids for densities proximal to the close-packing density. In fact, the FN and the HD solid problems are closely related: In the latter (HD) the centers of the disks are not allowed to approach their neighbors a distance smaller than a, the diameter of the disks, while in the former (FN) atoms are not allowed to depart from their neighbors a distance larger than the maximal extension of the

bond, b. For HD solids, one can define the ratio $\delta \equiv a/b_0 \leq 1$ between the diameter of the disks, a, and the mean lattice separation, b_0. In the limits $\gamma \to 1$ and $\delta \to 1$ (corresponding to the FN and HD problems, respectively), the elastic constants of both systems coincide, as can be seen from the following argument: Let Π_{FN} and Π_{HD} be phase spaces of allowed configurations of a FN with a certain value of γ and of a HD solid with $\delta = 1/\gamma$, respectively. Each configuration in one of these phase spaces can be described by the set $\{\mathbf{u}_i\}$ of deviations of either the atoms of the net or the centers of the disks from their mean lattice positions. In the $\gamma, \delta \sim 1$ asymptotic regimes, we can assume that the size of each one of the deviations is much smaller than the lattice spacing, b_0. One can easily check that if the set $\{\mathbf{u}_i\}$ represents an allowed microscopic configuration of the FN, then the set $\{-\mathbf{u}_i\}$ almost always corresponds to an allowed configuration of the HD system. Moreover, by this transformation we can generate almost all the configurations of Π_{HD}. The measure of the subgroup of configurations for which the mapping $\{\mathbf{u}_i\} \longleftrightarrow \{-\mathbf{u}_i\}$ between the two problems does not apply, diminishes proportionally to $\langle u_i{}^2 \rangle / b_0{}^2$. Thus, the mapping $\{\mathbf{u}_i\} \longleftrightarrow \{-\mathbf{u}_i\}$ is asymptotically a *one-to-one* transformation from Π_{FN} onto Π_{HD}. Since for both systems the Helmholtz free energy F is equal to $-kT \ln |\Pi|$, where $|\Pi|$ is the volume of the $2N$-dimensional configurations phase space (N is the number of atoms), and since the Jacobian of the above transformation is unity, we readily find that the free energies F_{HD} and F_{FN} of the HD and FN systems, respectively, are related by

$$F_{\mathrm{FN}}(N, \gamma) \simeq F_{\mathrm{HD}}(N, \delta = 1/\gamma), \qquad \text{for } \gamma \sim 1.$$

Suppose now that both systems are slightly deformed from their reference states. The displacements of the atoms from their original (undeformed) mean lattice positions can be divided into the set $\{\mathbf{u}_i\}$ of thermal fluctuations and the set $\{\mathbf{v}_i\}$ of small changes in mean lattice positions caused by the deformation. The transformation between Π_{FN} and Π_{HD}, in this case, maps both $\{\mathbf{u}_i\}$ to $\{-\mathbf{u}_i\}$ and $\{\mathbf{v}_i\}$ to $\{-\mathbf{v}_i\}$. The $\{\mathbf{v}_i\}$ mapping is equivalent to the reversal of the strain applied on the system. We, therefore, find that F_{HD} and F_{FN} will be equally modified, provided that opposite strains are applied on the FN and HD systems. The following asymptotic relations between the stress and elastic constants of these systems follow immediately: $\sigma_{\mathrm{FN}}(\gamma) \simeq P_{\mathrm{HD}}(1/\gamma)$, $\kappa_{\mathrm{FN}}(\gamma) \simeq \kappa_{\mathrm{HD}}(1/\gamma)$ and $C_{\mathrm{FN}44}(\gamma) \simeq C_{\mathrm{HD}44}(1/\gamma)$. These relations are very useful since the asymptotic expressions for P_{HD}, κ_{HD} and $C_{\mathrm{HD}44}$ are available [33], and can be used to find the stress and bulk modulus of the FN. This gives us the *exact* (asymptotic) expressions

$$\sigma_{\mathrm{FN}}(\gamma) \simeq \frac{4/\sqrt{3}}{(\gamma^2 - 1)} \frac{kT}{b_0^2}, \tag{4.1}$$

and

$$\kappa_{\mathrm{FN}}(\gamma) \simeq \frac{4/\sqrt{3}}{(\gamma^2 - 1)^2} \frac{kT}{b_0^2}. \tag{4.2}$$

For the elastic constant C_{44}, Ref. [33] finds only the asymptotic functional form, and therefore for our problem we have

$$C_{\mathrm{FN}44}(\gamma) \simeq \frac{A}{(\gamma^2 - 1)^2} \frac{kT}{b_0^2}, \tag{4.3}$$

with an unknown constant A. Our numerical results, presented in Fig. 4.2, confirm these relations, which seem to be accurate over quite a large range of γ values. In Eq. (4.3), the value $A = 1.80 \pm 0.02$ is used. It is obtained by fitting the asymptotic expression for C_{44} to the three data points corresponding to the smallest γ values. Note that while in Eqs. (4.1)–(4.3), P_{HD}, κ_{HD} and $C_{\mathrm{HD}44}$ are expressed in units of kT/b_0^2, in Fig. 4.2 they are given in units of kT/b^2. In this representation, the stress and elastic constants of the FN are scaled to depend on the parameter γ alone.
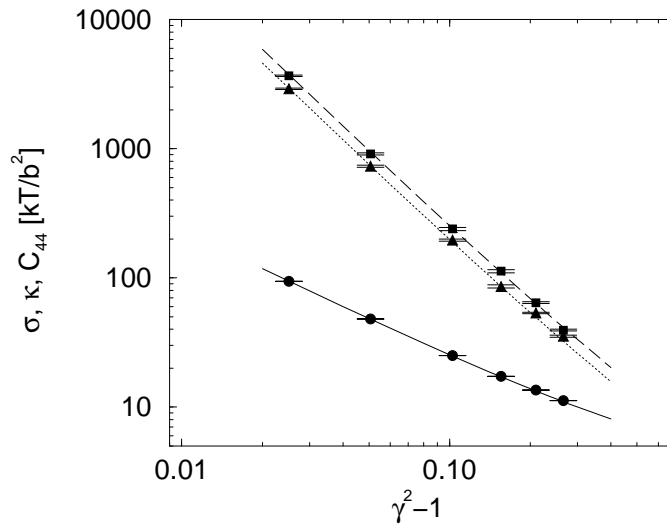
Figure 4.2: Numerical results for the stress σ (circles), the bulk modulus κ (squares), and the elastic constant C_{44} (triangles), as a function of the ratio γ between the maximal and actual extensions of the net. Results are in kT/b^2 units. The solid, dashed and dotted curves depict the expressions on the right sides of Eqs. (4.1)–(4.3), respectively [with $A = 1.80$ in Eq. (4.3)].

4.3   Weakly Stretched Fisherman's Nets

Fig. 4.3 shows the dependence of the stress and elastic constants on γ for weakly stretched nets. We observe a spectacular decay of elastic constants to almost zero

for $\gamma \sim 3$, and at the same time we note that the stress becomes independent of γ. The same result (for the critical value of γ and the γ-independent pressure) has been obtained in Ref. [45]. These observations indicate that a "loose" FN can be approximated by a network of Gaussian springs. The relation between the vanishing of the elastic constants and Gaussian elasticity has been discussed in detail in section 3.1.2. The decay of the stress to a γ-independent value (i.e., a value which does not depend on the extension of the net) can be also explained by the Gaussian model: The stress $\sigma = -P$ is opposite to the negative pressure needed to apply on the boundaries in order to balance the forces exerted by the net. In the case of a 2D Gaussian net, the lengths of the Gaussian springs forming the net and, consequently, also the network force pulling the boundaries inwards are proportional to length of the boundaries L. On the other hand, the external force created by the negative pressure is equal to $f = PL$. Since the force f should be also proportional to L, it follows that P must be independent of L. The size-independence of the stress is the reason for the vanishing of the bulk modulus κ of 2D Gaussian networks, and to the fact that such networks are not stable against homogeneous volume fluctuations (see section 3.1.3).
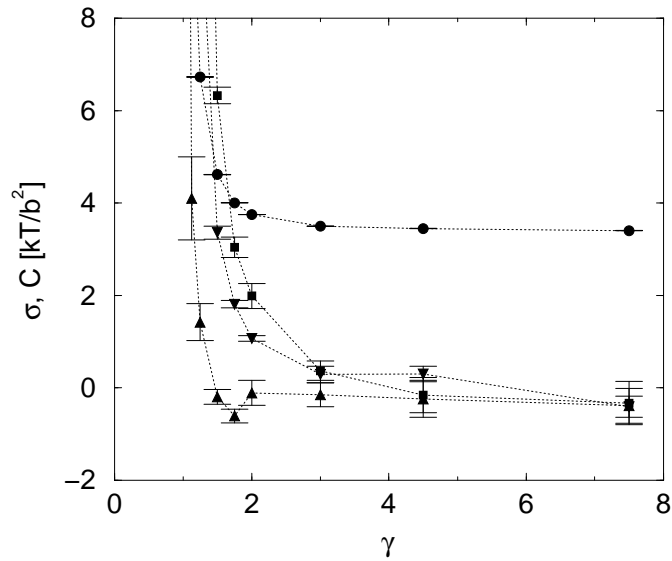
Figure 4.3: Numerical results for the stress σ (circles), and the elastic constants C_{11} (squares), C_{12} (triangles pointing up) and C_{44} (triangles pointing down), as a function of the ratio γ between the maximal and actual extensions of the net. Results are in kT/b^2 units. The lines are guides to the eye.

The similarity between *non-stressed* tethered and Gaussian one-dimensional (1D) nets, i.e., linear polymers, is a consequence of central limit theorem [10, 38]. For

topologically 2D regular (non-random) nets, such similarity was demonstrated by Kantor *et al.* [2]: In both tethered and Gaussian 2D nets, the mean squared distance in the embedding space, $r^2_{\mathbf{xx'}} = \langle|\mathbf{r}(\mathbf{x}) - \mathbf{r}(\mathbf{x'})|^2\rangle$, between two distant points whose internal positions in the net (measured in lattice constants) are $\mathbf{x}$ and $\mathbf{x'}$, grows proportionally to $\ln|\mathbf{x} - \mathbf{x'}|$. One can define the effective spring constant, K_{eff}, as the value of K of a Gaussian network with the same connectivity and statistical properties as of the tethered network. The value of K_{eff} is extracted from the ratio of the mean squared distance, $r^2_{\mathbf{xx'}}$, between two points $\mathbf{x}$ and $\mathbf{x'}$ on the FN, and the mean squared distance $\tilde{r}^2_{\mathbf{xx'}}$ between the same two points on a Gaussian network of unit spring constants:

$$K_{\text{eff}} = \tilde{r}^2_{\mathbf{xx'}}/r^2_{\mathbf{xx'}}. \tag{4.4}$$

$\tilde{r}^2_{\mathbf{xx'}}$ can be calculated exactly, while the value of the corresponding $r^2_{\mathbf{xx'}} = \langle|\mathbf{r}(\mathbf{x}) - \mathbf{r}(\mathbf{x'})|^2\rangle$ can be extracted from MC simulations of the FN with free boundaries conditions (i.e., in the absence of external pressure). We simulated a FN of $56^2 = 3136$ atoms and measured (using 10^7 different configurations) $r^2_{\mathbf{xx'}}$ for several pairs of points $\mathbf{x}$ and $\mathbf{x'}$ at different lattice separations. With these measurements we evaluated the effective spring constant [using Eq. (4.4)], and found, as shown in Fig. 4.4, that for the FN model $K_{\text{eff}} \simeq 1.96\ kT/b^2$. In order to support our conclusion about the crossover into the Gaussian regime, we need to show that the constant value to which the stress drops in Fig. 4.3, is just the stress applied by a Gaussian net with spring constants K_{eff} calculated for *non-stressed* FN. For a Gaussian net with $K \simeq 1.96$, one finds that $\sigma = \sqrt{3}K \sim 3.39\ kT/b^2$ which indeed coincides with the value of $3.4\ kT/b^2$, extracted from Fig. 4.3.

The persistence of the Gaussian regime to intermediate values of γ ($\gamma \sim 3$) is not unique for 2D nets, but is also found, for instance, in 1D polymers. For a polymer chain consisting of $N \gg 1$ tethers of maximal length b, the relation between the force f, stretching the chain, and the end-to-end separation $R = Nb_0 \equiv Nb/\gamma$ is [36]

$$\frac{R}{Nb} = \frac{1}{\gamma} = \left[\coth\left(\frac{fb}{kT}\right) - \left(\frac{kT}{fb}\right)\right] \equiv \mathcal{L}\left(\frac{fb}{kT}\right), \tag{4.5}$$

where $\mathcal{L}$ is the Langevin function. This relation is plotted in Fig. 4.5, together with the *approximate* linear force-extension relation

$$\frac{R}{Nb} = \frac{1}{\gamma} = \frac{fb}{3kT}. \tag{4.6}$$

The relative difference between the forces predicted by these two relations is about 7 percents for $\gamma = 3$, while for $\gamma > 10$ it becomes less than 1 percent. A simple argument explaining the accuracy of the linear relation (4.6) (which implies that the chain behaves as a Gaussian spring) for values $\gamma \gtrsim 3$ is the following: Gaussian
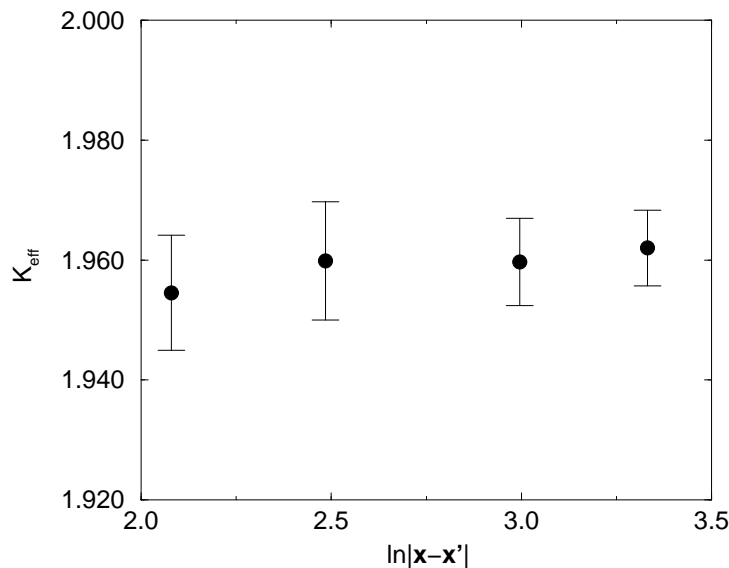
Figure 4.4: The effective spring constant K_{eff}, extracted from MC measurements of $r^2_{\mathbf{xx}'} = \langle|\mathbf{r}(\mathbf{x}) - \mathbf{r}(\mathbf{x}')|^2\rangle$ [see Eq. (4.4)]. The error bars correspond to one standard deviation in the estimated value of $r^2_{\mathbf{xx}'}$.

behavior is expected as long as the end-to-end separation $R = Nb_0$ does not exceed the order of magnitude of the root mean square size of the chain

$$l = Nb_0 \lesssim \sqrt{N}b. \tag{4.7}$$

However, the requirement that criterion (4.7) is satisfied by the whole chain is too restrictive. Criterion (4.7) should, in fact, be applied to small segments of the chain. If there exist a certain length scale at which the potential between the atoms becomes effectively quadratic, i.e., can be replaced by a Gaussian spring, then the whole chain is like a chain of Gaussian springs, and therefore it is itself Gaussian. For a linear polymer chain, the effective potential between non-neighboring atoms is calculated by integrating out the spatial degrees of freedom of the atoms located between them. Such calculations are usually done iteratively, where on each "rescaling" step every second atoms is integrated out. It appears that even elementary potentials which are very different from parabola, are brought into a quadratic form within a few "rescaling" steps. For the specific potential used in this work, three steps are sufficient, which means that a segment of $N \sim 10$ tethers may be justly considered as an effective Gaussian spring. Similarly to a macroscopically large chain, we expect that the Gaussian nature of this segment will persist as long as it is stretched to a length which does not exceed its root mean square size, namely, as long as $10b_0 \lesssim \sqrt{10}b$ [see criterion (4.7)]. This relation gives the lower limit, $\gamma = b/b_0 \gtrsim \sqrt{10} \sim 3$,
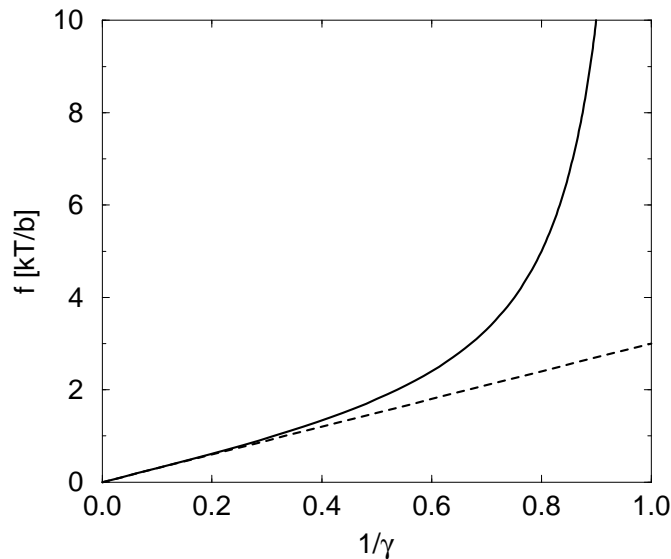
Figure 4.5: The force f (in kT/b units) stretching a 1D long polymer chain of tethers, as a function of γ, the ratio between the maximal and the actual extension of the chain. The solid line depicts the exact relation given by Eq. (4.5), while the dashed line shows the approximate linear force-extension relation (4.6).

of the Gaussian regime of a 1D chain of tethers. For a 2D regular phantom net, the effective potential becomes approximately quadratic also for a distance of number of bonds, $N \sim 10$ [2]. Root mean square distance between two such points is $b\sqrt{\ln N}$. Thus, in order to observe Gaussian elastic behavior, we require that $10 b_0 \lesssim b\sqrt{\ln 10}$, or, $\gamma = b/b_0 \gtrsim 10/\sqrt{\ln 10} \sim 4$, which is consistent with the value $\gamma \sim 3$, observed in Fig. 4.3.

4.4   Summary

In this chapter we have investigated the entropic elastic behavior of 2D tethered triangular networks. The Gaussian nature of entropic elasticity, observed for non-stressed phantom nets, was also found when stress was applied. It is expressed by the vanishing of the elastic constants and the size-independence of the stress. Corrections to Gaussian elasticity are observed when the net becomes very stretched. As the net approaches its fully extended size, the stress and elastic constants grow rapidly. In the asymptotic limit of maximal extension, the elastic constants of the nets can be related to the elastic constants of dense HD solids.

The correspondence between Gaussian and phantom networks is also a central issue of the next chapter, which deals with the critical elastic behavior of phantom percolating (bond-diluted) networks. One may expect that since percolating net-

works are much floppier than fisherman's nets, they would certainly exhibit a Gaussian elastic behavior. On the other hand, the elastic backbone of such networks is inhomogeneous and includes very tenuous parts where the tension applied on the network is distributed between very few stands. The presence of such strands may lead to deviations from Gaussian elasticity. Further complications with the Gaussian model arise from EV interactions which have not been discussed yet in relation to polymer networks. This will be the main subject of chapter 6.

Chapter 5

Elasticity of Phantom Percolation Networks

In the gelation process, monomers or short polymers in a fluid solution are randomly cross-linked. At a certain moment during the reaction, a macroscopically large network, *the gel*, spans the system. At this point, the system changes from a fluid-like (sol) to a solid-like (gel) phase which has a finite shear modulus. One of the models which has been proposed to describe the process of gelation is *percolation* [47]. In the percolation model, the sites or the bonds of a lattice are randomly occupied by, respectively, atoms or bonds, with an occupation probability p. In the site percolation model, one links every two neighboring occupied sites, while in the bond percolation model one assumes that all the sites are occupied by atoms and each pair of neighbors is linked if the bond between the atoms exists. Within the percolation model, the gel point is identified with the percolation threshold p_c, the critical site/bond concentration above which a spanning cluster is formed. The percolation model predicts that close to p_c, quantities like the mean cluster mass, typical cluster linear size, and gel fraction have power-law dependence on $(p - p_c)$. The relevant exponents are universal and depend only on the dimensionality of the system, but not on its atomic-scale features. The values of these exponents have been measured experimentally for various gel systems [48]. A fairly good agreement have been found between the measured exponents and their values as predicted by the percolation model, what proves the applicability of the percolation model to gelation.

Near the sol-gel transition typical polymer clusters are very large, tenuous and floppy. Elastic properties of such systems are primarily determined by the *entropy*, i.e., distortions of a sample barely modify its energy, but they decrease the available phase space (decrease entropy) and, thus, increase the free energy. Like geometrical quantities near p_c, the shear modulus is also expected to follow a power law: $\mu \sim (p - p_c)^f$. De Gennes [39] used an analogy between gel elasticity and conductiv-

ity of resistor networks, and conjectured that the exponent f should be equal to the exponent t describing the conductivity Σ of random resistor networks close to p_c: $\Sigma \sim (p - p_c)^t$. There is, however, a different approach based on scaling arguments which concludes that the elastic moduli of a gel are of the order of kT/ξ^d, where ξ is the percolation correlation length that diverges as $(p - p_c)^\nu$, and d is the dimensionality. Consequently, the relation $f = d\nu$ is obtained [49]. An exact calculation of the critical behavior of μ, which takes into account EV interactions and entanglements effects, is not yet available. Experimental measurements (which will be reviewed on the next chapter, in section 6.1), done on different polymeric systems, do not help to resolve the problem but rather give scattered results.

Numerical studies of elasticity at vanishing temperature T, showed that the *energetic* elastic behavior of percolation systems depends on the details of the interaction: For non-stressed central force networks the rigidity threshold occurs at a concentration of bonds much larger than p_c [50]. If bond bending forces are present, rigidity and percolation thresholds coincide; however the rigidity exponent f, is considerably larger than the conductivity exponent, t, suggesting that the two problems belong to different universality classes [51, 52]. As the number of models of elasticity of random systems increased, it became clear that de Gennes' conjecture about the identity of the rigidity exponent f to the conductivity exponent t can be justified only within models which "reduce" the thermodynamic behavior of gels to so called "scalar elasticity" models [53, 54, 55]. Recently, the equality $f = t$ was measured by Plischke *et al.* in a numerical study of *phantom* central force percolation networks at $T \neq 0$ [56]. The authors attributed this elastic behavior to the entropic part of the elastic free energy.

The present chapter deals with the entropic elasticity of phantom percolating networks [41, 57]. The critical behaviors, near p_c, of phantom Gaussian networks (PGNs) and phantom nearly Gaussian networks (PNGNs) are discussed in section 5.1. Numerical results describing the behavior of tethered phantom networks are presented in section 5.2. These numerical results show that the shear modulus behaves near p_c like the conductivity of random resistor networks as predicted by the PGN model, while the elastic stiffness tensor of the spanning cluster, which according to the PGN model is supposed to vanish, also exhibits a power law behavior near p_c with a significantly larger critical exponent. The last result is a consequence of the deviation from the Gaussian behavior, and can be understood within the PNGN model. A short summary of the chapter is included in section 5.3.

5.1   Gaussian and Nearly Gaussian Networks

In a phantom percolation system the contributions of the different clusters to the elastic properties of the system are additive. Each finite cluster, not connected to the boundaries of the system, contributes as a single atom of an ideal gas. Thus, N_0 free finite clusters confined within volume V at temperature T, produce stress equal to $\sigma = -P = -\frac{N_0 kT}{V}$, and elastic constants $C_{11} = \frac{2N_0 kT}{V}$, $C_{12} = 0$, and $C_{44} = \frac{N_0 kT}{V}$, where k is the Boltzmann constant (see section 3.1). Although both the elastic constants and the pressure P are affected by the presence of the finite clusters, we observe that the (ideal gas) contribution of the finite clusters cancels out in the definition of μ [Eqs.(1.10) and (1.11)]. Since the finite clusters play such an unremarkable role in the problem of elasticity, we will disregard them completely, and in the remainder of this chapter the stress, elastic constants and elastic moduli will refer to the contribution of the spanning cluster alone.

In the present section we apply the results from sections 3.1 and 3.2 to phantom percolation networks of identical springs having the energy $E = \frac{1}{2}KR^2$ (Gaussian network) or $E = \frac{1}{2}KR^2 + \frac{1}{4}aR^4$ (nearly Gaussian network). The critical elastic behavior of such networks is studied in a regime where the correlation length $\xi \sim (p - p_c)^{-\nu}$ is much larger than the characteristic atomic length scale b, but much smaller then the linear size of the system L. The correlation length is the length scale below which the spanning cluster has a fractal structure and above which the system is homogeneous. A quantity that follows a power law $\sim (p - p_c)^Y \sim \xi^{-(Y/\nu)}$ when $L \gg \xi$, scales as to $L^{-(Y/\nu)}$ when $\xi \gg L$. (At p_c the latter power law is always relevant because ξ is infinite.) Since $\xi \gg b$, we expect the structure of the spanning cluster to "forget" the details of the lattice on which its topology (connectivity) is defined, and have the elastic properties of an isotropic system. In the Gaussian case, the tensorial equality $\sigma_{ij} = \Sigma_{ij}$ (3.12) becomes a scalar equality $-P = \Sigma$. Also, because of the vanishing of the elastic constants of Gaussian networks [Eq.(3.14)], we have for the shear moduli of the spanning cluster that $\mu = \mu_1 = \mu_2 = -P = \Sigma$ [see Eqs.(1.10) and (1.11)]. Close to the percolation threshold, the conductivity scales as $\Sigma \sim (p - p_c)^t$, and therefore we conclude that for Gaussian networks

$$\mu = -P = \Sigma \sim (p - p_c)^t, \tag{5.1}$$

in accordance with de Gennes' argument. This result is not changed if we also include the finite clusters, since the latter make no contribution to the shear modulus (just as they do not contribute to the conductivity of the system). The equality of the shear modulus and the stress, a signature of Gaussian elasticity, was observed numerically in Ref. [56].

In the nearly Gaussian case, we have from Eq.(3.17) that the leading term in the expression for the stress is the Gaussian term, and therefore we expect the shear modulus to have the same scaling behavior as in Eq.(5.1). What distinguishes non-Gaussian networks from purely Gaussian ones is the non-vanishing elastic constants of the former. For percolation networks it is reasonable to assume that the elastic constants also follow a power law $C \sim (p - p_c)^g$. The elastic constants of a nearly Gaussian network should be "almost" zero, namely much smaller than the network stress. Therefore, the perturbative analysis in section 3.2 would be self-consistent only if it yields that the exponent $g > f$. We can use expression (3.19) for the elastic constants to derive bounds on the value of the exponent g. Consider a percolation network of linear size L in d dimensions at p_c. An upper bound on the exponent g is obtained by including only a partial set of the bonds of the spanning cluster in the sum in expression (3.19). We take the set of singly connected bonds (SCBs), which are such bonds that removal of each one of them disconnects the spanning cluster. Their number scales as $L^{1/\nu}$ [58]. The force acting on a SCB is the total force applied on the surface of the system, which is proportional to $PL^{(d-1)} \sim L^{(-t/\nu+d-1)}$. The length to which a SCB is stretched, $(R_{\text{SCB}})_0$, is proportional to the force, and therefore have the same scaling form

$$(R_{\text{SCB}})_0 \sim L^{(-t/\nu+d-1)}, \tag{5.2}$$

and consequently from Eq.(3.19) we get

$$C \sim L^{-g/\nu} \geq L^{-d} L^{1/\nu} L^{4(-t/\nu+d-1)},$$

which yields the upper bound $g \leq (4t - 1) - \nu(3d - 4)$. A lower bound for g is obtained by noting that for any bond other than the SCBs, $(R_{\text{bond}})_0 < (R_{\text{SCB}})_0$. That is because the SCBs are the only bonds which experience the total force acting on the system. We use this fact in expression (3.19) and write that

$$C \sim L^{-g/\nu} \leq [(R_{\text{SCB}})_0]^2 \left\{ \frac{1}{V} \sum_{\text{bonds}} a[(R_{\text{bond}})_0]^2 \right\}.$$

The term in braces in the above inequality is, however, proportional to the pressure [see Eq.(3.18)], which scales like $L^{-t/\nu}$. This, together with result (5.2), bring us to the lower bound $g \geq 3t - 2\nu(d - 1)$. Using the known values of the exponents $t \simeq 2.0$ [59] and $\nu \simeq 0.88$ [47] in three dimensions, we find that $2.48 \leq g \leq 2.6$ for 3D systems. In six dimensions both bounds coincide to give $g = 4$. This last result reflects the fact that in six dimensions essentially all the bonds which carry the force across the network are SCBs. In two dimensions we have $t \simeq 1.31$ [60] and $\nu = 4/3$ [47], and consequently $1.26 \leq g \leq 1.57$. However, we must mention a

special feature of the 2D case which questions the validity of the nearly Gaussian model. The model assumes that the contribution of the quartic term to the spring energy is small compared to the quadratic term [Eq.(3.15)]. This happens only if the bond length satisfies

$$R^{\alpha\beta} \ll \left(K^{\alpha\beta}/a^{\alpha\beta}\right)^{1/2}. \tag{5.3}$$

The longest bonds in the network are the bonds that *inside a cell of size* ξ^d serve as SCBs. Close to p_c, their length scales like

$$R \sim \xi^{-t/\nu+(d-1)} \sim (p - p_c)^{t-\nu(d-1)} \equiv (p - p_c)^y.$$

In two-dimensions the exponent $y < 0$, what implies that the length of the SCBs diverges, and certainly does not satisfy criterion (5.3). The problem is not limited to the SCBs only, but is relevant to a larger fraction of the bonds including the doubly-connected bonds, triply-connected bonds, and so on. It is difficult to predict, a priori, whether this observation should modify the results of the nearly Gaussian model from section 3.2. Note that we do not encounter such a problem for dimensionality larger than two, where the exponent y is positive.

5.2 Elasticity of Tethered Networks–Numerical Results

In this section we present numerical results describing the critical elastic behavior of phantom percolation networks consisting of tethers of maximal length b. The (quenched) topologies of the networks were generated by considering bond percolation problem on 2D triangular ($p_c = \frac{\pi}{9} \sim 0.349$) and 3D FCC ($p_c \simeq 0.12$) lattices, with a fraction p of bonds present. Each present bond was replaced by a tether, while each site became an "atom" without EV, and the system was allowed to move in *continuum*. Fig. 5.1 (a) depicts an initial 2D configuration of the system, which equilibrates into a configuration of the kind depicted in Fig. 5.1 (b). As expected, finite clusters and dangling ends of the spanning cluster contract relative to their linear sizes in the initial quenched construction [54]. The size of the backbone, on the other hand, is fixed by the boundary conditions, and therefore it looks like a collection of loops of the size of the percolation correlation length.

The non-interacting character of phantom networks significantly simplifies the numerical procedure: (1) Since the (trivial) contribution of the finite clusters is not interesting, they were removed from the simulations. (2) Dangling ends of the spanning cluster do not contribute neither to the stress nor to the elastic constants, and therefore they can also be removed. Thus, for every quench the backbone

(a)

(b)
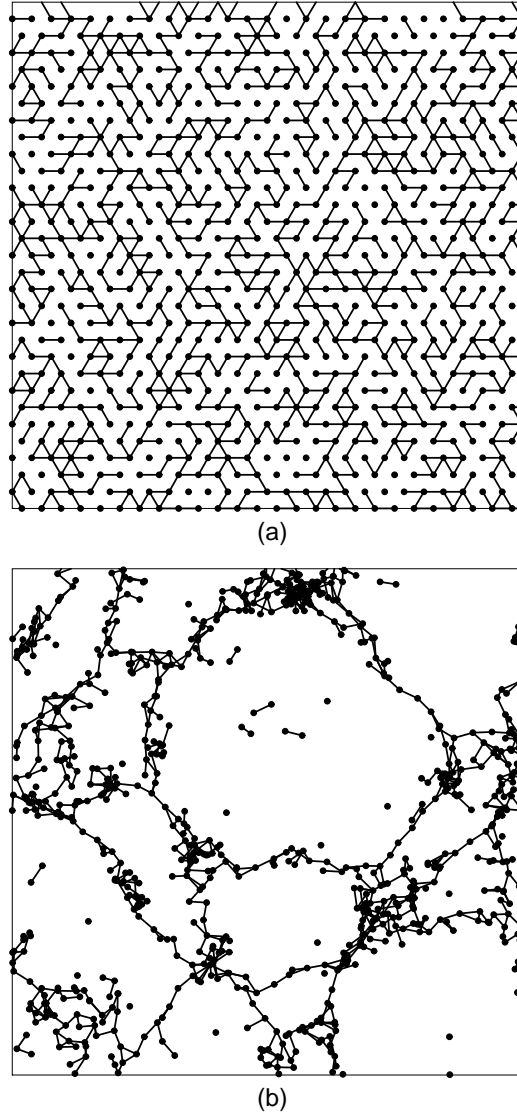
Figure 5.1: Part of initial (a) and equilibrated (b) configurations of the 2D system ($p = 0.405$, $b = 1.05$).

was identified (using the "burning" algorithm [61] which was slightly modified to deal with the periodic boundary conditions applied in our simulations), and its configurations phase space was explored using Jaster updating scheme [32]. At each MC time unit we made a number of move attempts (with acceptance probability ~ 0.5) equal to the number of atoms. In the 2D simulations, we used a 120×138 triangular lattice (that has an aspect ratio very close to 1) with nearest-neighbor spacing $b_0 \equiv 1$, and a number of quenched topologies that ranged from $N_t = 200$ for p closest to p_c, down to $N_t = 20$ far from p_c. In the 3D simulations we used systems of 24^3 cubic unit cells (each containing 4 atoms), i.e., of linear size $L = 24\sqrt{2}b_0$, with nearest-neighbor spacing $b_0 \equiv 1$, and $30 \leq N_t \leq 150$. The duration of the MC run of each individual sample was *at least* 50 times larger than the relaxation time

which we estimated from the expression

$$\tau = dkTL^2\tilde{\rho}/(\pi^2\mu s^2),\tag{5.4}$$

where s is the (average) distance an atom moves in one MC time unit, $\tilde{\rho}$ is the number density of atoms, and d is the dimensionality of the system.[1] The value of μ in this expression was taken, a posteriori, from the simulations. The stress and elastic constants were measured using expressions (2.9) and (2.10). The error estimates are affected by the fluctuations in the values of the measured quantities between the different quenches, and to lesser extent by the thermal uncertainties within each sample. The error bars appearing in the graphs correspond to one standard deviation of the averages.
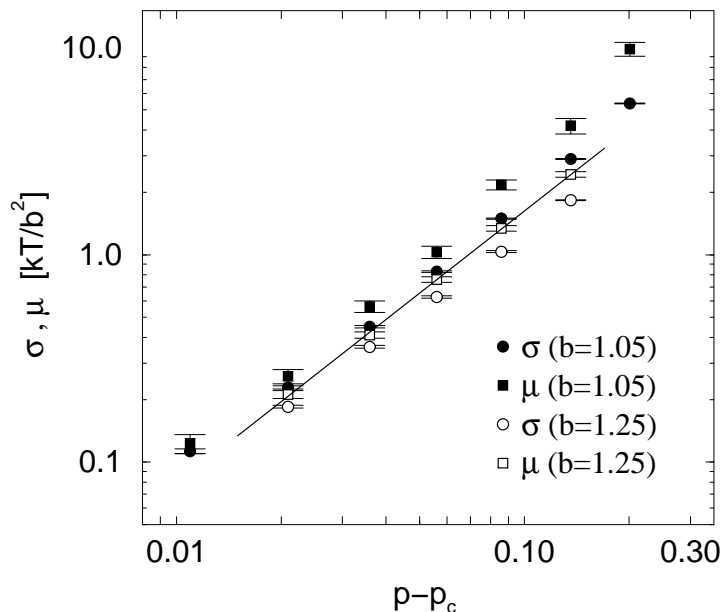
Figure 5.2: Logarithmic plot of the stress σ and the shear modulus μ as a function of $(p - p_c)$, for 2D systems. The slope of the solid line is 1.35. Results are in kT/b^2 units.

In phantom percolation systems we can vary only two non-trivial parameters: the bonds concentration p, and the maximal tether length b (measured in the units of the nearest-neighbor spacing b_0). Fig. 5.2 depicts the results for σ and μ as a function of $(p - p_c)$ for 2D systems with $b = 1.05$ and $b = 1.25$. It clearly demonstrates that close to p_c, the network becomes Gaussian: First, the difference between μ and σ decreases as we approach p_c, which implies that the elastic constant $C_{44} = \mu - \sigma$ vanishes faster than both quantities. Second, when plotted in kT/b^2 units, the values of σ and μ in systems with different b converge towards each other. This is explained by the facts that (1) the stress of a 2D PGN depends only on

---

[1]This expression is a generalization of Eq.(4.7) in Ref. [2].

the topology of the network and the value of the springs force constant K; and (2) for the tethered networks, the *effective* K is proportional to kT/b^2 (see chapter 4). Third, the value of f extracted from the the graphs is $f = 1.35 \pm 0.10$, very close to the value of the conductivity exponent $t \simeq 1.31$ in two dimensions [60]. Similar result for the exponent f has been obtained by Plischke *et al.* [56]. They used central force networks in which both entropy and energy contribute to the elastic properties and, by examining systems at several temperatures, removed the energetic component. Close to p_c the elasticity of central force systems is completely dominated by entropy, and their result for f reflects this fact.
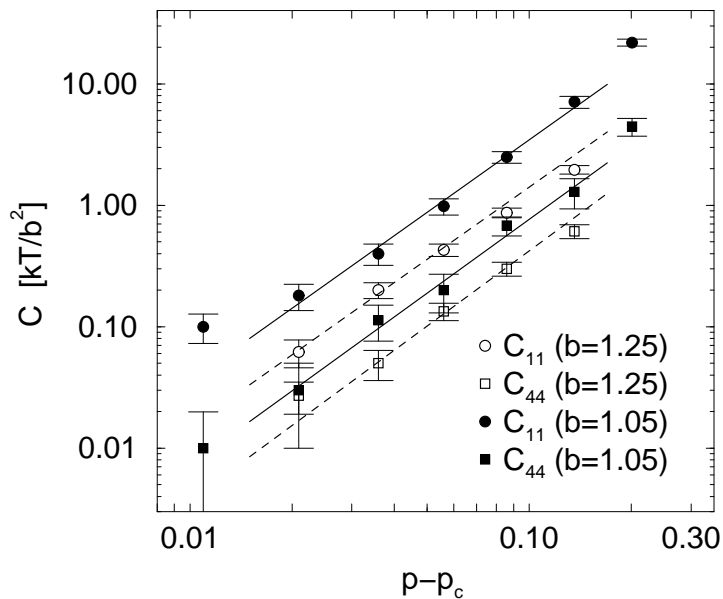
Figure 5.3: Logarithmic plot of the elastic constants C_{11} and C_{44} as a function of $(p - p_c)$, for 2D systems. The slope of the lines is ≈ 2. Results are in kT/b^2 units.

Fig. 5.3 depicts the results for the elastic constants C_{11} and C_{44}, which are supposed to vanish in the purely Gaussian case. Shorter tethers correspond to larger values of the elastic constants, since they represent more stretched networks, which exhibit stronger deviations from Gaussian behavior. Despite almost an order-of-magnitude difference between C_{11} and C_{44} for the same b, and half an order-of-magnitude difference between the same constants for the different values of b, all the results can be described by a power law $(p - p_c)^g$, with the same exponent $g = 2.0 \pm 0.2$, which is significantly larger than f. (We do not show the elastic constant C_{12}, which has large statistical uncertainties that prevent exact determination of the power law. Our results for this elastic constant are, however, consistent with the power laws for the other constants.) To further ascertain the universality of g, one would need to increase b to even larger values. This, however, would further decrease the values of the elastic constants and, simultaneously, increase the
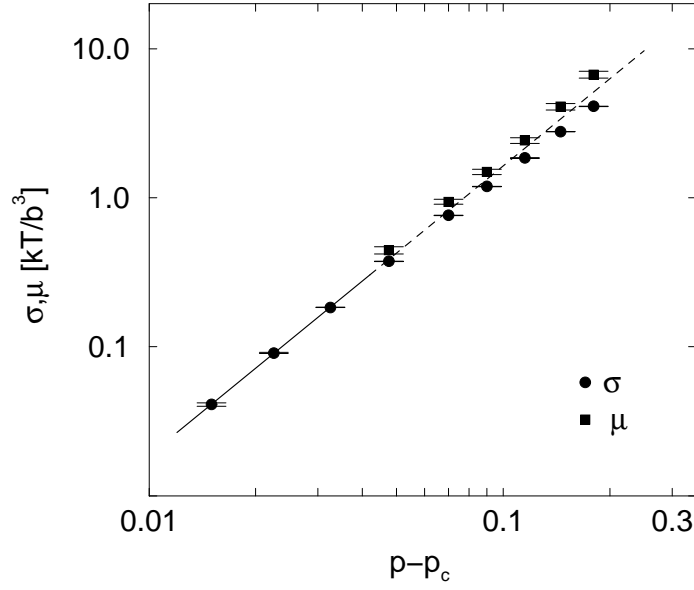
Figure 5.4: Logarithmic plot of the stress σ and the shear modulus μ as a function of $(p - p_c)$, for 3D systems with $b = 1.05$. The slope of the solid line is 1.95. Results are in kT/b^3 units.
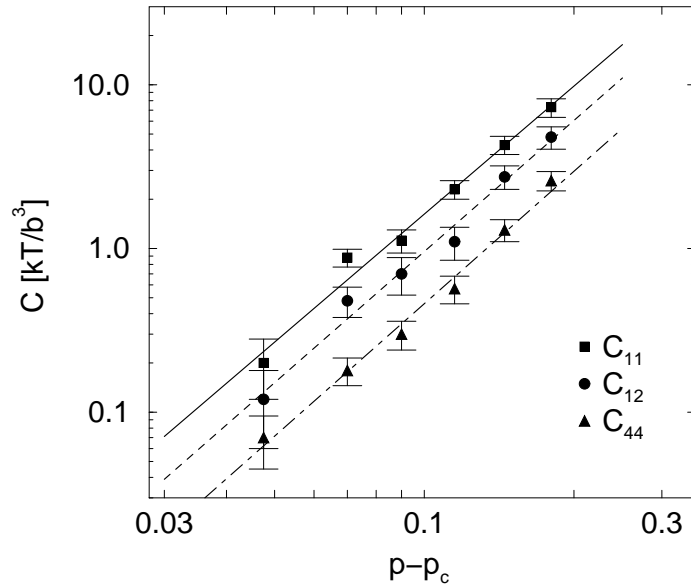
Figure 5.5: Logarithmic plot of the elastic constants C_{11}, C_{12}, and C_{44} as a function of $(p - p_c)$, for 3D systems with $b = 1.05$. The slope of different lines is ≈ 2.65. Results are in kT/b^3 units.

statistical uncertainties and require increase of the simulation length beyond our computational ability.

Our results for the 3D networks with $b = 1.05$ are shown in Figs. 5.4 and 5.5. Again, the validity of the PGN model is supported by the observation that σ and μ^2 converge towards each other as we approach p_c, following a power law with $f = 1.95 \pm 0.05$, which agrees with the conductivity exponent $t \simeq 2.0$ in three

---

[2] The shear modulus shown in Fig. 5.4 is $\mu_1 = C_{44} - P$.

dimensions [59]. The elastic constants also follow power laws with an exponent $g = 2.65 \pm 0.15$. This value is, within numerical uncertainty, consistent with the bounds $2.48 \leq g \leq 2.6$ derived for 3D nearly Gaussian networks (see section 5.1). One should keep in mind, however, that the PNGN model assumes that the coefficient of the quartic perturbation term to the Gaussian spring energy is a constant number, while for the tethered network model its effective value may depend on the mean stress and, thus, on the position of the bond in the network. Note that our numerical results for the elastic constants confirm relation (1.8), $C_{11} = C_{12} + 2C_{44}$, which indicates that close to p_c, percolating networks behave as isotropic systems. At $p = 1$ the system has a lower (cubic) symmetry, and there is a gradual deviation from relation (1.8) with increasing p beyond the regime shown in Fig. 5.5.

5.3 Summary

In this chapter we investigated the elastic behavior of phantom percolating networks close to the percolation threshold. The shear modulus of such systems follows the same power low, $\mu \sim (p - p_c)^t$, like the conductivity in random resistor networks. This result is due to the fact that percolating networks near p_c are very "floppy" so that on sufficiently large scales the pair potentials become effectively Gaussian. When the pair potential is not identical to that of a Gaussian spring, as in the nearly Gaussian or the tethered cases, one finds a power law dependence of the elastic constants $C \sim (p - p_c)^g$. This is an evidence for deviation from Gaussian elasticity. The critical behavior of the elastic constants is controlled by a critical exponent significantly larger than the exponent of conductivity. Since g characterizes a "sub-leading" behavior, a detailed study of a broad class of potentials is needed to verify its universality.

Chapter 6

Elasticity of Self-Avoiding Percolation Systems

The present chapter addresses the question of the critical elastic behavior of self-avoiding percolation systems [62, 63]. In the presence of EV interactions, the strands forming the network cannot, in principle, be treated as Gaussian springs. Hence, one cannot map this problem to conductivity of resistor networks and, in particular, cannot assume an equality between the critical exponents of both problems. Moreover, in self-avoiding systems the different clusters interact with each other. Therefore, the shear response cannot be related to the percolating cluster alone as in the phantom case. These features of the self-avoiding systems complicate the theoretical treatment of the entropic elasticity problem, and make it unsolvable to date.

Usually, one cannot neglect EV interactions without strongly modifying the physics of the system. For instance, the radius of gyration of non-stressed polymer networks is different for phantom and self-avoiding systems [2]. There are, however, some cases in which EV interactions are screened out, as in dense polymer melts [38]. The influence of EV interactions on the critical elastic behavior of gels has not been understood, yet. It has been suggested that they primarily influence the system by introducing osmotic pressure [55]. Thus, the true problem may be approximated by a mixture of phantom Gaussian network (PGN) and "pressure producing fluid". This reduces the self-avoiding system to *energetic* "scalar" elasticity problem [53, 54, 55], which is equivalent to PGN, and leads to the conclusion that the critical exponent of elasticity f is equal to the conductivity exponent t. However, as mentioned at the introduction of the previous chapter, a scaling approach to the problem leads to the conclusion that the elastic moduli of a gel behave as $(p - p_c)^{d\nu}$, where d is the dimensionality of the system and ν the correlation length exponent [49]. The experimental values of the exponent f, measured for different polymeric systems, are very scattered. Some experiments support the "scalar" elasticity model,

while others favor the prediction of the "scaling approach".

In this chapter we report the results of the first *direct* numerical measurement of the critical exponent f in entropy-dominated percolating systems with EV interactions. The simulations were performed for both 2D and 3D systems. In both cases, the numerically measured value of f was found to be similar to the corresponding value of the conductivity exponent, in agreement with the aforementioned qualitative theories which treat the system as a PGN with added pressure.

The chapter is organized in following way: Section 6.1 is devoted to a summary of the many experimental results for the critical exponent f. The numerical results for 2D and 3D percolating systems are presented in sections 6.2 and 6.3, respectively. In section 6.4, we summarize and discuss the results.

6.1 Experimental Results of the Critical Exponent

Table 6.1 summarizes various experimental results for the critical exponent f. In the first seven experiments presented in the table ([64]–[70]), the measured exponent is close to the conductivity exponent $t \simeq 2.0$ in three dimensions [59]. In the next four experiments ([71]–[74]) the exponent varies from 2.4 to 3.2, and seems to agree with $f = d\nu \simeq 2.7$. The gels formed by the materials in both groups of experiments are floppy, and the dominance of the entropic contribution to their elastic properties is fairly expected. Thus, the division of experimental works into these two groups is based on the values of the measured exponents rather than on the nature of the investigated materials. The origin of the discrepancy between the experimental results is not clear, and we can only list several possible reasons: In some cases the topology of the system does not correspond to the 3D percolation model of gels, but is somewhere between gel (cross-linking of monomers or short polymeric units) and rubber (cross-linking of a melt of long polymers).[1] Additional reasons are related to experimental difficulties, such as the imprecise determination of concentration of cross-links, or the difficulty to extract the static shear modulus from measurements of the low frequency behavior of the dynamic complex modulus.[2] A more fundamental reason for the wide range of experimental results is the energetic contribution to gel elasticity which mixes with the entropic contribution and influences the "effective"

---

[1] The classical theory of rubber elasticity (see Ref. [37]) gives a different set of critical exponents than the 3D percolation theory.

[2] In most of the experiments listed in Table 6.1, the rheological behavior of the system is studied. In rheological experiments, the measured quantity is the frequency-dependent complex modulus $G(\omega)$. The shear modulus μ is defined as the static ($\omega \to 0$) limit of the real part of G. For more details about these rheological experiments see, e.g., Refs. [67, 77].

Material	f	Ref.
Polyacrylamide + chromium III salt	1.9 ± 0.1	[64]
Gelatin	1.82 ± 0.15	[65]
Pectin (biopolymer)	1.93 ± 0.08	[66]
TEOS (Silica gel)	2.0 ± 0.1	[67]
PDMS	1.9 ± 0.15	[68]
Piezoelectric ceramics of PZT	2.2 ± 0.2	[69]
Gelatin	1.9 ± 0.1	[70]
Polyurethane gels	3.2 ± 0.5	[71]
TEOS (Silica gel)	2.4 ± 0.2	[72]
Polyester	3.0 ± 0.7	[73]
PVC/DOP gels	2.6 ± 0.1	[74]
Sintered silver powders	3.8 ± 0.5	[75]
Sintered copper powders	3.6 ± 0.5	[76]

Table 6.1: Various experimental results for the critical exponent f.

exponent. Energetic *bending elasticity* is characterized by a much larger exponent, $f \simeq 3.8$ [51, 52]. Such an exponent is measured only when the entropic contribution to elasticity is negligible, e.g, in the experiments in sintered metallic powders [75, 76]. When both energetic and entropic contributions coexist, we expect the elastic behavior near the gel point to be dominated by the latter, since the critical exponent of entropic elasticity (according to both approaches to entropic elasticity) is smaller than that of bending elasticity. However, the dominance of entropic elasticity near the transition may be limited to a very narrow regime, in which the shear modulus is small and difficult to measure.

In the following two sections we present numerical results describing the entropic elastic behavior of percolation systems consisting of spheres and tethers. Most of the difficulties encountered in experiments are avoided in the simulations: There

is no uncertainty about the correspondence between the topology of the system and percolation; the static shear modulus is measured directly, and the percolation threshold is known to a very high precision. The most important feature of the simulations is the fact that the elastic behavior of the system is purely entropic, and does not include any energetic contribution.

6.2   2D Systems

The topology of the network was defined by considering bond percolation problem of a triangular lattice ($p_c \simeq 0.349$), with a fraction p of bonds present. Each site of the lattice was replaced by a sphere of diameter a, while each present bond was replaced by a tether of maximal extension b, where the lattice spacing $b_0 \equiv 1$. Once the (quenched) topology was defined, the system was allowed to move in a *continuous* 2D space. Fig. 6.1 depicts a part of a typical equilibrium configuration. In our MC simulations we used a 52×60 site lattice (that has an aspect ratio very close to 1). Periodic boundary conditions were applied in order to fix the area of the systems. The MC configurations were generated using Jaster updating scheme [32]. We made a number of move attempts (with acceptance probability ~ 0.5) equal to the number of atoms at each MC time unit. The stress σ_{ij} and elastic constants C_{ijkl} were measured over a broad range of concentrations p above p_c. As p approached p_c, more quenches were needed to be studied because of the increasingly broader distribution of the values of μ between the different samples. For the system closest to p_c we used 40 quenches, while for the systems distant from p_c, 4 quenches sufficed. Close to p_c, the relaxation time becomes very large. We used expression (5.4) to estimate the relaxation time [where the value of μ in expression (5.4) was taken, a posteriori, from the simulations]. For each individual quench, the total duration of the MC run was *at least* 30 times larger than τ. The increase of the fluctuations in the value of μ, and the larger relaxation times close to p_c, affect the error estimates. The error bars appearing in the graphs correspond to one standard deviation of the average.

Fig. 6.2 depicts the pressure, bulk and shear modulus for a range of values of p for $a = 0.7$ and $b = 1.05$. The pressure and the bulk modulus do not vanish at p_c. The pressure decreases monotonically with p due to the increasingly larger negative contribution of the tethers to P. At $p \simeq 0.46$, the contribution of the tethers to the pressure overcomes the positive contribution of the hard spheres, and P becomes negative. The point of vanishing P depends on a and b. The bulk modulus does not change significantly near p_c, while at larger values of p it increases rapidly. The shear modulus becomes extremely small at p_c, signaling the sol-gel transition. (The
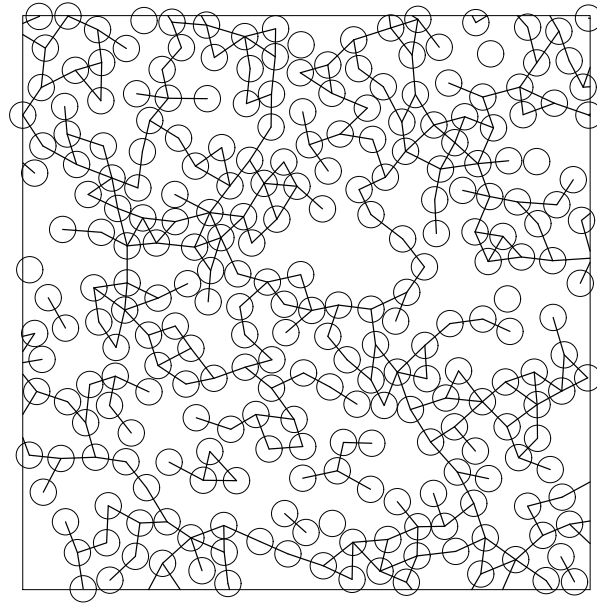
Figure 6.1: Equilibrium configuration of the system with $a = 0.7$, $b = 1.05$ and $p = 0.405$. Only part of the system is shown.
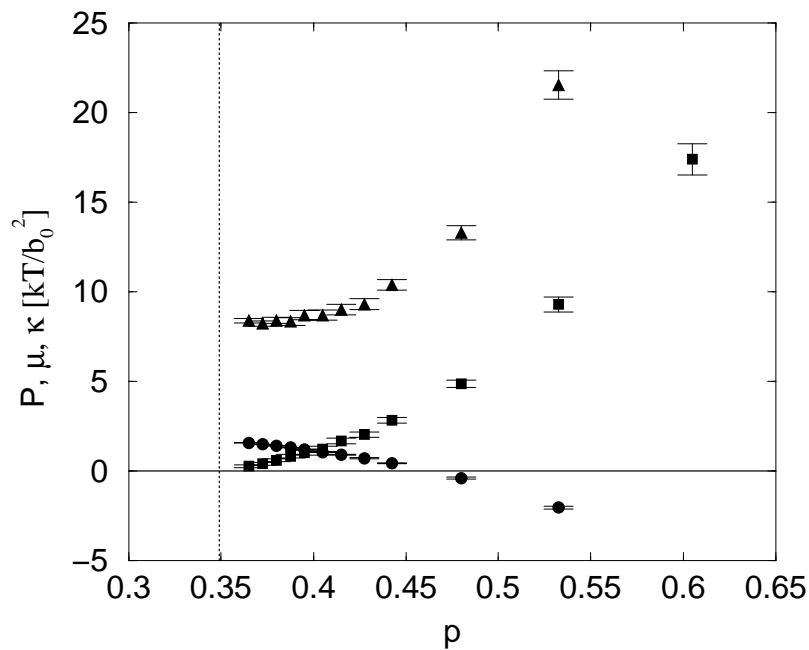
Figure 6.2: Pressure P (circles), shear modulus μ (squares) and bulk modulus κ (triangles), as a function of the bonds concentration p, for percolation networks with $a = 0.7$ and $b = 1.05$. Results are in kT/b_0 units. The vertical dotted line marks p_c.

elastic constants C_{ijkl} do not vanish near p_c.) In the presence of EV interactions it is not self evident that the transition from liquid (sol) to solid (gel) behavior appears at p_c. In the absence of tethers ($p = 0$), the behavior of the system depends on the diameter of the disks a, or rather the reduced density $\tilde{d} = \tilde{\rho}a^2$,[3] as indicated near

---

[3]Note that the definitions of the reduced densities in 2D hard disk systems ($\tilde{d}$) and in 3D hard sphere systems (ρ/ρ_0, see section 2.3.2) are slightly different.

the vertical axis of Fig. 6.3. The maximal possible packing is $\tilde{d} = 2/\sqrt{3} \simeq 1.15$. At slightly smaller densities the system is a 2D solid with quasi-long-range order. At $\tilde{d} \simeq 0.91$ the solid melts into a phase whose nature is controversial. Some numerical works [78] suggest that it is an hexatic phase with quasi-long-range orientational order, as predicted by the Kosterlitz–Thouless–Halperin–Nelson–Young (KTHNY) theory [79]. Other works [80] favor a fluid-solid coexisting phase (i.e., the usual first order transition), as proposed, for instance, by Chui [81]. At $\tilde{d} \simeq 0.89$, the system becomes a homogeneous liquid. For the purpose of our work, it is important to realize that close to $\tilde{d} \simeq 0.89$, corresponding to $a \simeq 0.88$, finite size effects make it difficult to distinguish between the phases, and therefore the largest a used in our simulations is $a = 0.85$, as indicated by the full circle in Fig. 6.3. (The open circle in Fig. 6.3 indicates the smaller density $\tilde{d} \simeq 0.57$, corresponding to $a = 0.7$, used in the simulations.) In the absence of EV interactions, the onset of rigidity is obviously at p_c. One might expect that the line separating the sol and the gel phases should move towards lower p with increasing a. However, within the accuracy of our simulations we were unable to distinguish between the rigidity threshold p_r and p_c. Thus, the sol and the gel are separated by essentially a vertical line depicted in Fig.6.3 at p_c.
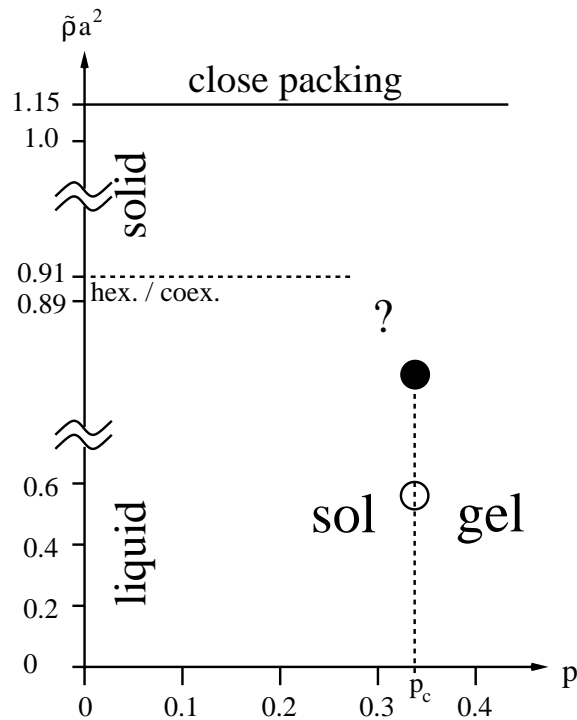
Figure 6.3: The phase diagram of the system. The horizontal and vertical axes represent the concentration of the tethers and the reduced density of the spheres, respectively.

Fig.6.4 depicts our results for μ as a function of $(p - p_c)$ for the two values of a. As expected, larger EV interactions correspond to larger values of shear modulus. However, both graphs exhibit similar power laws with $f = 1.3 \pm 0.1$ for $a = 0.7$, and

$f = 1.3 \pm 0.2$ for $a = 0.85$. This value of f is close to the value of the conductivity exponent $t \simeq 1.31$ in 2D [60], which is expected for phantom networks ($a = 0$) whose elastic behavior is Gaussian. It is, therefore, reasonable to conclude that f is independent of a over the entire range $a \leq 0.85$. Note that our result is inconsistent with an *indirect* estimate $f = 2.7 \pm 0.1$, which was obtained by Del Gado *et al.* [82]. Their simulations were performed on a discrete lattice, where the phase diagram differs from the one in Fig. 6.3, and used slightly correlated bond topologies.
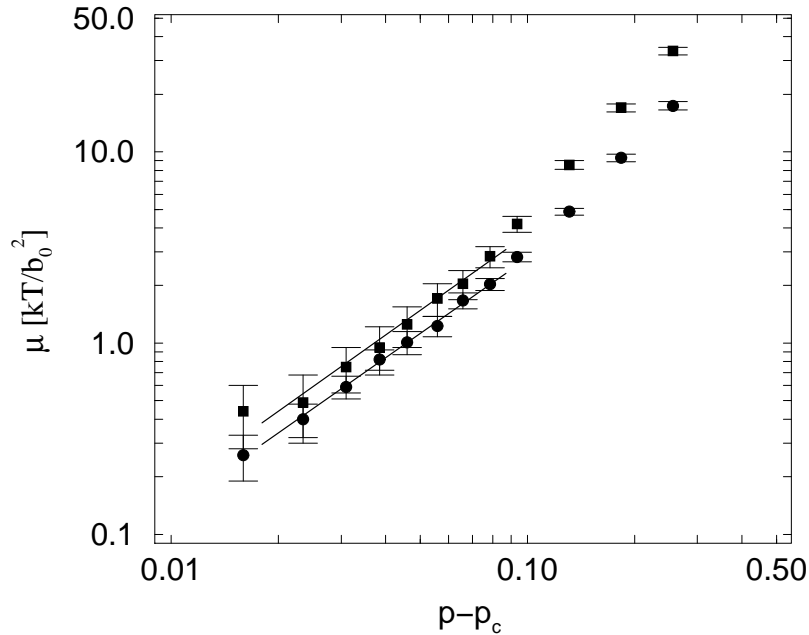
Figure 6.4: Logarithmic plot of the shear modulus μ as a function of $(p - p_c)$, for systems with $a = 0.7$ (circles) and $a = 0.85$ (squares). For both systems $b = 1.05$.

6.3   3D Systems

The topologies of the networks were defined by considering bond percolation problems on simple cubic (SC) and FCC lattices, with a fraction p of bonds present. Each site of the lattice was occupied by a sphere of diameter a, while each present bond was replaced by a tether of maximal extension b, which was larger than the nearest-neighbor distance b_0. Once the topology was defined, the systems were allowed to move in a continuous 3D space. For both types of topologies the volume fraction of the spheres was set to $\rho = 0.2$ (considerably below $\rho = 0.494$, the volume fraction at which hard sphere fluid begins to freeze, see section 2.3.1), and the ratio $b/a \sim 1.6$. The topologies of the SC and the FCC systems are quite different: In the latter the number of nearest-neighbor lattice sites is larger and, consequently, the percolation threshold is smaller: $p_c \simeq 0.12$ and $p_c \simeq 0.249$ for the FCC and

SC topologies, respectively. Thus, highly connected rigid regions are formed more rapidly (at lower p) in FCC networks. It has been suggested (see, e.g., Ref. [67]) that in real gels the creation of such rigid blobs tends to enhance the contribution of energetic bending elasticity and, thus, makes the entropy-dominated regime near p_c narrower. Therefore, it seems interesting to compare the SC and the FCC topologies in a purely entropic model. In the MC simulations we used box sizes $L = 18b_0$ and $L = 12\sqrt{2}b_0$ for the SC and FCC topologies, respectively, with periodic boundary conditions. Figure 6.5 depicts a typical equilibrium configuration of the FCC system. The stress σ_{ij} and elastic constants C_{ijkl} were measured over a broad range of concentrations above p_c. Strictly speaking, the rigidity threshold p_r is lower than the percolation threshold p_c due to effects of entanglements [83] (and, perhaps, also due to additional EV effects, see discussion in section 6.2). However, the two thresholds are so extremely close that they are practically indistinguishable in experiments and numerical studies. Therefore, we treat p_r and p_c as identical. The number of quenched topologies and the length of the MC run of each individual topology increased near the percolation threshold. For systems close to p_c, the relevant quantities were averaged over 10 different topologies, while far from p_c, only 2–3 quenches were needed. Close to p_c the duration of the MC runs is about 500 times larger than the relaxation time τ of the simulations [see the approximate expression (5.4) for τ in section 5.2]. During each MC run the systems were sampled several million times.

The systems whose elastic properties are discussed in this section posses a cubic symmetry since their topologies are defined on cubic lattices. Therefore, their elastic behavior is described by two distinct shear moduli rather than one, as in isotropic systems (see section 1.3). This property does not exist in experiments where the networks are isotropic because of randomness. Figure 6.6 depicts the two shear moduli, μ_1 and μ_2, as a function of $(p - p_c)$ for the SC and FCC systems. For each type of connectivity, its own p_c is used. The error bars appearing in Figs. 6.6 and 6.7 correspond to one standard deviation of the averaged quantities. For both systems close to p_c, μ_1 and μ_2 are practically indistinguishable, suggesting that the systems become isotropic. The shear moduli can be approximated by the power laws $\mu_1 \simeq \mu_2 \sim (p - p_c)^f$ with $f = 2.0 \pm 0.1$ for the SC system, and $f = 2.1 \pm 0.1$ for the FCC system. Within numerical uncertainty both values are similar and consistent with the conductivity exponent in 3D, $t \simeq 2.0$ [59]. In the previous section we saw that $f \simeq t \simeq 1.3$ in two dimensions, and therefore it is expected that $f \simeq t$ at any dimension. For phantom percolation networks we have $f = t$, due to the Gaussian nature of the elastic response (see chapter 5). Our results in this chapter indicate that a similar picture may also apply to systems with EV interactions.
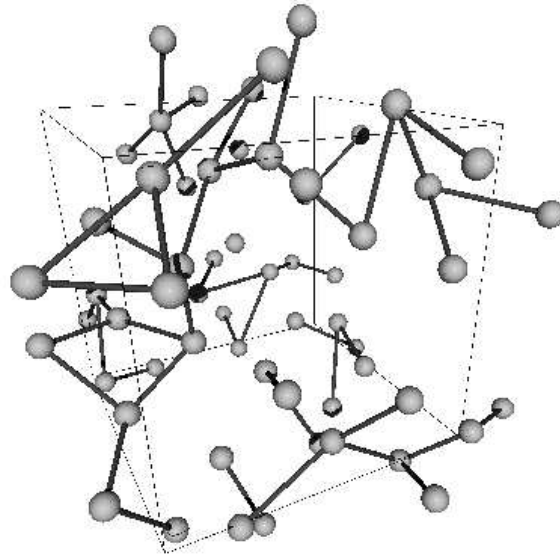
Figure 6.5: A part of an equilibrium configuration of the FCC bond percolating system with $p = 0.1975$. For clarity the spheres are shown as $\frac{1}{3}$ of their actual diameter.

In Fig. 6.6 we observe that the values of μ_1 and μ_2 gradually deviate from each other far from p_c because at large p the systems "remember" the lower (cubic) symmetry of their connectivities. For the FCC connectivity $\mu_1 > \mu_2$, while for the SC case $\mu_2 > \mu_1$. (The definitions of the shear moduli μ_1 and μ_2 depend on the orientation of the axes of the reference system, which in our simulations were taken along the edges of the conventional cubic unit cell.) Figure 6.7 shows that the difference $\Delta\mu \equiv |\mu_1 - \mu_2|$, follows, in both cases, quite similar power laws $\Delta\mu \sim (p - p_c)^h$ with $h = 3.95 \pm 0.15$ for the SC case and $h = 4.15 \pm 0.15$ for the FCC case. Because of the similarities of the values of h in SC and FCC systems, it is reasonable to assume that h is a new universal critical exponent which characterizes deviation from isotropic elastic behavior. While the power law dependence of $\Delta\mu$ is not surprising due to the self-similar nature of the large percolation clusters, we could only support this assumption by numerical data of limited accuracy. The validity of the power law dependence of $\Delta\mu$ on $(p - p_c)$ was verified by attempting (unsuccessfully) to fit the data to other functional forms.

We already saw that the exponent f (describing the leading critical elastic behavior) is very similar for self-avoiding and phantom percolating systems. Therefore, it is interesting to check whether this similarity applies to the exponent h, as well. For this purpose we measured $\Delta\mu$ for a phantom FCC bond percolating network
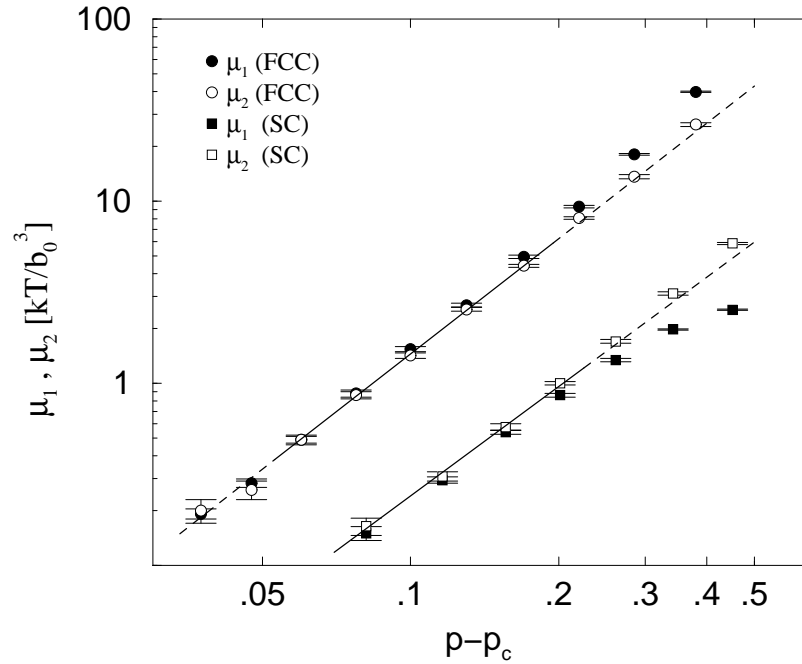
Figure 6.6: Logarithmic plot of the shear moduli μ_1 (solid symbols) and μ_2 (open symbols) as a function of $(p - p_c)$, for FCC (circles) and SC (squares) bond percolating systems. For each topology, its percolation threshold is used ($p_c \simeq 0.12$ for FCC, and, $p_c \simeq 0.249$ for SC). For both systems the volume fraction of the spheres is 0.2 and $b/a \sim 1.6$.

with the same values of b and b_0, but with $a = 0$. Our results of these simulations are also plotted in Fig. 6.7, revealing a power law with $h = 4.15 \pm 0.15$, as in the self-avoiding FCC case. The phantom Gaussian model which predicts that $f = t$, cannot be used to predict the value of h since it gives $\Delta\mu \equiv 0$ at any bond concentration p [40, 84]. Hence, $\Delta\mu$ represents deviation from a purely Gaussian behavior which originates in the non-Gaussian form of the tether potential and (in the self-avoiding case) EV interactions. The results for the exponent h imply that the similarity between the critical elasticity of phantom and self-avoiding percolating systems may not be restricted to the leading Gaussian behavior.

6.4   Summary

In this chapter we analyzed the elastic behavior of purely entropic percolation systems with EV interactions. The fact that the numerical values of the exponent f, found both for 2D and 3D systems, are (within error bars) equal to the corresponding exponents t of the conductivity, lends credibility to qualitative theories which assume that the finite clusters (1) do not contribute directly to the shear modulus (i.e., behave like a fluid medium) and (2) effectively screen out EV interactions in the elastic network. However, it must be noted that formal exact identity between
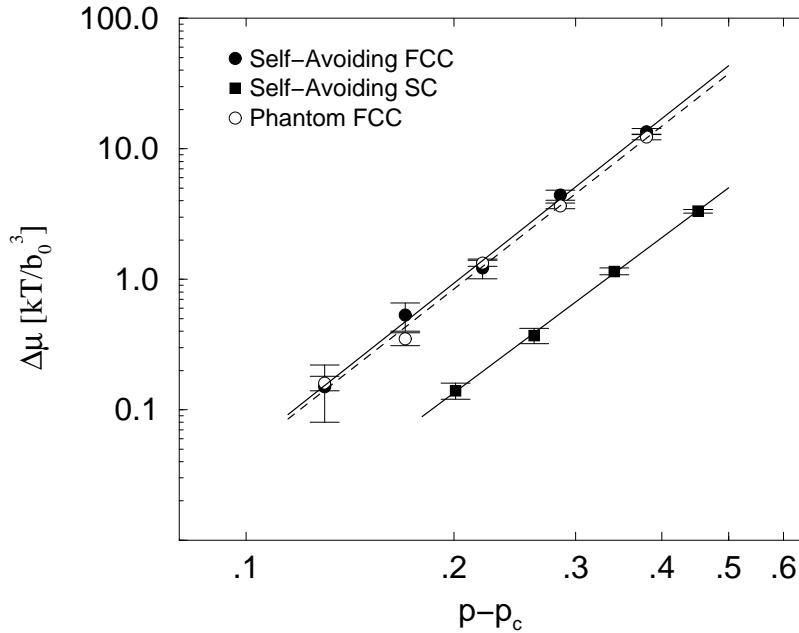
Figure 6.7: Logarithmic plot of the difference between the shear moduli $\Delta\mu$ as a function of $(p - p_c)$, for self-avoiding FCC (solid circles), self-avoiding SC (squares) and phantom FCC (open circles) bond percolating systems.

the elasticity and conductivity problems cannot exist in the same simple sense as it exists between the PGN problem and conductivity (see chapter 5). While for 2D systems one can only suspect that p_r may be lower than p_c in dense systems (see section 6.2), in three dimensions topological entanglements reduce p_r below p_c [83]. (Unfortunately, the decrease in p_r due to topological entanglements is very small and cannot be investigated in the context of elasticity.) This, and additional possible EV effects, bring p_r strictly below p_c, and therefore a simple mapping between the random resistor model and elasticity problem is impossible (unless it is used in some generalized sense). The fact that the exponent f is much smaller than the exponent predicted by the energetic bending elasticity model, implies that at finite T in the presence of bond-bending forces, sufficiently close to the rigidity threshold, the elastic behavior will be entropy-dominated. The lack of importance of central-force energetic elasticity for systems of this kind was already discussed in Ref. [56].

Further support to the heuristic approach which treat the system as a PGN with added pressure is given by our result for $\Delta\mu$ which is also described by similar exponents in phantom and self-avoiding systems. The exponent h that characterizes the decay of $\Delta\mu$ seems to be universal, namely independent of the lattice on which the geometry of the system is defined, but this point should be established more carefully by studying other lattice connectivities, and by measuring h for 2D (phantom and self-avoiding) percolation systems.

Chapter 7

Summary and Future Prospects

Materials like colloids and gels are characterized by their softness and great flexibility. The origin of these features is the entropic nature of their elastic response. This is also the main reason why the calculation of the elastic constants of such systems is, usually, highly non-trivial. More difficulties encountered in many theoretical studies of soft materials are related to the fact that these materials are often stressed and disordered, having both quenched and annealed degrees of freedom.

In this thesis we derived expressions for the stress and elastic constants of two generic models of entropy-dominated systems. One of them, the "phantom Gaussian model" (chapter 3 and appendix C), describes the elastic behavior of systems without EV interactions (or systems in which EV interactions are screened out). We found that the elastic behavior of phantoms Gaussian networks is characterized by the vanishing of their elastic constants. Therefore, the elastic moduli of such networks (which are related to the criteria of mechanical stability in the elasticity theory of stressed systems) are proportional to the stress. We showed that the components of the stress tensor of a Gaussian network coincide with the components of the conductivity tensor of an equivalent resistor network. For percolating Gaussian networks, this last result implies that the rigidity exponent, describing the elasticity of the system near the percolation threshold, is equal to the conductivity exponent in random resistor networks.

The other model, of "hard-spheres-and-tethers" systems (chapter 2 and appendix A), can be used to study the entropic elasticity of systems with EV interactions, as well as corrections to Gaussian elasticity in phantom systems. The stress and elastic constants of such purely entropic systems were expressed in terms of the probability densities of contact between hard spheres, and the probability densities of having stretched tethers. The major advantages of the new formalism are the facts that the different components of the stiffness tensor (elastic constants) are measured directly, and that the formalism is not restricted to systems with specific topologies. This

makes it an efficient tool for investigating a wide range of problems.

The new expressions for the stress and elastic constants of hard-spheres-and-tethers systems were used in MC simulations of various systems, leading to many new interesting results. In chapter 2 we calculated the elastic constants of 3D hard sphere fluids and solids. In particular, we were able to measure the elastic constants very close to maximal packing, i.e., in a regime which has not been studied by other, indirect, methods. In chapters 4 and 5 we studied the behavior of regular and random phantom tethered networks. It has been demonstrated that despite of the fact that the form of tether potential is very different from that of a Gaussian spring, the elastic properties of phantom tethered networks are described well by the Gaussian model. Yet, we were also able to detect deviations from the Gaussian model, which were manifested by non-vanishing values of the elastic constants.

In chapter 6 we discussed the long-standing question of the value of the critical rigidity exponent f in self-avoiding percolation systems. We performed simulations of both two- and three-dimensional systems. In both cases we found that the value of f is similar to the corresponding value of the conductivity exponent t (which is the value expected for phantom networks). These important results support qualitative theories claiming that EV interactions and entanglements are irrelevant as far as the critical behavior is concerned. However, one must keep in mind that at least for 3D systems we know that entanglements do affect the sol-gel transition by shifting the position of the rigidity threshold below the percolation threshold [83]. Thus, although the results presented in this thesis greatly improve our understanding of the problem of entropic elasticity at the sol-gel transition, a rigorous statistical-mechanical solution is still needed.

Finally, I would like to discuss, very briefly, other problems of entropic elasticity, for which the method and ideas presented in this thesis may be applied:

1. There has been an extensive research on the problem of *rubber elasticity* for already more than half a century [35, 36, 37]. Unlike gels, rubber is usually composed of a dense network of long polymers. Loops and knots should, therefore, play a more significant role in rubber elasticity than in gel elasticity. Various models of inter-penetrating networks have been investigated in order to analyze the influence of such entanglements on the elastic behavior [85]. The new method which enables accurate and efficient calculation of the elastic properties should be helpful in testing different theoretical predictions.

2. Another subject of active research is the thermodynamic properties of colloidal suspensions. Even the seemingly simple model of *binary hard–sphere mixtures*, exhibit a very rich phase behavior which depends on the volume fractions of the large and the small spheres, and on the ratio of their diameters. Due to the presence

of the small spheres, the large spheres are effectively attracted to each other by an entropic "depletion force" [86]. The main interest in such mixtures is the existence of a phase separation and the nature of the different phases [87]. These phase transitions may be accompanied by changes in the elastic properties. It is, therefore, interesting to study the elastic behavior of models of this type.

3. The controversy about the order of the *melting transition in two–dimensional hard disks systems* has been discussed in section 6.2. Despite the many numerical works which have been carried out for this problem in recent years [78, 80], the problem remains open, both due to numerical difficulties (finite size effects, choice of boundary conditions, etc.) and real physical problems (if a first order transition occurs, it is probably very weak). Investigating the elastic constants at the transition provides a new approach to this problem. The KTHNY theory [79], suggesting a continuous second order phase transition, predicts that the shear modulus suffers a discontinuity at the solid–hexatic transition. An even stronger prediction of the KTHNY theory is that the combination of the elastic moduli $4\kappa\mu/(\kappa+\mu)$ (measured in units of kT/b_0^2, where b_0 is the lattice spacing) takes the universal value of 16π just before melting (see the papers of Nelson and Halperin in Ref. [79]). These predictions were tested for Lennard–Jones–type systems [88], but the studies did not resolve the question about the nature of the transition. Inconclusive results for hard disk systems, obtained using indirect strain method simulations, were published recently [89]. Perhaps our new (direct) method for computing the elastic constants would lead to more accurate results.

Appendix A

Detailed Derivation of the Formalism

A.1 The Stress Tensor

The starting point of the derivation is the following expression for the stress tensor

$$
\begin{aligned}
\sigma_{ij} &= \left. \frac{1}{V} \frac{\partial F}{\partial \eta_{ij}} \right|_{\{\eta\}=0} \\
&= -\frac{kT}{V} \frac{1}{Z_C} \left\{ \int \prod_{\gamma=1}^{N} d\vec{R}^\gamma \left[\left(\sum_{\langle \alpha\beta \rangle} \frac{-\phi'\left(R^{\alpha\beta}\right)}{kT} \frac{R_i^{\alpha\beta} R_j^{\alpha\beta}}{R^{\alpha\beta}} \right) \exp\left(-\sum_{\langle \gamma\delta \rangle} \phi\left(R^{\gamma\delta}\right)/kT \right) \right. \right. \\
&\quad + \left. \left. \left. \frac{\partial J}{\partial \eta_{ij}} \right|_{\{\eta\}=0} \exp\left(-\sum_{\langle \gamma\delta \rangle} \phi\left(R^{\gamma\delta}\right)/kT \right) \right] \right\},
\end{aligned} \tag{A.1}
$$

which is easily derived from Eqs.(2.2) and (2.4). The first term in the square brackets on the r.h.s of Eq.(A.1), the configurational term, is composed of $N(N-1)/2$ terms, each corresponding to one distinct pair. Each of these terms can also be written as

$$
\int d\vec{R}^\alpha d\vec{R}^\beta \frac{d\left[\exp\left(-\phi\left(R^{\alpha\beta}\right)/kT \right) \right]}{dR^{\alpha\beta}} \times
$$

$$
\left\{ \frac{1}{Z_C} \int \prod_{\gamma\neq\alpha,\beta} d\vec{R}^\gamma \left[\exp\left(-\sum_{\langle \gamma\delta \rangle \neq \langle \alpha\beta \rangle} \phi(R^{\gamma\delta})/kT \right) \right] \right\} \frac{R_i^{\alpha\beta} R_j^{\alpha\beta}}{R^{\alpha\beta}}, \tag{A.2}
$$

where $\sum_{\langle \gamma\delta \rangle \neq \langle \alpha\beta \rangle}$ represents the sum over all pairs $\langle \gamma\delta \rangle$, distinct from the pair $\langle \alpha\beta \rangle$. Note that the limit $\{\eta\} = \{0\}$, was already taken at this stage.

If we now substitute an approximating potential, $\phi(r)$, in the Boltzmann factor, $\exp\left(-\phi\left(R^{\alpha\beta}\right)/kT \right)$, and take the "athermal limit" (see definitions in the last paragraph of section 2.1), we find the Boltzmann factor converging to a step function, where the discontinuity (from zero to unity) occurs at $R^{\alpha\beta} = a$ and an opposite discontinuity (from unity to zero) occurs at $R^{\alpha\beta} = b$ if the pair $\langle \alpha\beta \rangle$ is tethered.

70

The derivative of a step function is just the Dirac δ-function. Therefore, in the "athermal limit", the function $d\left[\exp\left(-\phi\left(R^{\alpha\beta}\right)/kT\right)\right]/dR^{\alpha\beta}$, which appears in the integrand in the expression (A.2), turns into

$$\frac{d\left[\exp\left(-\phi\left(R^{\alpha\beta}\right)/kT\right)\right]}{dR^{\alpha\beta}} \longrightarrow \left[\delta\left(R^{\alpha\beta}-a\right)-\nu^{\alpha\beta}\delta\left(R^{\alpha\beta}-b\right)\right] \equiv \Delta^{\alpha\beta}, \qquad (A.3)$$

where $\nu^{\alpha\beta}=1$ $(\nu^{\alpha\beta}=0)$ for a tethered (non-tethered) pair. The remaining part of the integrand,

$$\left\{\frac{1}{Z_C}\int\prod_{\gamma\neq\alpha,\beta}d\vec{R}^{\gamma}\left[\exp\left(-\sum_{\langle\gamma\delta\rangle\neq\langle\alpha\beta\rangle}\phi(R^{\gamma\delta})/kT\right)\right]\right\}\frac{R_i^{\alpha\beta}R_j^{\alpha\beta}}{R^{\alpha\beta}} \equiv \tilde{p}\left(\vec{R}^{\alpha},\vec{R}^{\beta}\right)\frac{R_i^{\alpha\beta}R_j^{\alpha\beta}}{R^{\alpha\beta}}$$

$$(A.4)$$

is a smooth function, including at $R^{\alpha\beta}=a$ or $R^{\alpha\beta}=b$. Since only the values of this function at $R^{\alpha\beta}=a$ and (if $\nu^{\alpha\beta}=1$) $R^{\alpha\beta}=b$ are relevant, the function might be replaced by any other function whose values at these points are the same. For $a<R^{\alpha\beta}<b$, the values of $\tilde{p}\left(\vec{R}^{\alpha},\vec{R}^{\beta}\right)$, coincide with the values of the following function

$$p\left(\vec{R}^{\alpha},\vec{R}^{\beta}\right)=\frac{1}{Z_C}\exp\left(-\phi\left(R^{\alpha\beta}\right)/kT\right)\int\prod_{\gamma\neq\alpha,\beta}d\vec{R}^{\gamma}\exp\left(-\sum_{\langle\gamma\delta\rangle\neq\langle\alpha\beta\rangle}\phi(R^{\gamma\delta})/kT\right),$$

which is the probability density to find atom α in $\vec{R}^{\alpha}$ and atom β in $\vec{R}^{\beta}$, since in that region $\phi\left(R^{\alpha\beta}\right)=0$. We thus find that for "hard" potentials, expression (A.2) becomes

$$\int d\vec{R}^{\alpha}d\vec{R}^{\beta}\left\{\frac{R_i^{\alpha\beta}R_j^{\alpha\beta}}{R^{\alpha\beta}}\Delta^{\alpha\beta}p\left(\vec{R}^{\alpha},\vec{R}^{\beta}\right)\right\}=\left\langle\frac{R_i^{\alpha\beta}R_j^{\alpha\beta}}{R^{\alpha\beta}}\Delta^{\alpha\beta}\right\rangle. \qquad (A.5)$$

[Unlike the function $\tilde{p}\left(\vec{R}^{\alpha},\vec{R}^{\beta}\right)$, the function $p\left(\vec{R}^{\alpha},\vec{R}^{\beta}\right)$ suffers a discontinuity at $R^{\alpha\beta}=a$ and (if $\nu^{\alpha\beta}=1$) $R^{\alpha\beta}=b$, and therefore the transition between the two sides of Eq.(A.5) should be made with some caution. The integral in equation (A.5) and in the following expressions of this type should be understood as if the delta functions reproduce the finite values $p(a+)$ and $p(b-)$. In practice, when we evaluate expression (A.5) by a numerical computation, this mathematically delicate point becomes unimportant.] When we sum all $N(N-1)/2$ terms corresponding to all pairs of atoms, we obtain

$$\sigma_{ij}^{\mathrm{conf}}=-\frac{kT}{V}\left\{\sum_{\langle\alpha\beta\rangle}\left\langle\frac{R_i^{\alpha\beta}R_j^{\alpha\beta}}{R^{\alpha\beta}}\Delta^{\alpha\beta}\right\rangle\right\}. \qquad (A.6)$$

The second term in Eq.(A.1) is known as the kinetic term. It appears even when $\phi\equiv 0$, i.e., for an ideal gas, and it contributes the term $-NkT\delta_{ij}/V$. To obtain this

contribution we start from Eq.(2.5), from which we find that

$$\frac{\partial J}{\partial \eta_{ij}} = \frac{N}{2} \left\{ \det \left(2[\eta] + [I] \right) \right\}^{[(N/2)-1]} \cdot \frac{\partial \left\{ \det \left(2[\eta] + [I] \right) \right\}}{\partial \eta_{ij}}. \tag{A.7}$$

When the explicit expression for $\det \left(2[\eta] + [I] \right)$ is written down and the derivative with respect to η_{ij} is taken, it is trivial to see that

$$\left. \frac{\partial J}{\partial \eta_{ij}} \right|_{\{\eta\}=0} = N \delta_{ij}, \tag{A.8}$$

which when substituted in Eq.(A.1) yields

$$\sigma_{ij}^{\text{kinetic}} = -N k T \delta_{ij} / V. \tag{A.9}$$

If we now combine Eqs.(A.6) and (A.9), we get expression (2.9) for the stress tensor:

$$\sigma_{ij} = \sigma_{ij}^{\text{conf}} + \sigma_{ij}^{\text{kinetic}} = -\frac{kT}{V} \left\{ \sum_{\langle \alpha \beta \rangle} \left\langle \frac{R_i^{\alpha\beta} R_j^{\alpha\beta}}{R^{\alpha\beta}} \Delta^{\alpha\beta} \right\rangle + N \delta_{ij} \right\}.$$

A.2 The Tensor of Elastic Constants

For the tensor elastic constants, we have

$$\begin{aligned} C_{ijkl} &= \left. \frac{\partial^2 F}{\partial \eta_{ij} \partial \eta_{kl}} \right|_{\{\eta\}=\{0\}} \\ &= \left. -\frac{kT}{V} \left[\frac{1}{Z_C} \frac{\partial^2 Z_C}{\partial \eta_{ij} \partial \eta_{kl}} - \left(\frac{1}{Z_C} \right)^2 \frac{\partial Z_C}{\partial \eta_{ij}} \frac{\partial Z_C}{\partial \eta_{kl}} \right] \right|_{\{\eta\}=\{0\}}. \end{aligned} \tag{A.10}$$

If we use Eq.(2.4), the first of the two terms on the r.h.s of Eq.(A.10) splits into four terms (which for the sake of later reference throughout this derivation we denote by T_{1-1}, T_{1-2}, T_{1-3} and T_{1-4}, respectively)

$$\begin{aligned} & -\frac{kT}{V} \frac{1}{Z_C} \int \prod_{\gamma=1}^{N} d\vec{R}^{\gamma} \left\{ J \frac{\partial^2 \exp\left(\sum_{\langle \alpha\beta \rangle} \phi\left(\left[R_m^{\alpha\beta} R_n^{\alpha\beta} (\delta_{mn} + 2\eta_{mn}) \right]^{1/2} \right) / kT \right)}{\partial \eta_{ij} \partial \eta_{kl}} \right. \\ & + \frac{\partial J}{\partial \eta_{kl}} \frac{\partial \exp\left(\sum_{\langle \alpha\beta \rangle} \phi\left(\left[R_m^{\alpha\beta} R_n^{\alpha\beta} (\delta_{mn} + 2\eta_{mn}) \right]^{1/2} \right) / kT \right)}{\partial \eta_{ij}} \\ & + \frac{\partial J}{\partial \eta_{ij}} \frac{\partial \exp\left(\sum_{\langle \alpha\beta \rangle} \phi\left(\left[R_m^{\alpha\beta} R_n^{\alpha\beta} (\delta_{mn} + 2\eta_{mn}) \right]^{1/2} \right) / kT \right)}{\partial \eta_{kl}} \\ & \left. + \frac{\partial^2 J}{\partial \eta_{ij} \partial \eta_{kl}} \exp\left(\sum_{\langle \alpha\beta \rangle} \phi\left(\left[R_m^{\alpha\beta} R_n^{\alpha\beta} (\delta_{mn} + 2\eta_{mn}) \right]^{1/2} \right) / kT \right) \right\} \bigg|_{\{\eta\}=0}. \tag{A.11} \end{aligned}$$

The most challenging term in expression (A.11) is, of course, the first one, T_{1-1}. If we perform the two derivatives in this term, it yields the following three terms (which we denote by T_{1-1-1}, T_{1-1-2} and T_{1-1-3}, respectively):

$$
-\frac{kT}{VZ_C} \int \prod_{\gamma=1}^{N} d\vec{R}^\gamma \left\{ \frac{1}{kT} \exp\left(-\sum_{\langle\gamma\delta\rangle} \phi\left(R^{\gamma\delta}\right)/kT\right) \left[\sum_{\langle\alpha\beta\rangle} \frac{\phi'\left(R^{\alpha\beta}\right)}{\left(R^{\alpha\beta}\right)^3} R_i^{\alpha\beta} R_j^{\alpha\beta} R_k^{\alpha\beta} R_l^{\alpha\beta}\right] \right.
$$

$$
-\frac{1}{kT} \exp\left(-\sum_{\langle\gamma\delta\rangle} \phi\left(R^{\gamma\delta}\right)/kT\right) \left[\sum_{\langle\alpha\beta\rangle} \frac{\phi''\left(R^{\alpha\beta}\right)}{\left(R^{\alpha\beta}\right)^2} R_i^{\alpha\beta} R_j^{\alpha\beta} R_k^{\alpha\beta} R_l^{\alpha\beta}\right]
$$

$$
+ \left(\frac{1}{kT}\right)^2 \exp\left(-\sum_{\langle\gamma\delta\rangle} \phi\left(R^{\gamma\delta}\right)/kT\right) \left[\sum_{\langle\alpha\beta\rangle} \frac{\phi'\left(R^{\alpha\beta}\right)}{R^{\alpha\beta}} R_i^{\alpha\beta} R_j^{\alpha\beta}\right] \times
$$

$$
\left. \left[\sum_{\langle\alpha\beta\rangle} \frac{\phi'\left(R^{\alpha\beta}\right)}{R^{\alpha\beta}} R_k^{\alpha\beta} R_l^{\alpha\beta}\right] \right\}. \qquad (A.12)
$$

[Note that in Eq.(A.12) the limit $\{\eta\} = \{0\}$, at which $J = 1$, was already taken]. Following the derivation of the configurational stress tensor [Eq.(A.5)], it can be easily shown that in the "athermal limit", the term T_{1-1-1} becomes

$$
\frac{kT}{V} \sum_{\langle\alpha\beta\rangle} \left\langle \frac{R_i^{\alpha\beta} R_j^{\alpha\beta} R_k^{\alpha\beta} R_l^{\alpha\beta}}{\left(R^{\alpha\beta}\right)^3} \Delta^{\alpha\beta} \right\rangle. \qquad (A.13)
$$

A straightforward generalization of this derivation shows that the *non-diagonal* elements in term T_{1-1-3}, i.e. these terms for which $\langle\alpha\beta\rangle \neq \langle\gamma\delta\rangle$, gives

$$
-\frac{kT}{V} \sum_{\langle\alpha\beta\rangle} \sum_{\langle\gamma\delta\rangle\neq\langle\alpha\beta\rangle} \left\langle \frac{R_i^{\alpha\beta} R_j^{\alpha\beta} R_k^{\gamma\delta} R_l^{\gamma\delta}}{R^{\alpha\beta} R^{\gamma\delta}} \Delta^{\alpha\beta} \Delta^{\gamma\delta} \right\rangle. \qquad (A.14)
$$

Note that the non-diagonal terms include both 3-particles terms $[\langle\alpha\beta\rangle, \langle\alpha\gamma\rangle]$ and 4-particles terms $[\langle\alpha\beta\rangle, \langle\gamma\delta\rangle]$.

We were thus left with the T_{1-1-2} term and with the *diagonal* elements of the T_{1-1-3} term, which may be written in the following combined form

$$
\frac{1}{VZ_C} \int \prod_{\gamma=1}^{N} d\vec{R}^\gamma \left\{ \exp\left(-\sum_{\langle\gamma\delta\rangle} \phi\left(R^{\gamma\delta}\right)/kT\right) \times \right.
$$

$$
\left. \sum_{\langle\alpha\beta\rangle} \left[\left(\phi''\left(R^{\alpha\beta}\right) - \phi'\left(R^{\alpha\beta}\right)^2/kT\right) \left(\frac{R_i^{\alpha\beta} R_j^{\alpha\beta} R_k^{\alpha\beta} R_l^{\alpha\beta}}{\left(R^{\alpha\beta}\right)^2}\right)\right] \right\}.
$$

Let us now look at one of these expressions, corresponding to the pair $\langle\alpha\beta\rangle$. After performing the integrations over the rest of the coordinates, $\{\vec{R}^\gamma | \gamma \neq \alpha, \beta\}$, we are left with

$$
-\frac{kT}{V} \int d\vec{R}^\alpha d\vec{R}^\beta \, \tilde{p}\left(\vec{R}^\alpha, \vec{R}^\beta\right) \frac{R_i^{\alpha\beta} R_j^{\alpha\beta} R_k^{\alpha\beta} R_l^{\alpha\beta}}{\left(R^{\alpha\beta}\right)^2} \frac{d^2 \left[\exp\left(-\phi\left(R^{\alpha\beta}\right)/kT\right)\right]}{d\left(R^{\alpha\beta}\right)^2} \qquad (A.15)
$$

$[\tilde{p}\left(\vec{R}^\alpha, \vec{R}^\beta\right)$ is defined in Eq.(A.4)]. At this point we change the variables of integration from $d\vec{R}^\alpha d\vec{R}^\beta$ to $d\vec{R}^{\alpha\beta} d\vec{R}^\beta$, where $\vec{R}^{\alpha\beta} = \vec{R}^\alpha - \vec{R}^\beta$, and then change $d\vec{R}^{\alpha\beta}$

to spherical coordinates $\left(R^{\alpha\beta} \right)^{d-1} dR^{\alpha\beta} d\Omega^{\alpha\beta}$, where $\Omega^{\alpha\beta}$ is the solid angle aperture around $\vec{R}^{\alpha\beta}$ and d is the dimensionality of the system. We also note that the terms $\left(R_i^{\alpha\beta} R_j^{\alpha\beta} R_k^{\alpha\beta} R_l^{\alpha\beta} \right) / \left(R^{\alpha\beta} \right)^2$ in Eq.(A.15) can be written as $\left(R^{\alpha\beta} \right)^2 f_{ijkl} \left(\Omega^{\alpha\beta} \right)$, where f_{ijkl} is a function of the solid angle alone (for instance, for a 2D system, $f_{xxxx} = \cos^4 \Omega$, $f_{yyyy} = \sin^4 \Omega$, $f_{xyxy} = f_{yxyx} = f_{xxyy} = f_{yyxx} = \cos^2 \Omega \sin^2 \Omega$, etc.). Thus, Eq.(A.15) takes the form

$$-\frac{kT}{V} \int d\vec{R}^{\alpha} d\Omega^{\alpha\beta} dR^{\alpha\beta} \left\{ \left(R^{\alpha\beta} \right)^{d+1} \tilde{p} \left(\vec{R}^{\alpha}, \vec{R}^{\beta} \right) f_{ijkl} \left(\Omega^{\alpha\beta} \right) \frac{d^2 \left[\exp \left(-\phi \left(R^{\alpha\beta} \right) / kT \right) \right]}{d \left(R^{\alpha\beta} \right)^2} \right\}.$$

When integration by parts is performed over the variable $R^{\alpha\beta}$ this expression becomes

$$= \frac{kT}{V} \int d\vec{R}^{\alpha} d\Omega^{\alpha\beta} f_{ijkl} \left(\Omega^{\alpha\beta} \right) dR^{\alpha\beta} \frac{\partial \left[\left(R^{\alpha\beta} \right)^{d+1} \tilde{p} \left(\vec{R}^{\alpha}, \vec{R}^{\beta} \right) \right]}{\partial R^{\alpha\beta}} \frac{d \left[\exp \left(-\phi \left(R^{\alpha\beta} \right) / kT \right) \right]}{dR^{\alpha\beta}}$$

$$= \frac{kT}{V} \int d\vec{R}^{\alpha} d\Omega^{\alpha\beta} f_{ijkl} \left(\Omega^{\alpha\beta} \right) dR^{\alpha\beta} \frac{\partial \left[\left(R^{\alpha\beta} \right)^{d+1} \tilde{p} \left(\vec{R}^{\alpha}, \vec{R}^{\beta} \right) \right]}{\partial R^{\alpha\beta}} \Delta^{\alpha\beta} \qquad \text{(A.16)}$$

(Integration is taken from 0 to ∞ and, therefore, the boundary terms vanish.) The second expression in Eq.(A.16) is obtained for the "athermal limit" using substitution (A.3). In order to bring this expression into a more useful form, we perform the derivative in Eq.(A.16):

$$\frac{\partial \left[\left(R^{\alpha\beta} \right)^{d+1} \tilde{p} \left(\vec{R}^{\alpha}, R^{\alpha\beta}, \Omega^{\alpha\beta} \right) \right]}{\partial R^{\alpha\beta}} = (d+1) \left(R^{\alpha\beta} \right)^d \tilde{p} \left(\vec{R}^{\alpha}, R^{\alpha\beta}, \Omega^{\alpha\beta} \right)$$

$$+ \left(R^{\alpha\beta} \right)^{d+1} \frac{\partial \left[\tilde{p} \left(\vec{R}^{\alpha}, R^{\alpha\beta}, \Omega^{\alpha\beta} \right) \right]}{\partial R^{\alpha\beta}}. \quad \text{(A.17)}$$

After the first term on the r.h.s of Eq.(A.17) is substituted in Eq.(A.16), we may switch back to the original integration variables, $d\vec{R}^{\alpha} d\vec{R}^{\beta}$, and again, use substitution (A.3). In fact, we get an expression which is identical with the expression (A.13), except for the a prefactor $(d+1)$. Thus, their *joint* contribution is

$$(d+2) \frac{kT}{V} \sum_{\langle \alpha\beta \rangle} \left\langle \frac{R_i^{\alpha\beta} R_j^{\alpha\beta} R_k^{\alpha\beta} R_l^{\alpha\beta}}{\left(R^{\alpha\beta} \right)^3} \Delta^{\alpha\beta} \right\rangle. \qquad \text{(A.18)}$$

The task imposed by the second term in Eq.(A.17) is slightly more complicated: We need to evaluate $\partial \left[\tilde{p} \left(\vec{R}^{\alpha}, \vec{R}^{\beta} \right) \right] / \partial R^{\alpha\beta}$. We remind the reader that $\tilde{p} \left(\vec{R}^{\alpha}, \vec{R}^{\beta} \right)$ is defined in Eq.(A.4). The dependence of $\tilde{p}$ on $R^{\alpha\beta}$ in this expression comes from the exponent

$$\sum_{\langle \gamma\delta \rangle \neq \langle \alpha\beta \rangle} \phi \left(R^{\gamma\delta} \right), \qquad \text{(A.19)}$$

appearing in (A.4). Instead of the set of variables $\{\vec{R}^\gamma \mid \gamma = 1 \ldots N\}$, we may use the set of *independent* variables $\{\vec{R}^\alpha, \vec{R}^\gamma - \vec{R}^\alpha = \vec{R}^{\gamma\alpha} \mid \gamma = 1 \ldots N, \gamma \neq \alpha\}$, to express the terms in the exponent (A.19). Since we look for the derivative of $\tilde{p}\left(\vec{R}^\alpha, \vec{R}^\beta\right)$ with respect to $R^{\alpha\beta}$ (the size of one of the variables, $\vec{R}^{\beta\alpha}$), we need to find which of the terms in expression (A.19) actually depend on this variable. One can easily find that the terms included in the set $\left\{\phi\left(R^{\beta\gamma}\right) \mid \gamma = 1 \ldots N; \gamma \neq \alpha, \beta\right\}$ are the relevant terms. $\vec{R}^{\beta\gamma}$ and $\vec{R}^{\alpha\beta}$ are two of the edges of a triangle whose vertices are the positions of atoms α, β and γ. It is not difficult to show that if the length of $\vec{R}^{\alpha\beta}$ is slightly changed, while the length of $\vec{R}^{\alpha\gamma}$ is fixed, then the change in the length of the third edge, $\vec{R}^{\beta\gamma}$, obeys

$$\frac{\partial R^{\beta\gamma}}{\partial R^{\alpha\beta}} = \frac{\vec{R}^{\alpha\beta} \cdot \vec{R}^{\gamma\beta}}{R^{\alpha\beta} R^{\gamma\beta}}.$$

With this identity, we find in a straightforward manner that

$$\frac{\partial\left[\tilde{p}\left(\vec{R}^\alpha, R^{\alpha\beta}, \Omega^{\alpha\beta}\right)\right]}{\partial R^{\alpha\beta}} = \tilde{p}\left(\vec{R}^\alpha, R^{\alpha\beta}, \Omega^{\alpha\beta}\right) \sum_{\gamma \neq \alpha, \beta} -\frac{1}{kT}\phi'\left(R^{\beta\gamma}\right)\frac{\vec{R}^{\alpha\beta} \cdot \vec{R}^{\gamma\beta}}{R^{\alpha\beta} R^{\gamma\beta}}.$$

In this expression the indices α and β appear in an asymmetrical way. If we interchange their roles we obtain the following symmetrical form

$$\frac{\partial\left[\tilde{p}\left(\vec{R}^\alpha, R^{\alpha\beta}, \Omega^{\alpha\beta}\right)\right]}{\partial R^{\alpha\beta}} = \frac{\tilde{p}\left(\vec{R}^\alpha, R^{\alpha\beta}, \Omega^{\alpha\beta}\right)}{-2kT} \times$$
$$\sum_{\gamma \neq \alpha, \beta} \left\{\phi'(R^{\beta\gamma})\frac{\vec{R}^{\alpha\beta} \cdot \vec{R}^{\gamma\beta}}{R^{\alpha\beta} R^{\gamma\beta}} + \phi'(R^{\alpha\gamma})\frac{\vec{R}^{\alpha\beta} \cdot \vec{R}^{\alpha\gamma}}{R^{\alpha\beta} R^{\alpha\gamma}}\right\}. \tag{A.20}$$

We now need to substitute this last identity into the integrand of (A.16), switch back to the original integration variables, $d\vec{R}^\alpha d\vec{R}^\beta$, and use transformation (A.3), to finally obtain that the contribution of the second term in (A.17) is

$$-\frac{kT}{2V}\sum_{\langle\alpha\beta\rangle}\sum_{\gamma\neq\alpha,\beta}\left\langle\left\{\frac{R_i^{\alpha\beta} R_j^{\alpha\beta} R_k^{\alpha\beta} R_l^{\alpha\beta}}{(R^{\alpha\beta})^2}\Delta^{\alpha\beta}\left(\frac{\vec{R}^{\alpha\beta} \cdot \vec{R}^{\alpha\gamma}}{R^{\alpha\beta} R^{\alpha\gamma}}\Delta^{\alpha\gamma} + \frac{\vec{R}^{\alpha\beta} \cdot \vec{R}^{\gamma\beta}}{R^{\alpha\beta} R^{\gamma\beta}}\Delta^{\beta\gamma}\right)\right\}\right\rangle. \tag{A.21}$$

We still need to treat terms T_{1-2}, T_{1-3} and T_{1-4} in Eq.(A.11) and the second term in Eq.(A.10). Term T_{1-2} is identical to the configurational stress term [Eq.(A.6)], except for the multiplicative term, $\partial J/\partial\eta_{kl}$, which appears in the former. Therefore, using result (A.8), we find that the contribution of this term is

$$N\delta_{kl}\sigma_{ij}^{\text{conf}}. \tag{A.22}$$

Similarly, the T_{1-3} term yields

$$N\delta_{ij}\sigma_{kl}^{\text{conf}}. \tag{A.23}$$

The second term in Eq.(A.10) is obviously equal to

$$\frac{kT}{V}\left\{\sum_{\langle\alpha\beta\rangle}\left\langle\frac{R_i^{\alpha\beta}R_j^{\alpha\beta}}{R^{\alpha\beta}}\Delta^{\alpha\beta}\right\rangle + N\delta_{ij}\right\}\left\{\sum_{\langle\alpha\beta\rangle}\left\langle\frac{R_k^{\alpha\beta}R_l^{\alpha\beta}}{R^{\alpha\beta}}\Delta^{\alpha\beta}\right\rangle + N\delta_{kl}\right\}. \qquad (A.24)$$

Finally we need to differentiate expression (A.7) with respect to η_{kl}, in order to calculate term T_{1-4} which is given by

$$-\frac{kT}{V}\frac{\partial^2 J}{\partial\eta_{ij}\partial\eta_{kl}}\bigg|_{\{\eta\}=\{0\}} = -\frac{kT}{V}\left\{N^2\delta_{ij}\delta_{kl} - 2N\delta_{il}\delta_{jk}\right\}. \qquad (A.25)$$

When we combine these four terms [(A.22)–(A.25)], we find that their *joint* contribution to the expression for the tensor of elastic constants is

$$\frac{2NkT}{V}\delta_{il}\delta_{jk} + \frac{kT}{V}\left\{\sum_{\langle\alpha\beta\rangle}\left\langle\frac{R_i^{\alpha\beta}R_j^{\alpha\beta}}{R^{\alpha\beta}}\Delta^{\alpha\beta}\right\rangle\right\}\left\{\sum_{\langle\alpha\beta\rangle}\left\langle\frac{R_k^{\alpha\beta}R_l^{\alpha\beta}}{R^{\alpha\beta}}\Delta^{\alpha\beta}\right\rangle\right\}. \qquad (A.26)$$

To this contribution we need to add terms (A.14), (A.18) and (A.21) to obtain the following final expression for the tensor of elastic constants (2.10):

$$\begin{aligned}
C_{ijkl} =\ & \frac{2NkT}{V}\delta_{il}\delta_{jk} + \frac{kT}{V}\Bigg\{(d+2)\sum_{\langle\alpha\beta\rangle}\left\langle\frac{R_i^{\alpha\beta}R_j^{\alpha\beta}R_k^{\alpha\beta}R_l^{\alpha\beta}}{(R^{\alpha\beta})^3}\Delta^{\alpha\beta}\right\rangle \\
& -\frac{1}{2}\sum_{\langle\alpha\beta\rangle}\sum_{\gamma\neq\alpha,\beta}\left\langle\left[\frac{R_i^{\alpha\beta}R_j^{\alpha\beta}R_k^{\alpha\beta}R_l^{\alpha\beta}}{(R^{\alpha\beta})^2}\Delta^{\alpha\beta}\left(\frac{\vec{R}^{\alpha\beta}\cdot\vec{R}^{\alpha\gamma}}{R^{\alpha\beta}R^{\alpha\gamma}}\Delta^{\alpha\gamma} + \frac{\vec{R}^{\alpha\beta}\cdot\vec{R}^{\gamma\beta}}{R^{\alpha\beta}R^{\gamma\beta}}\Delta^{\beta\gamma}\right)\right]\right\rangle \\
& +\left[\sum_{\langle\alpha\beta\rangle}\left\langle\frac{R_i^{\alpha\beta}R_j^{\alpha\beta}}{R^{\alpha\beta}}\Delta^{\alpha\beta}\right\rangle\right]\left[\sum_{\langle\alpha\beta\rangle}\left\langle\frac{R_k^{\alpha\beta}R_l^{\alpha\beta}}{R^{\alpha\beta}}\Delta^{\alpha\beta}\right\rangle\right] \\
& -\sum_{\langle\alpha\beta\rangle}\sum_{\langle\gamma\delta\rangle\neq\langle\alpha\beta\rangle}\left\langle\frac{R_i^{\alpha\beta}R_j^{\alpha\beta}R_k^{\gamma\delta}R_l^{\gamma\delta}}{R^{\alpha\beta}R^{\gamma\delta}}\Delta^{\alpha\beta}\Delta^{\gamma\delta}\right\rangle\Bigg\}.
\end{aligned}$$

Appendix B

Computing the Averages of Quantities with Dirac δ-functions

Suppose we perform a MC investigation of a system consisting of N particles, in which we try to evaluate the thermal average of a certain quantity $g(\{\vec{R}^\alpha\})$ that depends on the positions of the particles $\{\vec{R}^\alpha \; ; \; 1 \leq \alpha \leq N\}$. The average is estimated by

$$\langle g \rangle \approx \frac{1}{\mathcal{N}_c} \sum_{p=1}^{\mathcal{N}_c} g\left(\{\vec{R}_p^\alpha\}\right),$$

where $\vec{R}_p^\alpha$ is the value of $\vec{R}^\alpha$ at the p-th sampled configuration, and $\mathcal{N}_c$ is the total number of MC configurations used in the simulation. Clearly, this sum does not lead to the correct mean when the averaged quantities include δ-functions, as we have in expressions (2.9) and (2.10), because such quantities vanish at almost every configuration (except for a group of configurations whose measure vanishes — at which their values are not defined at all). This is just a restatement of the fact that in MC simulations we measure probabilities rather than probability densities.

In systems of hard spheres the averages in expressions (2.9) and (2.10) can be approximated by measuring the relevant quantities every time we detect a pair of spheres whose separation is smaller than $a + \epsilon$ ($\epsilon \ll a$) and, then, dividing (normalizing) the sum by the size of ϵ. In a more formal language, this approximation is obtained by replacing the delta function $\delta(R^{\alpha\beta} - a)$ with a square function of width ϵ and height $1/\epsilon$, centered at $R^{\alpha\beta} = a + \epsilon/2$. In systems consisting of both spheres and tethers, we identify bond stretching with tethers whose lengths are larger than $b - \epsilon$, i.e., we approximate the function $\Delta^{\alpha\beta} \equiv \left[\delta\left(R^{\alpha\beta} - a\right) - \nu^{\alpha\beta}\delta\left(R^{\alpha\beta} - b\right)\right]$ [Eq.(A.3)] by the function

$$\tilde{h}_1(R^{\alpha\beta}) = \begin{cases} 1/\epsilon, & \text{for } a \leq R^{\alpha\beta} < a + \epsilon \\ -\nu^{\alpha\beta}/\epsilon, & \text{for } b - \epsilon < R^{\alpha\beta} \leq b \\ 0, & \text{otherwise} \end{cases} , \tag{B.1}$$
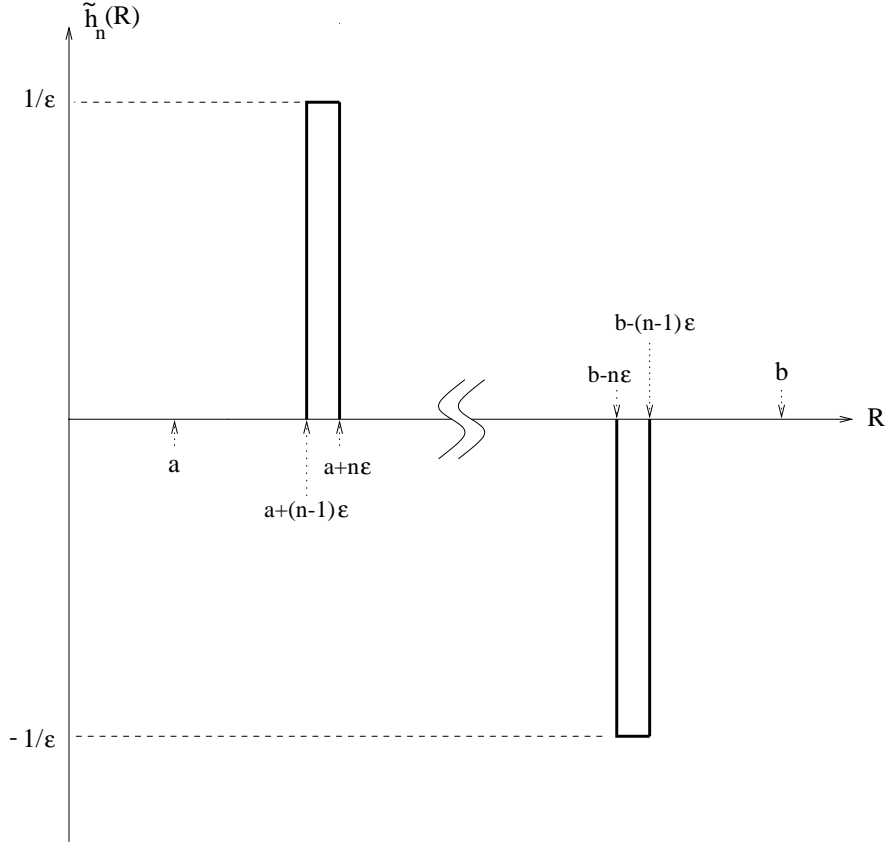
Figure B.1: The function $\tilde{h}_n(R)$ [Eq.(B.2)] (with $\nu = 1$) used as an approximation of the function $\Delta \equiv [\delta(R - a) - \delta(R - b)]$.

which (if $\nu^{\alpha\beta} = 1$) is equal to the difference between two square functions centered at $R^{\alpha\beta} = a + \epsilon/2$ and $R^{\alpha\beta} = b - \epsilon/2$, respectively. If the probability density of finding the pair separation equal to R is described by a smooth function, this approximation would lead to an error which is at most of the order of the small parameter ϵ/a. Obviously, one would like to set the size of ϵ as small as possible, in order to minimize this correction. However, there is a limit to the extent to which ϵ can be reduced, imposed by $\mathcal{N}_c$, the number of MC configurations. As ϵ gets smaller, one needs more MC samplings in order to count a sufficient number of events at which the distance between spheres satisfies $a \leq R < a + \epsilon$ (as well as events at which the length of a tether satisfies $b - \epsilon < R \leq b$). An elegant way to minimize the error (without making ϵ smaller) is to make a set of approximations using a set of functions (that one of them is depicted at Fig. B.1)

$$\tilde{h}_n(R) = \begin{cases} 1/\epsilon, & \text{for } a + (n-1)\epsilon \leq R < a + n\epsilon \\ -\nu/\epsilon, & \text{for } b - n\epsilon < R \leq b - (n-1)\epsilon \\ 0, & \text{otherwise} \end{cases}, \qquad (B.2)$$

defined similarly to Eq.(B.1), but with the square functions centered at $R = a + \epsilon_n$

and $R = b - \epsilon_n$, where

$$\epsilon_n \equiv (n - 1/2)\epsilon, \tag{B.3}$$

and $n = 1, 2, 3, \ldots$. When we use the function $\tilde{h}_n(R)$ in expressions (2.9) and (2.10), the averages are evaluated using the pairs of spheres whose separations are found inside the small "bin" interval $a + (n - 1)\epsilon \leq R < a + n\epsilon$, and the tethers whose lengths are found inside the "bin" $b - n\epsilon < R \leq b - (n - 1)\epsilon$. After evaluating these averages (which are statistically independent quantities since the "bins" corresponding to different values of n do not overlap each other, and therefore each average is computed using the contributions of different events) we plot the value of the average as a function of ϵ_n, the distance of the center of the relevant "bin" from a and b. We get our final estimate for the "correct" average by extrapolating this function to the limit $\epsilon_n \to 0$. In Fig. B.2 we demonstrate this extrapolation procedure for MC measurements of the pressure and elastic constants of hard sphere FCC crystal at a reduced density $\rho/\rho_0 = 0.8$. The curves are the weighted (i.e., each point was weighted by the reciprocal to its error bar) least squares fits of the data to polynomials of the third order in ϵ_n.
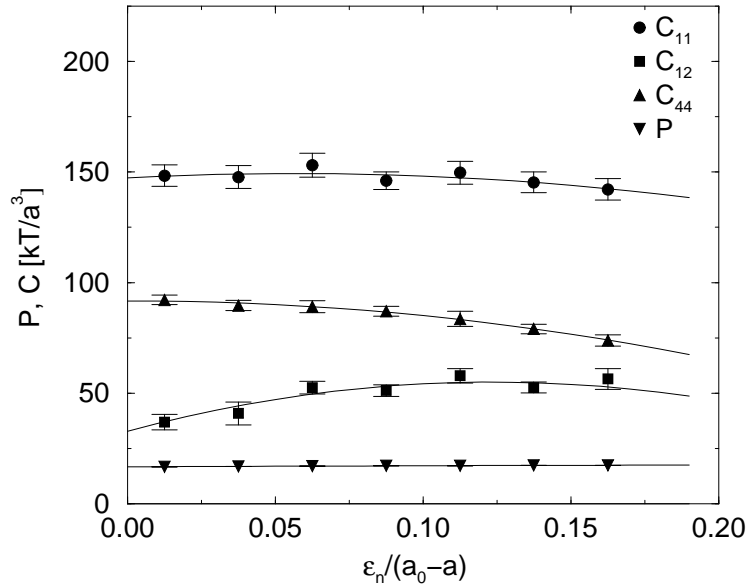
Figure B.2: The pressure, P, and the three elastic constants, C_{11}, C_{12}, C_{44}, of a hard sphere crystal at $\rho/\rho_0 = 0.8$, as a function of ϵ_n [see definition in Eq.(B.3)]. ϵ_n was normalized by $a_0 - a$, where a and a_0 are the spheres diameters at ρ and ρ_0, respectively. The curves are the weighted least squares fits of the third order polynomials in ϵ_n to the data.

Expression (2.10) for the elastic constants comprises of two types of terms - those including a single Δ function, and terms including the product of two Δ functions, corresponding to two distinct pairs. The former represent events of a single spheres'

contact (or tether stretching), while the latter correspond to events in which two contacts (or two stretches, or one contact and one stretch) occur simultaneously. The evaluation of the averages of the "double Δ" terms is far more difficult than that of the "single Δ" terms since they represent rarer events and, consequently, their statistics is much noisier. In the simulations described in chapters 2–5, we used the product $\tilde{h}_n(R^{\alpha\beta})\tilde{h}_n(R^{\gamma\delta})$ to approximate the product $\Delta^{\alpha\beta}\Delta^{\gamma\delta}$. Thus, the values of the computed averages depend on a single variable, ϵ_n [Eq.(B.3)], as shown in Fig. B.2. In the simulations of self-avoiding percolation systems (chapter 6) we evaluated the "double Δ" terms using the products $\tilde{h}_n(R^{\alpha\beta})\tilde{h}_m(R^{\gamma\delta})$, with n not necessarily equal to m. Now, the values of the computed averages should be plotted as a function of two variables, ϵ_n and ϵ_m, and the "correct" average is obtained by taking the limits $\epsilon_n \to 0$ and $\epsilon_m \to 0$. In Fig. B.3 we show the results for C_{12}^*, defined as the sum of all "double Δ" terms in the expression for the elastic constant C_{12}. The data corresponds to one of the 3D percolation topologies defined on an FCC lattice with fraction of tethers $p = 0.1975$. The surface represents the linear (both in ϵ_m and ϵ_n) weighted least squares fit of the data.
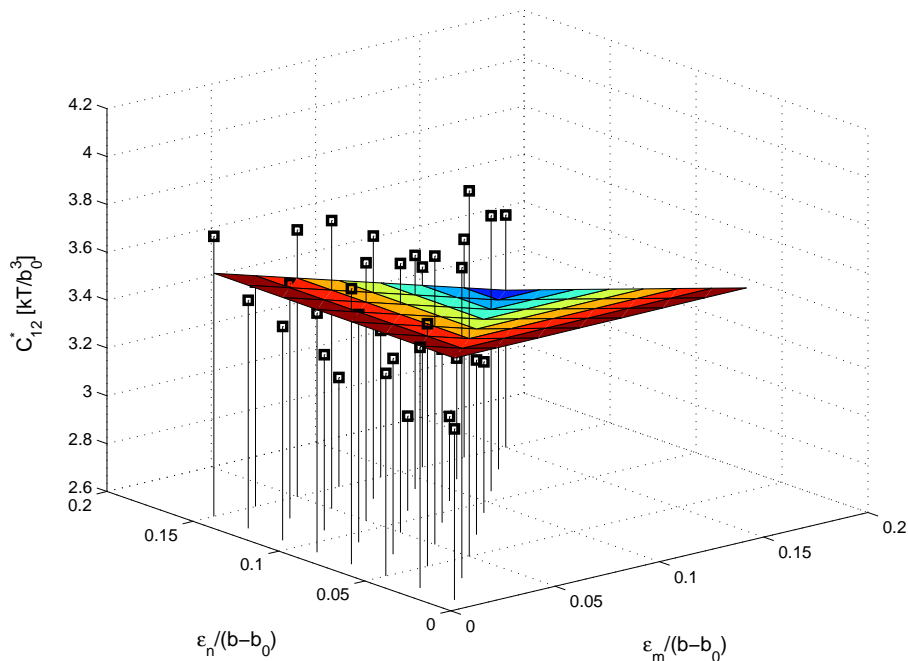
Figure B.3: The sum of "double Δ" terms, C_{12}^*, of a 3D percolation system defined on an FCC lattice with $p = 0.1975$, as a function of ϵ_m and ϵ_n. ϵ_m and ϵ_n were normalized by $b - b_0$, where b and b_0 are the maximal length of the tether and lattice spacing, respectively. The squares depict the data points, while the surface represents the linear (in ϵ_m and ϵ_n) weighted least squares fit of the data. For clarity, we draw a vertical line from each data point to the bottom of the grid.

Two important remarks should me made regarding the two variables extrapolation method: (1) The number of MC events used with this method is larger than that used with the single variable extrapolation. Thus, we greatly improve the accu-

racy of the results. (2) In the case that $m \neq n$ we computed the averages using the contributions of all the events in which one of the contacts (or stretches) belongs to the "bin" $a + (n-1)\epsilon \leq R < a + n\epsilon$ [or, $b - n\epsilon < R \leq b - (n-1)\epsilon$], while the other belongs to the "bin" $a + (m-1)\epsilon \leq R < a + m\epsilon$ [or, $b - m\epsilon < R \leq b - (m-1)\epsilon$]. The sums obtained in this way were eventually divided by 2, to obtain the correct normalization. Mathematically, this is equivalent to using the function $1/2\left[\tilde{h}_n(R^{\alpha\beta})\tilde{h}_m(R^{\gamma\delta}) + \tilde{h}_m(R^{\alpha\beta})\tilde{h}_n(R^{\gamma\delta})\right]$.

Appendix C

The Conductivity Tensor of Finite Resistor Networks

Consider a network whose bonds are resistors of conductance $K^{\alpha\beta}$, where the superscripts α and β label the nodes which the particular resistor connects. The network is finite and has an arbitrary topology, i.e., we make no assumption on the symmetry. We denote by $\vec{R}^{\beta}$ the position of the node β and by φ^{β} the electric potential at the node. The network is placed inside a rectangular box of volume $V = L_1 \times L_2 \times \ldots \times L_d$, where L_i is the length of the box along the ith Cartesian direction. (The derivation presented here can be easily generalized to systems of arbitrary shape.) The nodes of the network which are located on the surface of the system are called surface nodes, and we label them with the superscript s. The rest of the nodes are called the internal nodes, which we denote with the superscript α. The superscripts β and γ will be used to denote nodes of both types.

The conductivity of an electrical system is a tensor, Σ_{ik}, defined by

$$\langle j_i \rangle = \Sigma_{ik} \langle E_k \rangle, \tag{C.1}$$

where the subscripts denote Cartesian coordinates and summation over repeated indices is implied, while $\langle \vec{j} \rangle$ and $\langle \vec{E} \rangle$ are the volume averages of the current density and the electric field, respectively. This definition of Σ_{ik} applies to continuous electrical systems. It can be generalized to discrete networks, if we define the current density by a set of Dirac δ-functions representing the currents in the bonds. Let us assume now that the electric potential, φ, applied on the surface of the network is such that on each surface point it is equal to the jth Cartesian coordinate of the point. Since $\vec{E} = -\vec{\nabla}\varphi$, we have

$$\langle E_k \rangle = \frac{1}{V} \int E_k \, dV = -\frac{1}{V} \int \frac{\partial \varphi}{\partial x_k} \, dV = \frac{1}{V} \left[-\int_{x_k = L_k} \varphi \, dS + \int_{x_k = 0} \varphi \, dS \right],$$

where the surface integration is over the boundaries $x_k = 0$ and $x_k = L_k$, normal to the kth direction. However, with our choice for the electric potential on the

boundaries, $\varphi = x_j$, it is easy to see that $\langle E_k \rangle = -\delta_{kj}$, where δ_{kj} is the Kronecker delta.

The mean current density $\langle j_i \rangle$, is given by

$$\langle j_i \rangle = \frac{1}{V} \int j_i \, dV. \qquad (C.2)$$

As we have already noted, the above definition (C.2) applies to continuous electrical systems. To make it applicable to resistor networks we need to write the current density as a sum of Dirac δ-functions representing the currents in the "linear" resistors. With this formal representation, the contribution to $\langle j_i \rangle$ of each resistor is given by the line-integral

$$\int_{\vec{R}^\alpha}^{\vec{R}^\beta} I^{\alpha\beta} \, dx_i = K^{\alpha\beta} \left(\varphi^\alpha - \varphi^\beta \right) \left(R_i^\beta - R_i^\alpha \right),$$

where $I^{\alpha\beta} = K^{\alpha\beta} \left(\varphi^\alpha - \varphi^\beta \right)$ is the current across the resistor between nodes α and β. Adding the contributions of all the resistors we find that

$$\langle j_i \rangle = \frac{1}{V} \sum_{\langle \alpha\beta \rangle} K^{\alpha\beta} \left(\varphi^\alpha - \varphi^\beta \right) \left(R_i^\beta - R_i^\alpha \right).$$

We may write the last result in a slightly different way

$$\begin{aligned}
\langle j_i \rangle &= \frac{1}{2V} \left\{ \sum_\gamma \sum_\beta K^{\gamma\beta} \Theta^{\gamma\beta} \left(\varphi^\gamma - \varphi^\beta \right) \left(-R_i^\gamma \right) + \sum_\gamma \sum_\beta K^{\gamma\beta} \Theta^{\gamma\beta} \left(\varphi^\gamma - \varphi^\beta \right) R_i^\beta \right\} \\
&= \frac{1}{V} \left\{ \sum_\gamma \left(-R_i^\gamma \right) \left[\sum_\beta K^{\gamma\beta} \Theta^{\gamma\beta} \left(\varphi^\gamma - \varphi^\beta \right) \right] \right\},
\end{aligned}$$

where the variable $\Theta^{\gamma\beta}$ takes the value 1 if the nodes γ and β are connected by a resistor and if at least one of them is an internal node; and the value 0, otherwise. The sums in square brackets corresponding to internal nodes $\gamma = \alpha$ vanish due to the Kirchoff "junction rule" for the vanishing of the sum of currents entering an internal node:

$$\sum_\beta K^{\alpha\beta} \Theta^{\alpha\beta} \left(\varphi^\alpha - \varphi^\beta \right) = 0.$$

We are left with the contribution of the surface nodes $\gamma = s$ only, i.e.,

$$\langle j_i \rangle = \frac{1}{V} \left\{ \sum_s R_i^s \sum_\beta K^{\beta s} \Theta^{\beta s} \left(\varphi^\beta - \varphi^s \right) \right\}.$$

This last result can be also represented by summation over all the resistors $\langle \alpha s \rangle$, between surface and internal nodes

$$\langle j_i \rangle = \frac{1}{V} \left[\sum_{\langle \alpha s \rangle} K^{\alpha s} R_i^s \left(\varphi^\alpha - \varphi^s \right) \right].$$

Finally, since the electric field is equal to $\langle E_k \rangle = -\delta_{kj}$, we have from Eq.(C.1) that

$$-\langle j_i \rangle = \Sigma_{ij} = \frac{1}{V} \left[\sum_{\langle \alpha s \rangle} K^{\alpha s} R_i^s \left(\varphi^s - \varphi^\alpha \right) \right].$$

We have obtained expression (3.13), which we constructed by mapping expression (3.9) for σ_{ij} into the electrostatic problem. This proves that indeed $\sigma_{ij} = \Sigma_{ij}$. Note that Σ_{ij} does not depend on the positions of the internal nodes but only on the details of the conductivity. In large random networks the relation (C.1) suffices to define Σ_{ij} without need of a detailed specification of boundary conditions. However, our *exact* result is valid also for small networks of arbitrary topology, provided that the electric field $\vec{E}$ is generated using the very specific boundary conditions specified in this appendix.

Bibliography

[1] K. Kremer and G. S. Grest, J. Chem. Phys. **92**, 5057 (1990).

[2] Y. Kantor, M. Kardar and D. R. Nelson, Phys. Rev. A **35**, 3056 (1987).

[3] H. Lekerkerker, in *Soft and Fragile matter - Nonequilibrium dynamics, metastability, and flow*, Proceedings of the Fifty Third Scottish Universities Summer School in Physics, eds. M. E. Cates and M. R. Evans (Institute of Physics Publishing, Bristol, 2000), pp. 305.

[4] A. Cauchy, Exercices de Mathematiques **3**, 317 (1828).

[5] M. Born and Th. von Kármán, Physik Z. **13**, 297 (1912); Physik Z. **14**, 15 (1913).

[6] L. D. Landau and E. M. Lifshits, *Theory of Elasticity* (Pergamon Press, Oxford, 1986).

[7] M. Born and K. Huang, *Dynamical Theory of Crystal Lattices* (Oxford University Press, Oxford, 1954), p. 129-154.

[8] W. Voigt, *Lehrbuch der Kristallphysik* (Teubner, Berlin, 1928).

[9] D. C. Wallace, in *Solid State Physics*, eds. H. Ehrenreich, F. Seitz and D. Turnbull (Academic, New York, 1970), Vol. 25, pp. 301.

[10] J. H. Weiner, *Statistical Theory of Elasticity* (John Wiley and Sons, New York, 1983).

[11] Z. Zhou and B. Joós, Phys. Rev. B **54**, 3841 (1996).

[12] K. J. Runge and G. V. Chester, Phys. Rev. A **36**, 4852 (1987).

[13] D. Frenkel and A. J. C. Ladd, Phys. Rev. Lett. **59**, 1169 (1987).

[14] R. Everears, K. Kremer and G. S. Grest, Macromol. Symp. **93**, 53 (1995).

[15] S. J. Barsky, M. Plischke, B. Joós and Z. Zhou, Phys. Rev. E **54**, 5370 (1996).

[16] D. R. Squire, A. C. Holt and W. G. Hoover, Physica (Amsterdam) **42**, 388 (1969).

[17] Versions of the fluctuation method applicable to other thermodynamic ensembles are found in M. Parrinello and A. Rahman, J. Chem. Phys. **76**, 2662 (1982). For more recent discussions and additional references on the fluctuation method see: A. A. Gusev, M. M. Zehnder and U. W. Suter, Phys. Rev. B **54**, 1 (1996); S. Sengupta, P. Nielaba, M. Rao and K. Binder, Phys. Rev. E **61**, 1072 (2000).

[18] O. Farago and Y. Kantor, Phys. Rev. E **61**, 2478 (2000).

[19] K. Huang, *Statistical Mechanics* (John Wiley and Sons, New York, 1963).

[20] J. A. Barker and D. Henderson, Mol. Phys. **21**, 187 (1971).

[21] For a recent review article on hard spheres see A. P. Gast and W. B. Russel, Phys. Today **51** No.12, 24 (1998), and references therein.

[22] N. Metropolis, A. W. Rosenbluth, M. N. Rosenbluth, A. H. Teller and E. Teller, J. Chem. Phys. **21**, 1087 (1953).

[23] J. G. Kirckwood, J. Chem. Phys. **7**, 911 (1939).

[24] B. J. Alder and T. E. Wainwright, J. Chem. Phys. **27**, 1208 (1957).

[25] W. W. Wood and J. D. Jacobson, J. Chem. Phys. **27**, 1207 (1957).

[26] W. G. Hoover and F. H. Ree, J. Chem. Phys. **49**, 3609 (1968); B. J. Alder, W. G. Hoover and D. A. Young, J. Chem. Phys. **49**, 3688 (1968).

[27] A. D. Bruce, N. B. Wilding and G. J. Ackland, Phys. Rev. Lett. **79**, 3002 (1997).

[28] S. Pronk and D. Frenkel, J. Chem. Phys. **110**, 4589 (1999).

[29] P. N. Pusey and W. van Megen, Nature **320**, 340 (1986).

[30] J. Zhu, M. Li, R. Rogers, W. Meyer, R. H. Ottewill, STS-73 Space Shuttle Crew, W. B. Russel and P. M. Chaikin, Nature **387**, (1997).

[31] E. Velasco and P. Tarazona, Phys. Rev. A **36**, 979 (1987); H. Xu and M. Baus, Phys. Rev. A **38**, 4348 (1988); B. B. Laird, J. Chem. Phys. **97**, 2699 (1992).

[32] A. Jaster, Physica A **264**, 134 (1999).

[33] F. H. Stillinger Jr. and Z. W. Salsburg, J. Chem. Phys. **46**, 3962 (1967).

[34] M. Luban and J. P. J. Michels, Phys. Rev. A **41**, 6796 (1990).

[35] P. J. Flory, J. Chem Phys **10**, 51 (1942); F. T. Wall, J. Chem. Phys. **10**, 132 (1942). A detailed review on the classical theory of rubber elasticity is found in R. G. Treloar, Rep. Prog. Phys. **36**, 755 (1973).

[36] H. M. James and E. Guth, J. Chem. Phys. **11**, 455 (1943).

[37] Developments in the field of rubber elasticity are described in the following monographs (which also include many references to different theories): R. T. Deam and S. F. Edwards, Phil. Trans. R. Soc. A **280**, 317 (1976);J. E. Mark and B. Erman, *Rubberlike Elasticity. A Molecular Primer* (Wiley-Interscience, New York, 1988); R. Everears, Euro. Phys. J. B **4**, 341 (1998).

[38] P. G. de Gennes, *Scaling Concepts in Polymer Physics* (Cornell Univ. Press, Ithaca, N.Y. 1979).

[39] P. G. de Gennes, J. Phys. (Paris) Lett. **37**, L1 (1976).

[40] O. Farago and Y. Kantor, Phys. Rev. E **62**, 6094 (2000).

[41] O. Farago and Y. Kantor, Euro. Phys. J. E **3**, 253 (2000).

[42] *Statistical Mechanics of Membranes and Surfaces*, Proceedings of the Fifth Jerusalem Winter School for Theoretical Physics, eds. D. R. Nelson, T. Piran and S. Weinberg (World Scientific, Singapore, 1989).

[43] J. H. Fendler and P. Tundo, Acc. Chem. Res. **17**, 3 (1984).

[44] D. H. Pearson and R. J. Tonucci, Science **270**, 68 (1995).

[45] D. H. Boal, U. Seifert and J. C. Shillcock, Phys. Rev. E **48**, 4274 (1993).

[46] D. E. Discher, D. H. Boal and S. K. Boey, Phys. Rev. E **55**, 4762 (1997); W. Wintz, R. Everaers and U. Seifert, J. Phys. I (France) **7**, 1097 (1997).

[47] D. Stauffer and A. Aharony, *Introduction to Percolation Theory* (Taylor and Francis, London, 1992).

[48] A review article containing many relevant references: M. Adam and D. Lairez, in *Physical Properties of Polymeric Gels*, ed. J. P. Cohen Addad (J. Wiley and Sons, Chichester U. K., 1996), pp. 87.

[49] M. Daoud and A. Coniglio, J. Phys. A **14**, L301 (1981); M. Daoud, Macromol. **33**, 3019 (2000), and references therein.

[50] S. Feng and P. N. Sen, Phys. Rev. Lett. **52**, 216 (1984); D. J. Bergman and Y. Kantor, Phys. Rev. Lett. **53**, 511 (1984); S. Feng, M. F. Thorpe and E. Garboczi, Phys. Rev. B **31**, 276 (1985); S. Arbabi and M. Sahimi, Phys. Rev. B. **47**, 695 (1993).

[51] Y. Kantor and I. Webman, Phys. Rev. Lett. **52**, 1891 (1984); J. G. Zabolitzki, D. J. Bergman and D. Stauffer, J. Stat. Phys. **44**, 211 (1986); S. Arbabi and M. Sahimi, Phys. Rev. B. **47**, 703 (1993).

[52] Numerical evidence and heuristic arguments [see, M. Sahimi, J. Phys. C **19**, L79 (1986), and S. Roux, J. Phys. A **19**, L351 (1986)] indicate that for bending elasticity, the exponent f is well approximated by $t + 2\nu$, where ν is the correlation length exponent.

[53] S. Alexander and R. Orbach, J. Phys. (Paris) Lett. **45**, L625 (1982).

[54] M. E. Cates, Phys. Rev. Lett. **53**, 926 (1984).

[55] S. Alexander, Phys. Rep. **296**, 66 (1998).

[56] M. Plischke and B. Joós, Phys. Rev. Lett. **80**, 4907 (1998); M. Plischke, D.C. Vernon, B. Joós and Z. Zhou, Phys. Rev. E **60**, 3129 (1999).

[57] O. Farago and Y. Kantor, Europhys. Lett. **52**, 413 (2000).

[58] A. Coniglio, Phys. Rev. Lett. **46**, 250 (1981).

[59] J. P. Clerc, V. A. Podolskiy and A. K. Sarychev, Euro. Phys. J. B **15**, 507 (2000); G. G. Batrouni, A. Hansen and B. Larson, Phys. Rev, E **53** 2292 (1996); J. M. Normand and H. J. Herrmann, Int. J. Mod. Phys. **6**, 813 (1995); D. B. Gingold and C. L. Lobb, Phys. Rev. B **42**, 8220 (1990).

[60] P. Grassberger, Physica A **262**, 251 (1999).

[61] H. J. Herrmann, D. C. Hong and H. E. Stanley, J. Phys. A: Math. Gen. **17**, L261 (1984).

[62] O. Farago and Y. Kantor, Phys. Rev. Lett. **85**, 2533 (2000).

[63] O. Farago and Y. Kantor, cond-mat/0105469.

[64] F. C. Schilling, M. A. Gomes, A. E. Tonelli, F. A. Bovey and A. E. Woodward, Macromol. **20**, 2957 (1987).

[65] M. Djabourov, J. Leblond and P. Papon, J. Phys. (Paris) **49**, 333 (1988).

[66] M. A. V. Axelos and M. Kolb, Phys. Rev. Lett. **64**, 1457 (1990).

[67] F. Devreux, J. P. Boilot, F. Chaput, M. Mailier and M. A. V. Axelox, Phys. Rev. E **47**, 2689 (1993).

[68] M. Adam, D. Lairez, K. Karpasas and M. Gottlieb, Macromol. **30**, 5920 (1997).

[69] F. Carciun, C. Galassy and E. Roncari, Europhys. Lett. **41**, 55 (1998).

[70] G. C. Fadda, D. Lairez, and J. Pelta, Phys. Rev. E **63**, 061405 (2001).

[71] M. Adam, M. Deksanti and D. Durand, Macromol. **18**, 2285 (1985).

[72] D. F. Hodgson and E. J. Amis, Macromol. **23**, 2512 (1990).

[73] R. H. Colby, J. R. Gillmor and M. Rubinstein, Phys. Rev. E **48**, 3712 (1993).

[74] L. Lin and Y. Aoki, Macromol. **31**, 740 (1998).

[75] D. Deptuck, J. P. Harrison and P. Zawadzki, Phys. Rev. Lett **54**, 913 (1985).

[76] M. C. Maliepaard, J. H. Page, J. P. Harrison and R. J. Stubbs, Phys. Rev. B **32**, 6261 (1985).

[77] T. McLeish, in *Soft and Fragile matter - Nonequilibrium dynamics, metastability, and flow*, Proceedings of the Fifty Third Scottish Universities Summer School in Physics, eds. M. E. Cates and M. R. Evans (Institute of Physics Publishing, Bristol, 2000), pp. 79.

[78] S. Sengupta, P. Nielaba and K. Binder, Phys. Rev. E **61**, 6294 (2000); A. Jaster, Phys. Rev. E **59**, 2594 (1999).

[79] J. M. Kosterlitz and D. J. Thouless, J. Phys. C **6**, 1181 (1973); B. I. Halperin and D. R. Nelson, Phys. Rev. Lett. **41**, 121 (1978); D. R. Nelson and B. I. Halperin, Phys. Rev. B **19**, 2457 (1979); A. P. Young, Phys. Rev. B **19**, 1855 (1979).

[80] See e.g., A. C. Mitus, H. Weber and D. Marx, Phys. Rev. E **55**, 6855 (1997), and references therein.

[81] S. T. Chui, Phys. Rev. Lett. **48**, 933 (1982); Phys. Rev. B **28**, 178 (1983).

[82] E. Del Gado, L. De Arcangelis and A. Coniglio, Europhys. Lett. **46**, 288 (1999).

[83] Y. Kantor and G. N Hassold, Phys. Rev. Lett. **60**, 1457 (1988).

[84] Z. Zhou, Pik-Yin Lai and B. Joós, Phys. Rev. E **62**, 7490 (2000).

[85] For a review of this subject see K. Kremer, in *Soft and Fragile matter - Nonequilibrium dynamics, metastability, and flow*, Proceedings of the Fifty Third Scottish Universities Summer School in Physics, eds. M. E. Cates and M. R. Evans (Institute of Physics Publishing, Bristol, 2000), pp. 145.

[86] Y. Mao, M. E. Cates and H. N. W. Lekkerkerker, Physica A **222**, 10 (1995); T. Biben, P. Bladon and D. Frenkel, J. Phys.: Cond. Mat. **8**, 10799 (1996); R.

Dickman, P. Attard and V. Simonian, J. Chem. Phys. **107**, 205 (1997); and references therein.

[87] See e.g., W. C. K. Poon and P. B. Warren, Europhys. Lett. **28**, 513 (1994); A. D. Dinsmore, A. G. Yodh and D. J. Pine, Phys. Rev. E **52**, 4045 (1995); A. Imhof and J. K. Dhont, Phys. Rev. Lett. **75**, 1662 (1995); T. Coussaert and M. Baus, J. Chem. Phys. **109**, 6012 (1998); A. Bohot and W. Krauth, Phys. Rev. Lett. **80**, 3787 (1998); M. Dijkstra, R. van Roij and R. Evans, Phys. Rev. Lett. **81**, 2268 (1998).

[88] F. F. Abraham, Phys. Rev. B **23**, 6145 (1981); J. Tobochnik and G. V. Chester, Phys. Rev. B **25**, 6778 (1982); J. Q. Broughton, G. H. Glimer and J. D. Weeks, Phys. Rev. B **25**, 4651 (1982).

[89] M. A. Bates and D. Frenkel, Phys. Rev. E **61** 5223 (2000).

אלסטיות של מערכות נשלטות-אנטרופיה

חיבור לשם קבלת התואר

דוקטור לפילוסופיה

מאת

עודד פרגו

הוגש לסנט של אוניברסיטת תל אביב

יוני 2001

העבודה הוכנה בהנחייתו של

פרופסור יעקב קנטור